DISLOCATION MOBILITY IN PURE COPPER SINGLE CRYSTALS

Thesis by

William Franklin Greenman

In Partial Fulfillment of the Requirements

For the Degree of

Doctor of Philosophy

California Institute of Technology

Pasadena, California

1967

(Submitted July 29, 1966)

ACKNOWLEDGMENTS

The author wishes to express his sincere appreciation to Professor Thad Vreeland, Jr., who directed this research and whose aid and encouragement made the work possible. Throughout the course of the research, many valuable comments and suggestions were proffered by Professors David S. Wood and Donald S. Clark. Messrs. G. R. May and R. C. Blish were of great assistance in the experimentation.

The author is very grateful for fellowships provided by the Garrett Corporation and the R. C. Baker Foundation.

The torsion impulse machine was constructed and this research was performed under a contract with the United States Atomic Energy Commission.

Finally, the author wishes to express his appreciation to his wife, Penelope, for her patience, wisdom, and encouragement which also made this work possible.

ABSTRACT

This thesis presents the results of an experimental investigation of the stress dependence of dislocation velocity in 99.999 per cent copper single crystals. Dislocation displacements were detected by etch pitting dislocation sites on {100} planes. Stress pulses of microsecond duration were applied to single crystal test specimens by means of a torsion impulse machine. Maximum applied, resolved shear stresses ranged from 29 g/mm^2 to 236 g/mm^2, and calculated dislocation velocities ranged from 160 cm/sec to 710 cm/sec. The dislocations were presumably predominantly edge-oriented.

The growth of copper single crystals, the spark and chemical machining of single crystal test specimens, and the behavior of the etchants which reveal dislocation sites on {100} planes are also discussed.

The experimental data have been found to obey a linear relation between dislocation velocity and applied, resolved shear stress. This finding does not correlate with the explanation of the low strain rate sensitivity of the flow stress in copper as proposed by Cottrell (46)*, which predicts that dislocation velocity should be proportional to stress raised to a power of about 200. The low strain rate sensitivity of the flow stress in copper is explained by the high velocity of dislocations at low stresses and the strong stress dependence of the mobile dislocation density. This high velocity is interpreted as enabling the strain essentially to achieve its equilibrium value even at relatively high strain rates.

---

*One- and two-digit numbers appearing in parentheses indicate references listed at the end of the thesis.

TABLE OF CONTENTS

LIST OF FIGURES

I. INTRODUCTION

Measurement of dislocation velocity provides information from which theories of the influence of strain rate effect upon mechanical properties of crystalline solids may be derived. Further, such measurements provide information concerning the dynamic interactions between moving dislocations and the crystal lattice, other dislocations, and other lattice defects. This thesis presents the first direct measurements of dislocation velocity in a face-centered cubic metal, copper.

A theory of the influence of strain rate upon mechanical properties can be derived from a knowledge of the dynamical behavior of dislocations in crystals because of the direct dependence of plastic strain rate on dislocation velocity. This dependence is due to the fact that dislocation motion results in plastic deformation as expressed by the relation

$$\gamma_p = Ab/V = A_o b \qquad [1]$$

where γ_p is the plastic shear strain resulting from dislocations of Burgers vector b sweeping out a total slip plane area of A in a crystal of volume V. (A_o is then the area per unit volume swept out by the dislocations.) Equation 1 relates a macroscopic quantity, plastic shear strain, to the microscopic dislocation parameters A_o and b for the case of single slip. Differentiation of Equation 1 with respect to time gives the rate of plastic deformation for single slip,

$$\dot{\gamma}_p = \dot{A}_o b = b \oint v d\ell \qquad [2]$$

where v is the velocity of an element $d\ell$ of dislocation line and the

integral is taken over all the dislocations in a unit volume. If the integral in Equation 2 is replaced by a product of the average velocity $\bar{v}$ and the length of dislocation line per unit volume ρ, there results the relation

$$\dot{\gamma}_p = \rho b \bar{v} \quad . \qquad [3]$$

The dislocation density ρ could be the total length of all dislocations per unit volume, and $\bar{v}$, the average velocity of all dislocations. However, if all those dislocations which move do so with velocities of the same order of magnitude, then it is more useful to take ρ and $\bar{v}$ to be the density and average velocity, respectively, of only those dislocations which actually move. The dislocation density and the average dislocation velocity, and, consequently, the strain rate, are functions of stress and strain.

Equation 3, which relates the macroscopic shear strain rate to the dislocation parameters of density, Burgers vector, and velocity, may be extended to the case in which slip on different slip systems is occurring simultaneously. The contribution to the total deformation rate from slip on a given slip system is given by Equation 3 modified by an appropriate orientation factor. Gilman has pointed out that the description of plastic deformation in terms of dislocation mechanics represents a significant advance over classical plasticity theory (1). When the variables $\bar{v}$ and ρ can be described as functions of the applied stress and the instantaneous strain, the macroscopic plastic strain rate can then be related to the macroscopic stress and strain. This relation permits the response of the crystal to be predicted for

any stress-time history, or alternately, it permits calculation of the stresses required to deform a crystal on a given strain-time path.

The dislocation dynamics description of plastic deformation has been employed to predict the dynamic stress-strain response of a crystal (2), to describe transient creep behavior (3), and to explain some observations in high-velocity impact experiments (4), none of which could be adequately predicted by the classical plasticity theories. However, extension of the dislocation dynamics description of plastic deformation to single crystals of materials other than those for which velocity and density data exist or to polycrystalline aggregates, if feasible at all, awaits experimental data for a greater range of materials, both single crystal and polycrystalline, and a statistical approach to cope with the orientation factors in a multiple slip system.

Experimental techniques which permit dislocation velocity to be measured directly have become available only recently. "Direct experiments" is a term used here to denote those experiments in which the position of a dislocation is observed either continuously or intermittently with time. The early information about dislocation velocity was based on indirect measurements in internal friction experiments, and the information obtained from these experiments depended upon the model used to interpret the data. No model of or major presupposition about dislocation behavior is necessary in order to interpret the data in the direct experiments on dislocation motion employing transmission electron microscopy, dislocation etch pitting, or x-ray diffraction, although there is no certainty that dislocation behavior in the thin specimens employed in transmission electron

microscopy is identical to that in thick samples. Dislocation etch pitting has been the technique used most extensively in direct experiments on dislocation mobility. Until very recently, the x-ray diffraction techniques had not been employed for dislocation mobility studies (5, 6). While the continuous observation of moving dislocations is only possible in the techniques of electron microscopy and continuous etching, both of these techniques are limited to measuring low dislocation velocities. The intermittent observation of dislocation position as a function of time by means of etch pitting has, therefore, been employed in most studies of dislocation velocity and mobility.

The present knowledge of dislocation mobility in single crystals of several materials has resulted from experiments in which a stress pulse of known magnitude and duration was applied to a single crystal specimen and dislocation displacement was detected by etch pitting before and after the application of the pulse. Various minor assumptions are implicit in the etch-pulse-etch experiments, but no model is needed to interpret the results. For example, it is assumed that the dislocation velocity is in phase with the stress, i.e., that at every instant of time the dislocation velocity at a given stress is equal to the equilibrium or steady-state value of the velocity at that stress. Obviously, this assumption is not valid during the time of acceleration of the dislocation to the steady state velocity. Therefore, the effect or magnitude of the acceleration time must be determined.

The stress dependence of dislocation velocity may be determined most easily if the applied resolved shear stress on the disloca-

tion(s) is constant over a given duration of time, i.e., when an essentially "square" (actually trapezoid-shaped) stress pulse is applied. Then the velocity of the dislocation is just the dislocation displacement divided by the time at constant stress. However, if the acceleration time of the dislocation is longer than the rise time of the stress pulse, the above calculation of velocity can lead to erroneous results. It is also important that the specimen be subjected to only one known stress pulse and to no unknown stresses which would add to or subtract from the dislocation displacements produced by the pulse and upon which the velocity is calculated.

The so-called double etch technique uses the characteristics of certain etchants to facilitate determination of dislocation displacement. The specimen is etched before application of the stress pulse, the pulse is applied, and the specimen is re-etched without first removing the previous dislocation etch pits by chemical or electrolytic polishing. The re-etching produces small, sharp-bottomed pits at the new sites of dislocations which have moved during the stress pulse and large flat-bottomed pits at their previous sites. Large, sharp-bottomed pits form at the sites of dislocations which did not move. Thus, a sharp-bottomed pit and a flat-bottomed pit lying adjacent to one another along the direction of slip give the amount of dislocation displacement. Difficulties in determining the initial and final positions of a dislocation arise when dislocation displacements are greater than one-half the initial dislocation spacing and when dislocations are moving on more than one slip system.

Johnston and Gilman (7) were the first investigators to deter-

mine dislocation mobility in a material, the ionic compound lithium fluoride, with the technique of etch pitting. The dislocation mobility data in lithium fluoride is quite extensive, velocity having been studied as a function of applied stress, temperature, annealing treatment, and irradiation. Dislocation velocity has also been determined as a function of applied stress for silicon-iron (8, 9), sodium chloride (10), tungsten (11), and various semiconductor crystals (12, 13). Adams (14) has investigated basal and non-basal dislocation mobility in high purity and impurity-doped zinc. Although dislocation mobility data exist for a variety of materials, no studies have yet produced any direct information about dislocation velocity in the face-centered cubic metals.

Among the face-centered cubic metals of high purity (99.999 per cent), there are only two for which dislocation etchants exist, silver (15) and copper (16-19). Utilizing the etch pitting technique to determine dislocation density, Young (20), Livingston (18), and Hordon (21) have performed tension tests on high-purity copper single crystals of various orientations to determine the relationships among dislocation density, resolved shear stress, and shear strain for such tests. Studies of dislocation motion in high-purity copper single crystals have been made by Young (22, 23), Livingston (17, 24), and Petroff (25), but no quantitative work on the stress dependence of dislocation velocity was reported. From the results of indirect experiments by Conrad (26) on low-purity (99.98 per cent) copper, as analyzed according to the following treatment, it might be inferred that the dislocation velocity in copper is a very sensitive function of

the applied stress.

Subsequent to the dislocation mobility studies of Johnston and Gilman (7) and Stein and Low (8), Guard (27) suggested an indirect method of determining the stress dependence of dislocation velocity for those materials for which dislocation etchants did not exist -- the change of strain rate test during the usual tension or compression test. How this technique might be useful in determining the dependence of dislocation velocity on applied stress may be seen from Equation 3. Taking logarithms of both sides of the equation, differentiating with respect to the logarithm of the applied resolved shear stress τ, and defining the quantity m' as with Johnston and Stein (28),

$$m' = \frac{\partial \ell n \dot{\gamma}_p}{\partial \ell n \tau} = \frac{\partial \ell n \bar{v}}{\partial \ell n \tau} + \frac{\partial \ell n \rho}{\partial \ell n \tau} \quad . \qquad [4]$$

Now m' or $(\partial \ell n \dot{\gamma}_p)/(\partial \ell n \tau)$ can be approximated by

$$\frac{\ell n (\dot{\gamma}_2/\dot{\gamma}_1)}{\Delta\tau/\tau}$$

where $\dot{\gamma}_1$ is the strain rate before the change, $\dot{\gamma}_2$ is the strain rate after the change, and $\Delta\tau$ is the change of stress accompanying the change of strain rate ($\Delta\tau << \tau$). Over most of the range of dislocation velocities in the materials mentioned above, the data may be represented by the relation

$$\bar{v} = A\tau^m , \qquad [5]$$

where A and m are constants for a given material and temperature. Equation 4 then reduces to

$$m' = m + \frac{\partial \ell n \rho}{\partial \ell n \tau} \quad . \qquad [6]$$

If the moving dislocation density is independent of or rather insensi-

tive to the change of stress, the inverse strain rate sensitivity m' should be approximately equal to the mobility exponent m. Guard (27) found no agreement between m' and the directly measured m (8) for change of strain rate tests in silicon-iron, indicating that the moving dislocation density is sensitive to the change of stress. Johnston and Stein (28) reopened the question of the validity of strain rate tests, reasoning that for very small strains m' should equal m or, correspondingly, extrapolating a curve of m' versus strain to zero strain would give $m' = m$. Using this technique, they obtained reasonable agreement between m' at zero strain for change of strain rate tests and the directly measured values of m for lithium fluoride and silicon-iron. Of course, a major assumption in this change of strain rate treatment is that the dislocation velocity in the material has the functional dependence on stress as expressed by Equation 5.

Conrad (26) has performed such change of strain rate tests in copper; however, the tensile axis of the single crystals was such as to produce multiple slip initially, and also the specimens were subjected to very large strains. These facts alone might preclude the use of the data from these tests in order to determine the mobility exponent. The inverse strain rate sensitivity, m', calculated from the results of the experiments by Conrad, is plotted versus shear strain in Figure 1. The strain rate ratio was 10. If any curve can be fitted to the data at all, it would at least indicate a value of m large relative to those obtained for other materials (lithium fluoride - 15 to 25, silicon-iron - 40). It is clear from the scatter of the data that a change of strain rate test in copper might not allow an unambiguous

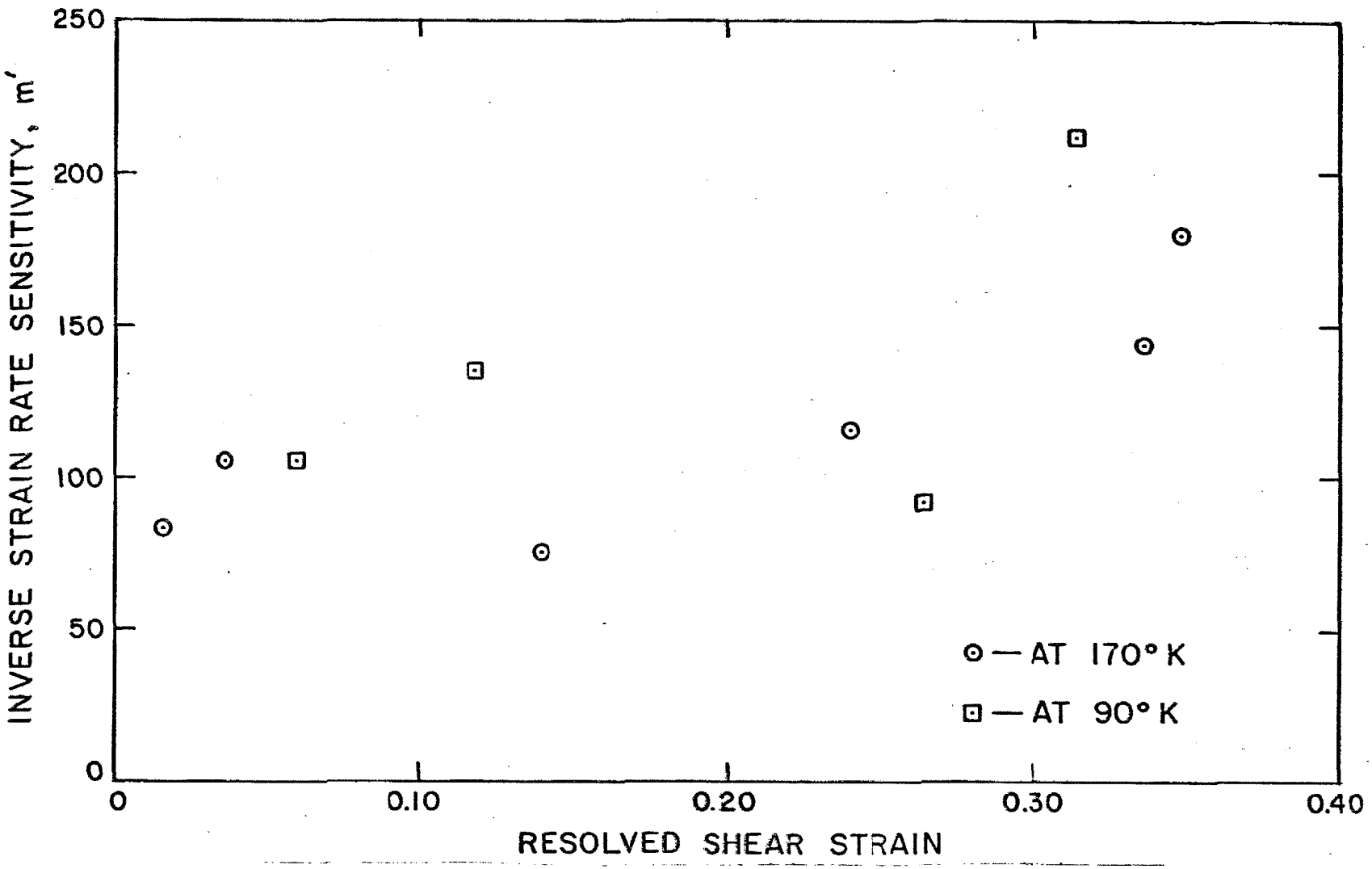

Figure 1. Inverse Strain Rate Sensitivity Versus Resolved Shear Strain for Copper from Data of Conrad (26).

determination of the stress dependence of dislocation velocity. Moreover, it is not certain that the extrapolation method of Johnston and Stein gives the mobility exponent, for Adams (14) found that in zinc single crystals, change of strain rate tests gave $m' = 83$ and direct measurements gave $m = 5$. Also, Schadler (11) found that the extrapolation procedure was inaccurate for tungsten single crystals.

With the validity of indirect tests of dislocation mobility in copper in question and with the lack of any quantitative data obtained directly, it was decided to embark upon a program to determine the stress dependence of dislocation velocity in copper as a representative face-centered cubic metal. It was, therefore, the purpose of the present work to make direct measurements of dislocation velocity by determining dislocation displacement produced by the application of a stress pulse of known magnitude and duration. All test specimens were to be of high-purity (99.999 per cent) copper, and the tests envisioned above were to be conducted at room and several lower temperatures. The data from the low-temperature tests were not available at the time this thesis was written but are to be included in a later report. Finally, the experimental results were to be compared with the stress dependence of dislocation velocity as predicted by various current theories in an attempt to determine which theory or theories give the most valid prediction of the actual behavior.

Various considerations enter into the experiments outlined above. Single crystals should be employed such that the applied resolved shear stress may be known with as little uncertainty as possible; and to minimize the effects of unknown impurities, the purity of

the single crystals should be as high as possible (in this case, 99.999 per cent). Since etch pitting was to be employed to determine initial and final dislocation positions, the spacing between dislocation etch pits should be at least twice the contemplated dislocation displacement due to the stress pulse in order to know with a fair degree of certainty the initial and final position of the dislocation. A restriction of low dislocation density was thereby imposed upon the single-crystal test specimens. It was assumed that a stress pulse of microsecond duration would be required, since other investigators in copper had available to them testing machines capable of producing square stress pulses of millisecond, second, and longer time duration and had reported no quantitative data on dislocation velocity. Also, the experience of Adams (14) with zinc, the only soft metal yet studied, would indicate that dislocations might move very fast in copper. For specimens of reasonable dimensions, the microsecond duration dictated application of the stress pulse by a wave propagation technique. Since the validity of the etch-pulse-etch technique depends to a large extent upon the application of a square or trapezoid-shaped stress pulse, the rise and decay time of the stress pulse should be short, here, less than five microseconds; and, therefore, the wave propagation should be non-dispersive. The orientation dependence of the available dislocation etchants for copper restricted the surface on which dislocation displacement could be observed to within a few degrees of {111}, {100}, or {110} surfaces. These etchants are for both fresh, undecorated dislocations and aged dislocations; no aging treatment is required after dislocation displacement.

Section II of this thesis is concerned with experimental equipment and techniques. The testing machine used to apply a stress pulse to a single-crystal specimen is described. The measurement of stress and time and the techniques employed to determine dislocation displacement are also described. Section III deals with the preparation of single-crystal test specimens with the proper orientation and shape from large single crystals. Section IV describes the experimental procedure followed in applying the stress pulse to a specimen and in determining dislocation displacement. Section V presents the experimental results of this investigation, the means of obtaining the data, and the calculations to reduce the data. Section VI analyzes the results in light of current theories and discusses physical mechanisms which might govern dislocation mobility in copper. Section VII is a summary and presents conclusions derived from this investigation.

II. EXPERIMENTAL EQUIPMENT AND TECHNIQUES

A. Torsion Impulse Machine

The most difficult of the requirements outlined above for the proposed project would appear to be the application of the stress pulse. A wave propagation technique must be employed for such loading, and the type and mode of the waves must be such that the pulse is not distorted as it propagates through the loading fixture and the specimen. These conditions are satisfied by zero-order mode torsional waves in isotropic, cylindrical bars, for which the phase and group velocities are independent of frequency (29). A testing machine capable of applying a single, square stress pulse of microsecond duration to a cylindrical, single-crystal specimen of proper crystallographic orientation has been developed at the W. M. Keck Laboratory of Engineering Materials at the California Institute of Technology (30).

The torsion testing machine generates stress pulses in the following manner. An initial static torque is applied to a section of a cylindrical rod which is a part of the torsion rod or load train shown schematically in Figure 2. The torque is applied to the top of the section by dead weight loading of a cranking disc attached to the rod through a rubber sleeve. A thin glass disc fastened to the bottom of the section transmits this torque to a bakelite fixture which is attached to a fixed bearing tube surrounding the rod. A 0.006 mm thick aluminum foil is attached between the glass disc and bakelite with Eastman 910 adhesive. The lower section of the torsion rod or load train is attached to the opposite side of the glass disc by means

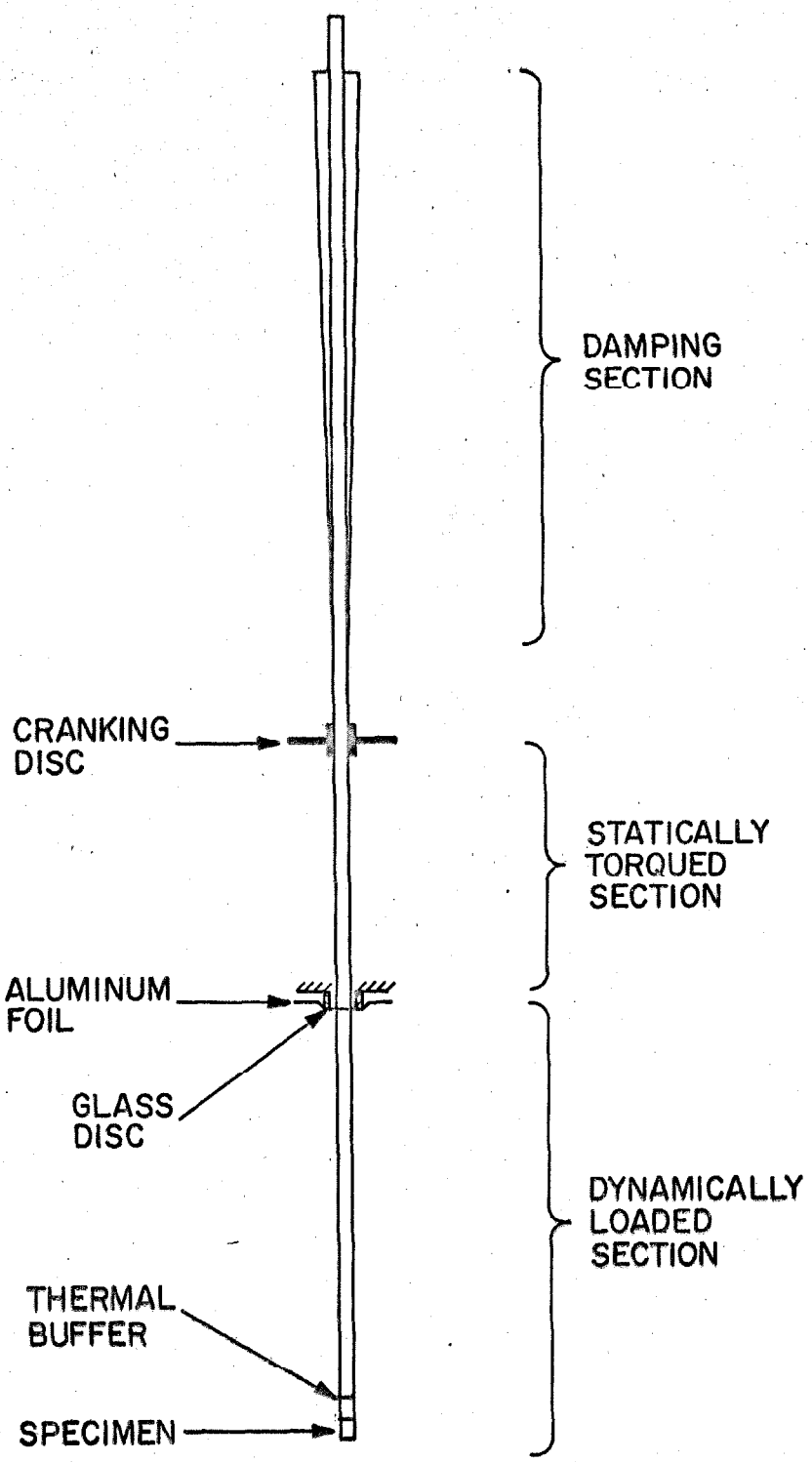

Figure 2. Schematic of Torsion Pulse System.

of a butt adhesive bond. This section of the torsion rod is coaxial with the upper section but does not carry any static torque. The specimen is attached to the bottom end of this lower section of the torsion rod, and the bottom end of the specimen is the free end of the torsion rod system. The section of the rod above the cranking disc is coated with a viscoelastic material and attenuates the waves propagating away from the specimen. The application of the stress pulse to the specimen is initiated by a high-voltage capacitor discharge through the aluminum foil. Explosion of the foil releases the static torque and results in elastic waves which propagate away from the glass disc interface of the torsion rod. The duration of the stress pulse at any point in the specimen is the time required for the wave to propagate from that point to the free end and return. The amplitude of the dynamic torque in the lower section of the torsion rod is one-half the initial static torque applied to the machine and, therefore, proportional to the weight hung on the cranking disc.

The requirements imposed upon the crystallographic orientation of the test specimens by the orientation dependence of the dislocation etch and the characteristics of the torsion machine could fortunately be reconciled. The effect of elastic anisotropy of a single crystal specimen upon the dispersion of the torsion pulse and the stresses produced thereby have been calculated and are presented in Appendix A. The form of the single-crystal test specimens chosen for this investigation was that of a right circular cylinder, the cylinder axis and torsion axis being coincident with the <100> direction of the crystal. This specimen orientation was not dispersive of the

stress pulse and provided four {100} observation surfaces upon which a double etch pit technique could be employed.

The testing system described above and in reference 30, with the modifications described below, was used to apply the stress pulse to test specimens. The governing consideration in altering this machine to test copper single crystals was that the acoustic impedance at the interfaces between different materials in the load train or torsion rod should be equal. The acoustic impedance for torsional waves in circular rods is given by (31)

$$Z_o = \frac{\pi a^4}{2} \sqrt{\mu\rho} \qquad [7]$$

where

a = radius of rod,

μ = shear modulus, or, for <100> oriented specimens, $c_{55'} = c_{66'} = c_{44}$,

ρ = density (mass/unit volume).

It was decided that the diameter of the torsion rods should be maintained at one-half inch in order to minimize the alteration of the machine. In this way, only the torsion rods needed to be changed; that is, only the material of which they were made needed to be changed; and modifications of other parts of the machine, such as the pillow blocks and bearing which supported the torsion rods, were avoided. Acoustic impedance can be made equal or matched for materials of slightly different shear impedance $\sqrt{\mu\rho}$ (32) by adjusting the diameters of the rods; however, a large change of diameter at the torsion rod - specimen interface was avoided by selecting a specimen diame-

ter of approximately one-half inch. It was felt that this diameter would allow sufficient surface area to observe dislocation motion. The torsion rods were made of steel (SAE 1040), a material which closely meets the requirement of shear impedance matching with the specimen.

The shear impedance for a copper single crystal of <100> torsion axis orientation may be calculated from

$$Z_s = \sqrt{\mu\rho} \qquad [8]$$

where

$$\mu = C_{55'} = C_{44} = 7.51 \times 10^{11} \text{ dynes/cm}^2 \text{ , (33)}$$
$$\rho = 8.93 \text{ g/cm}^3 \text{ ,}$$

which gives

$$(Z_s)_{cu} = 25.9 \times 10^5 \text{ g/cm}^2\text{-sec} \text{ .}$$

The subscript "cu" refers to the specimen. Correspondingly, for SAE 1040 steel (Young's modulus = 29×10^6 lb/in^2),

$$\mu = 11.3 \times 10^6 \text{ lb/in}^2 = 7.75 \times 10^{11} \text{ dynes/cm}^2 \text{ ,}$$
$$\rho = 7.84 \text{ g/cm}^3 \text{ ,}$$

and

$$(Z_s)_{1040} = 24.6 \times 10^5 \text{ g/cm}^2\text{-sec} \text{ ,}$$

where the subscript "1040" refers to the torsion rod. From equality of acoustic impedance across the interface, the following relation is derived.

$$\left(\frac{d_{cu}}{d_{1040}}\right)^4 = \frac{(Z_s)_{1040}}{(Z_s)_{cu}} \qquad [9]$$

where

d_{cu} = diameter of copper specimen,

d_{1040} = diameter of steel torsion rod = 0.499 in.

As calculated from Equation 9, the diameter required for the specimen is

$$d_{cu} = 0.493 \text{ in.}$$

To avoid spurious stresses in the specimen produced by differential thermal expansion of the steel and copper, a thermal buffer was placed between the steel torsion rod and the copper specimen. This thermal buffer would have ideally been another copper single-crystal specimen hardened such that its yield stress was much larger than the highest stress contemplated (about 400 g/mm^2 resolved shear stress), thus preventing dispersion of the torsion pulse due to plastic flow in the thermal buffer. Since such hardening was deemed unfeasible and since thermal expansion is isotropic in cubic symmetry crystals, the thermal buffer was made of polycrystalline, 99.9 per cent copper rod, which remained elastic at the stresses for testing single crystals. To match the acoustic impedance of the thermal buffer to the steel, the calculation given above is repeated for polycrystalline copper where

$$\mu = 4.6 \times 10^{11} \text{ dynes/cm}^2,$$

$$\rho = 8.9 \text{ g/cm}^2,$$

and

$$(Z_s)_{tb} = 20.2 \times 10^5 \text{ g/cm}^2\text{-sec} \quad (31)$$

(the "tb" subscript refers to the thermal buffer). Using Equation 9 again, $d_{tb} = 0.525$ in. In matching the acoustic impedance between

polycrystalline and single-crystal copper, it can be seen that d_{cu} = 0.493 in., as before. The length of the thermal buffer was 0.91 in., a length judged sufficient to attenuate the thermal stresses arising at the steel - copper interface.

As in reference 30, a 30° taper joint 3 in. from the end of the torsion rod was employed to facilitate removal of a specimen for polishing and etching. A photograph of a specimen attached to a thermal buffer, which is, in turn, attached to the end of the torsion rod, is shown in Figure 3. This part of the torsion rod, one end of which is tapered to fit the taper joint, will be referred to subsequently as the specimen holder. The end of the specimen which is attached to the thermal buffer will be referred to subsequently as the fixed end of the specimen.

Another modification on the torsion machine was made in the damping rod, the upper section of the torsion rod system in which the torsional wave traveling away from the specimen is attenuated. On the original version of the torsion machine, the damping material was Solithane 113, a polymer produced by Thiokol Chemical Company, Trenton, New Jersey, which was composed of 50 per cent prepolymer and 50 per cent catalyst by volume. In changing the torsion machine in order to test copper crystals, the damping material was also Solithane 113, but the ratio of components was 60 per cent prepolymer and 40 per cent catalyst by volume. Although this mixture was thought to attenuate the outgoing wave more effectively, it was, in fact, a less effective damping material. Nevertheless, the effect of the reflected pulses was negligible, as will be demonstrated later.

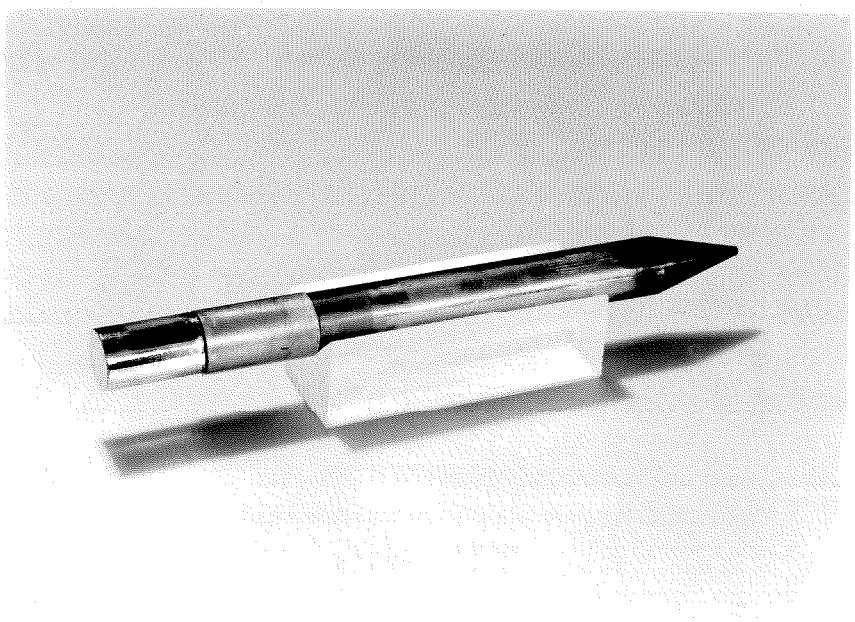

Figure 3. Specimen Mounted on Thermal Buffer and Specimen Holder.

Two aspects of the operation of the torsion machine should be mentioned here. First, it was found in this investigation that a rise time for the stress pulse of 2 μsec was quite reproducible. This value is very close to the time which a shear wave in steel requires to travel the radius of the rod (2 μsec). Secondly, it would seem likely that the release of the static torque might produce torsional wave modes of higher order than zero. After giving a solution of the Pochhammer equations for torsional waves in cylindrical bars, Mason states (34)

> If, however, the frequencies of all the components of the signal are below the critical frequency f_c, all the higher modes are highly attenuated and after a short distance the only mode transmitted is the zero-order mode which does not have any dispersion (34).

He states an inequality for the maximum frequency such that higher order modes are attenuated,

$$f < \frac{3}{4} f_c = \frac{3}{4} \times \frac{5.136\ V}{2\pi a} \qquad [10]$$

where V is the torsional wave velocity, which in steel is 0.315×10^6 cm/sec ; a is again the radius of the rod, in this case, 6.35 mm; and the numerical factor 5.136 is the first root of a secular equation. Using the above values, inequality 10 becomes

$$f < 1.5 \times 10^5 \text{ cps} \ . \qquad [11]$$

An indication of the torsion pulse component with the maximum frequency is given by the rise time, 2 μsec. The period of this component would then be 8 μsec, and the frequency, 1.25×10^5 cps, satisfying inequality 11. If higher modes are produced in releasing the static torque, they should be greatly attenuated before the torsion pulse enters the specimen, which is about 24 in. from the place of

initiation of the torsion pulse.

B. Stress and Time Measurement

Measurement of the stress pulse amplitude and duration was accomplished by means of silicon strain-gage circuits whose output was displayed on the screen of a Tektronix type 555 oscilloscope. The strain gages, which were 0.050 in. long and had a 500 Ω nominal resistance and a gage factor of 140, were obtained from Micro-systems, Inc., Pasadena, California, and were cemented (with epoxy cement) to the steel torsion rod at a point 7.125 in. from the end. A drawing of the lower section of the torsion rod is shown in Figure 4. They were placed at 45^{o} to the cylindrical axis and at positions 90^{o} apart around the periphery of the rod. The strain gages were connected in a voltage divider circuit such that bending and extensional strains were cancelled. The input voltage to the divider circuit was supplied by a 1/2 per cent regulated D.C. power supply, and the output voltage was conducted to the oscilloscope amplifiers through an electrical noise filter (1000 Ω - 270 pF). The oscilloscope sweep circuit was triggered by the capacitor discharge, as in reference 30.

The calibrated sweep rates of the oscilloscope provided a time base from which to determine stress pulse duration and the occurrence of other events. The strain-gage output voltage was displayed on both beams of the oscilloscope. The upper beam was triggered by the capacitor discharge and had a sweep rate of 200 μsec/cm for a time span of 2000 μsec, thus providing information about any reflected stress pulses applied to the specimen. The initiation of the

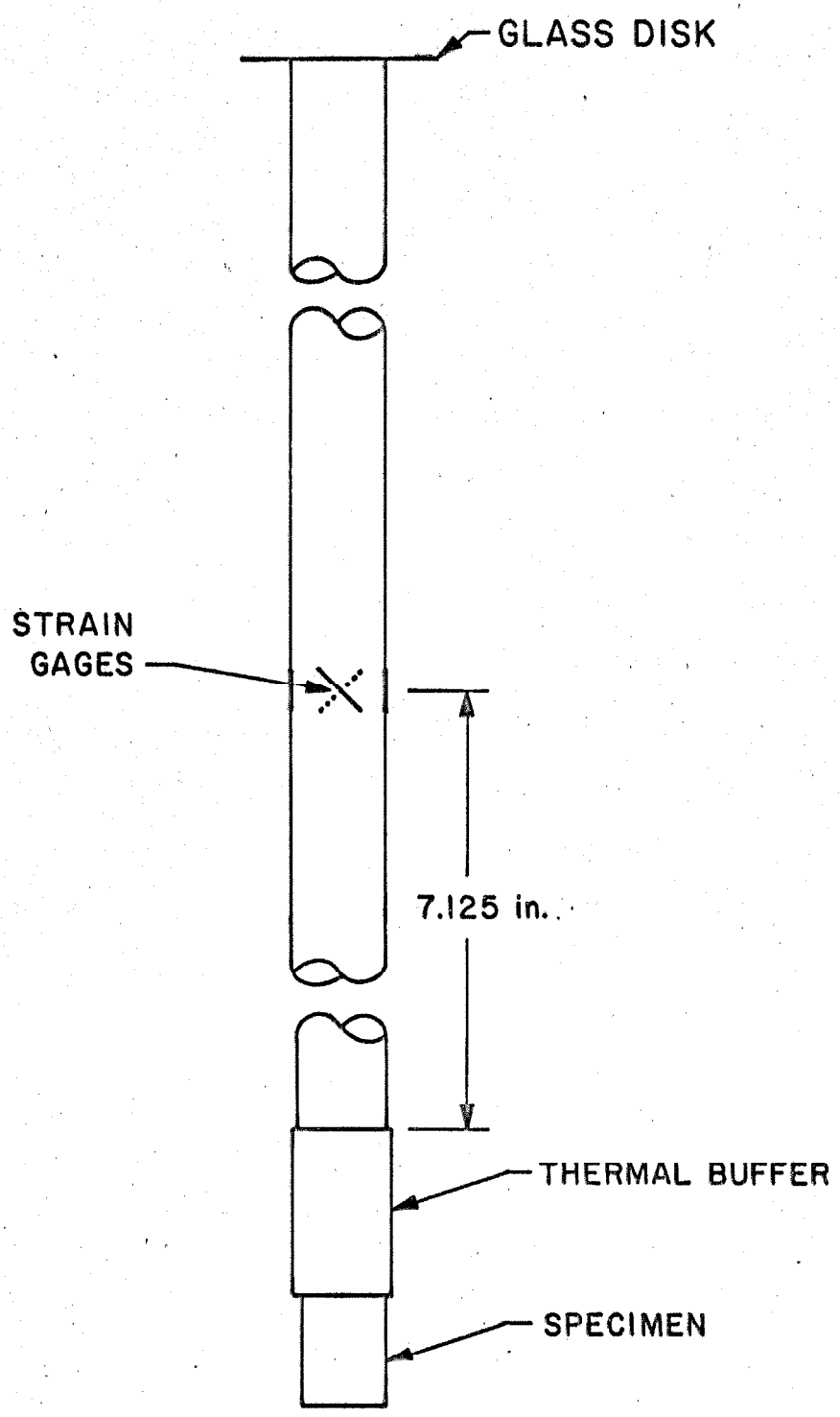

Figure 4. Lower Section of Torsion Rod.

lower trace was delayed about 116 μsec from that of the upper trace, and the trace covered a time span of 200 μsec, thus providing more detailed information about the stress pulse as detected by the strain gages. The oscilloscope screen was photographed with a Polaroid camera.

C. Scratching Apparatus

When fresh dislocations were introduced into a specimen, they were created by scratching the {100} observation surface with a diamond phonograph stylus or an alumina whisker while the specimen was in a special scratching apparatus. The scratching element was at the end of a lever arm on which a weight might be placed such that a known force was exerted by the scratching element. The specimen, attached to the thermal buffer and specimen holder, was moved slowly under the scratching element such that the scratch began at the fixed end of the specimen and ended at the free end. A photograph of a specimen, thermal buffer, and specimen holder combination in the scratching apparatus is shown in Figure 5.

D. Specimen Polishing and Etching

The chemical polish for copper employed in this investigation was reported by Livingston (24) and consisted of the following in volume per cent (acid concentration in parentheses),

20% HNO_3 (70%)
24% $HC_2H_3O_2$ (99.7%)
52% H_3PO_4 (85%)
2% HCl (38%)
2% H_2O .

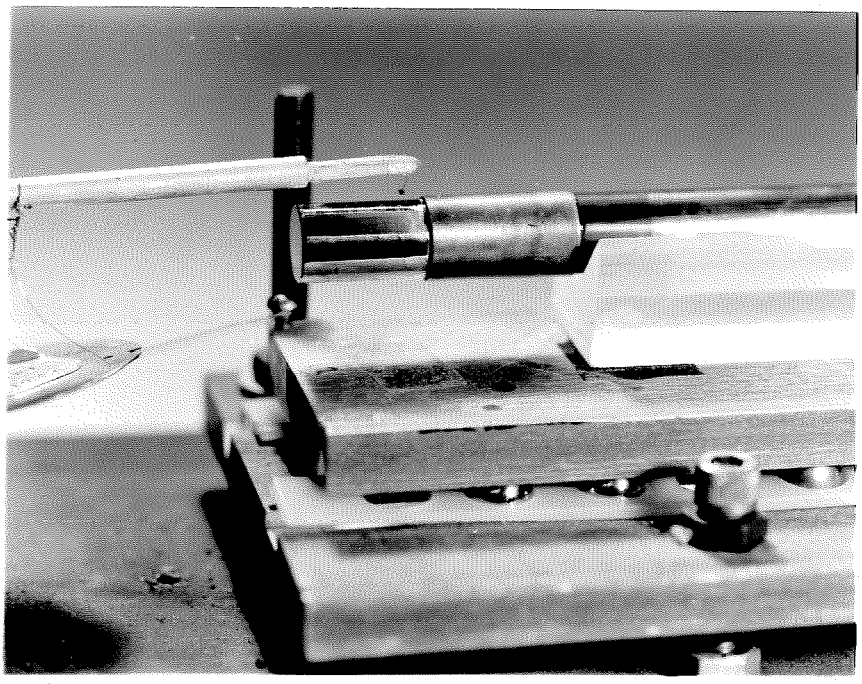

Figure 5. Specimen, Thermal Buffer, and Specimen Holder Combination in Scratching Apparatus.

The removal rate of this polish, whether a quiescent or agitated solution, was 1 to 2 μ/min.

Two etches were used to observe dislocations at the {100} observation surfaces. One etchant, designated EB1, was reported by Livingston (24) and is composed to 50 g of anhydrous ferric chloride ($FeC\ell_3$) in 100 ml of hydrobromic acid (HBr - 48 per cent). The other etchant, designated EB2, was discovered by Young (19) and contains the following concentrations of components:

$$2M \quad FeC\ell_3 \cdot 6\ H_2O$$

$$7.8M \quad HBr$$

Immersion in either etchant was followed by a rinse in hydrobromic acid. The etching or removal rate of EB1 was about twice as fast as that of EB2 as judged from the fact that an etching time of 5 sec was required to produce the same pit size with EB2, whereas 3 sec was required with EB1. The {100} observation surfaces were etched before and after the application of a stress pulse to a specimen. If the observation surfaces were scratched, they were etched after scratching and after application of a stress pulse.

E. Specimen Surface Records

A record of an as-etched surface was obtained by making a replica of the surface on cellulose acetate film with Ladd replicating solution, manufactured by Ladd Research Institute, Inc., Burlington, Vermont. After drying, the replica was peeled from the surface and mounted on a stiff Mylar sheet with Scotch Brand double-stick tape. The Mylar sheet prevented curling of the replica. After further drying for 24 h , the replica was made opaque and reflecting by vacuum

depositing aluminum on the replica surface. This process rendered the replicas suitable for examination in a metallurgical microscope.

A microscope system for comparing the "before" and "after" replicas which has been described previously (35) was used here to determine dislocation displacement.

III. PREPARATION OF TEST SPECIMENS

A. Crystal Growth

The single crystal specimens used in this investigation were machined by various methods from much larger single crystals. These parent single crystals were grown by a modified Bridgman technique according to a procedure developed by Young and Savage (36). Their technique for producing low dislocation density crystals was to employ a very smooth crucible wall and to adjust the temperature gradients such that the gradient along the crucible axis was the major one.

The procedure described in reference 36 was modified for use in this investigation, but the essential features were maintained. A graphite crucible, similar to that described in reference 36, was used to contain the initial material charge, the molten material, and the resulting single crystal.

Crucibles were machined from a block of graphite which is designated 3499 by the manufacturer, Speer Carbon Company, St. Marys, Pennsylvania. The maximum ash content of this graphite was 0.1 per cent, which was considerably greater than that for the graphite crucibles used by Young and Savage. They reported that the smoothness of the crucible wall was due to the purity of the graphite from which the crucible was machined. The walls of the crucibles, as machined, which were used in this investigation were not smooth, but an attempt was made to increase the smoothness by coating the inside of the crucibles with Dag Dispersion No. 154, a suspension of colloidal graphite in alcohol produced by Acheson Colloids Company,

Port Huron, Michigan.

The graphite crucible rested inside a Mullite tube closed at one end and with an inside diameter of 1 $\frac{1}{2}$ in. This assembly was enclosed in a Vycor tube which was connected to a vacuum system through a ground quartz joint. Induction heating of the graphite crucible was used to melt the copper charge. A copper-tube induction coil surrounding the Vycor tube and driven by an rf generator was translated along the axis of the tube to provide the moving temperature gradient. A chromel-alumel thermocouple whose bead was situated at the tip of the crucible between the Mullite tube and the crucible and whose output was read on a Leeds and Northrup chart recorder provided temperature measurement.

The procedure in crystal growth was as follows. A charge of 99.999 per cent copper rod obtained from American Smelting and Refining Company was placed in a "Dag" coated crucible. The copper rod was etched in concentrated nitric acid before placing in the crucible. The Vycor tube enclosing the crucible and Mullite tube was placed in the induction coil and connected to the vacuum system. After a vacuum of 1×10^{-5} mm Hg was reached, the power to the induction coil was increased from zero such that the pressure in the system, as measured at the port of the vacuum system, never exceeded 5×10^{-4} mm Hg. The initial position of the induction coil was such that the center of the coil was at the tip of the crucible. Heating and melting of the charge took place while the coil was in this position. After the thermocouple had indicated a temperature of 2200 to 2300°F for about 1$\frac{1}{2}$ h , the coil raising mechanism was started; and the coil

moved at 1.2 in/h . The coil continued moving until the bottom of the coil passed the plane of the end of the crystal, at which time the coil raising mechanism was stopped and the power to the coil was gradually lowered. When cooling was complete, the system was vented to atmosphere and disassembled; and the crystal was carefully withdrawn from the crucible. The crystal was etched in concentrated nitric acid to determine if more than one grain had nucleated. The crystals were usually about 5 in. long. They seemed to have a preferred growth direction of <110> .

About one-half of the test specimens in this investigation were machined from crystals obtained from the Sandia Corporation, Albuquerque, New Mexico. These crystals were grown in essentially the same manner as above, except that the environment was one atmosphere of helium.

B. Spark and Acid Machining

Major shaping operations to obtain the desired shape and orientation of specimens were performed in spark erosion machines, the Servomet spark-erosion machine, Model C, manufactured by Metals Research, Ltd., Cambridge, England, and the Agietron spark-erosion machine, type AB, manufactured by AG. für industrielle Elektronik, Locarno, Switzerland.

For future reference, some of the energy ranges and associated capacitances in the discharge circuit are given below for the Servomet and Agietron machines. (The number of energy ranges on the Agietron machine has been augmented from those existing on the production machine.)

SERVOMET

Range	Capacitance (μF)	
4	.5	↑ increasing energy and damage to crystals
5	.25	
6	.05	
7	.01	

AGIETRON

Range	Capacitance (μF)	
3	.1	
2	.03	↑ increasing energy and damage to crystals
1	.01	
C	.005	
B	.002	
A	.0004	

In order to determine the crystallographic orientation of the crystal relative to its cylindrical axis, the tip of the crystal was cut off perpendicular to the axis. This operation was performed by a traveling wire electrode attachment in the Servomet machine operated on range 6. The surface of the crystal thus exposed was etched in concentrated nitric acid (to remove spark machining damage), and a Laue back-reflection x-ray photograph of that surface was taken while the crystal was in a V-shaped cradle which was interchangeable between an x-ray machine track and the Servomet machine. The crystallographic orientation of the crystal was determined from the Laue photograph, and the crystal was cut along {100} planes with the wire attachment to the Servomet machine operated on range 4 or 6.

The crystal was thus sliced into <100> oriented segments 15 to 20 mm long. A given segment was then mounted on a large goniometer

which was interchangeable between an x-ray machine track, the Servomet machine, and the Agietron machine. A photograph of a typical segment mounted on the goniometer, which is on the adapter fixture to the x-ray machine, is shown in Figure 6. With the aid of the goniometer and a rotating electrode in the Servomet (a so-called planing wheel), a wire-cut surface on a crystal segment could be planed flat and parallel to a {100} surface within 1°.

The next operation in specimen preparation from these oriented segments was the machining of a right circular cylinder whose axis was <100>. This was accomplished by using a thin-walled tube of copper, brass, or more commonly, copper-tungsten alloy as the electrode in either spark machine and "trepanning" with the electrode perpendicular to the {100} surface. The energy range used was 6 in the Servomet machine, C on the Agietron machine. A photograph of the trepanning operation in the Agietron machine is shown in Figure 7. The diameter of the resulting cylinder was approximately 0.525 in.

The rough specimen was then reduced in diameter on a chemical or acid lathe of a design similar to that reported in reference 37. The essential features were a rotating, cloth-covered Lucite wheel which carried the solution to the specimen and a specimen-rotating drive whose axis was accurately parallel to that of the latheing or acid wheel. The specimen was placed at the end of a lever so that contact with the acid wheel and consequent damage could be controlled. A short piece of 3/8 in. copper rod whose ends were parallel was attached to the spark-planed {100} end surface with Duco cement. The 3/8 in. copper rod facilitated attachment to the specimen drive. A

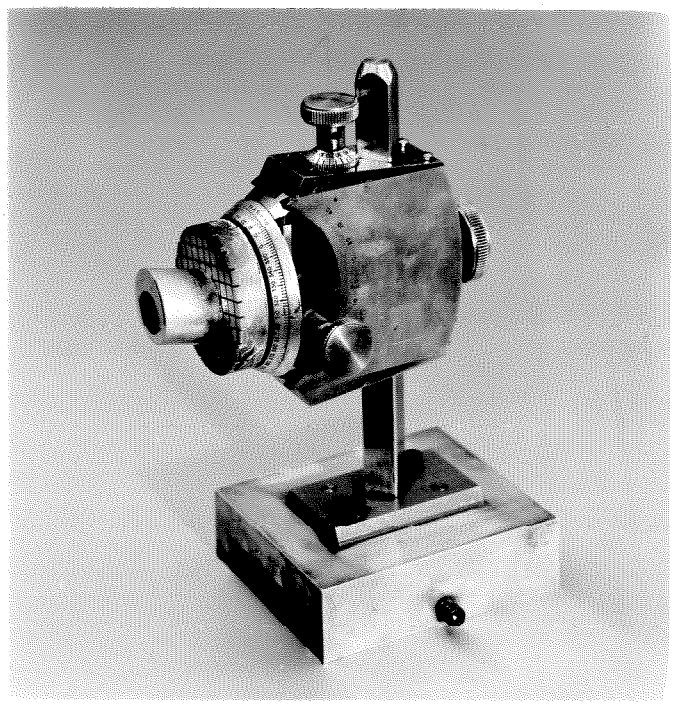

Figure 6. Crystal Segment on Goniometer in X-Ray Fixture.

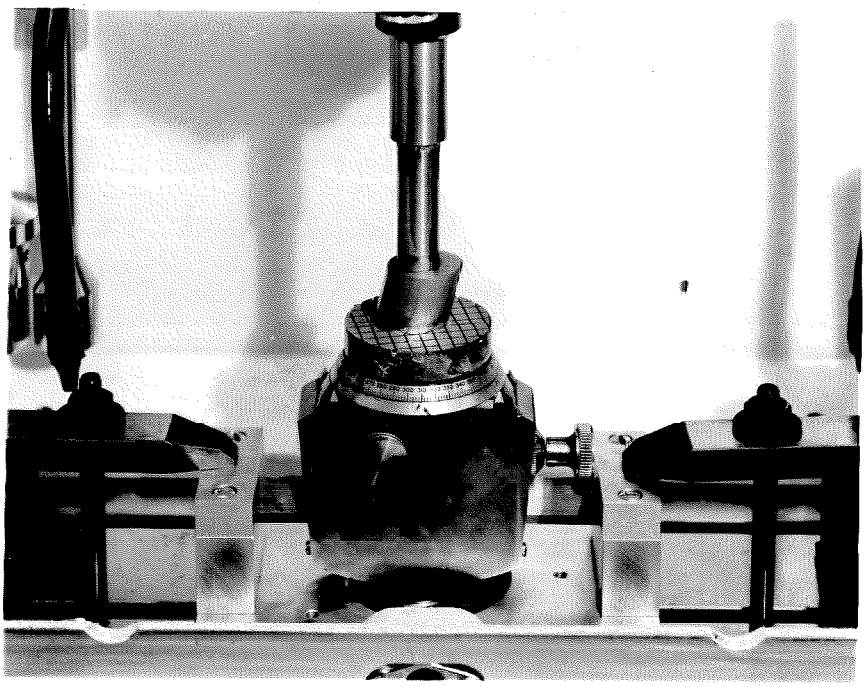

Figure 7. Trepanning Operation in Agietron Machine.

solution of 50 per cent (by volume) concentrated nitric acid and 50 per cent water was first employed, but a saturated solution of cupric chloride in concentrated hydrochloric acid proved more reliable and facilitated a subsequent orientation procedure by producing etched bands at the {100} surfaces on the cylindrical surface. A photograph of a typical specimen being reduced in diameter in the acid lathe is shown in Figure 8. The result of the acid latheing operation was a right circular cylinder with a diameter 0.495 to 0.490 in., an axis accurately <100>, one end accurately {100}, and the other end within 4° of {100}.

In order to increase the size of the {100} observation area, it was decided to machine narrow flats at the {100} planes on the cylindrical surface of the specimens. These flats were, on the average, about 3 mm wide and extended the length of the specimen. For a specimen with a diameter of 0.49 in. or 12.45 mm, the reduction in diameter at the flats was 3 per cent. The variation of resolved shear stress across the flats was, therefore, judged to be negligible.

To align the specimen such that these flats might be machined, the specimen was first polished and etched to produce square pits on the {100} end surfaces. The edges of these square pits were <100>. A stainless steel block with accurately perpendicular faces was aligned with the cross-hairs of an eyepiece in a metallurgical microscope. The accurate {100} end of the specimen was attached to the steel block with Duco cement, at the same time aligning the edges of the square pits on the inaccurate {100} specimen end with the eyepiece cross-hairs and, consequently, with the edges of the steel block.

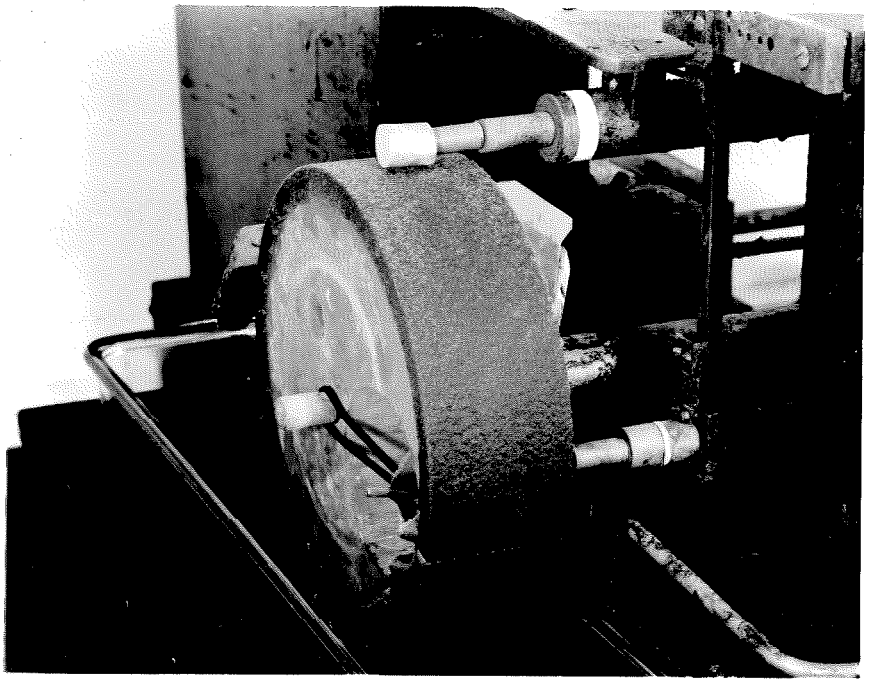

Figure 8. Typical Specimen in Acid Lathe.

Using the steel block as a holder and alignment fixture for the specimen, the flats were then spark planed in the Servomet machine on range 7. Attempts at acid or chemical planing of the flats were not successful because the chemicals used degraded the Duco cement bond to the extent that it failed, causing the crystal to drop off. Subsequent to this writing, chemical planing of the flats has become possible. The surfaces produced by spark planing of the flats were within 2^{o} of {100}. The other end of the specimen was then spark planed accurately to {100} on ranges 6 and 7 of the Servomet machine. The resulting specimen had accurately parallel {100} ends, flats at the {100} observation surfaces, and approximately the proper diameter for acoustic impedance matching in the torsion testing machine.

C. Annealing

After specimens were demounted from the stainless steel blocks and polished for about 30 min in the chemical polish to remove some spark-machining damage, they were placed on graphite in a tube furnace through which dry hydrogen was passed. Specimens were annealed in this fashion at 1020 - 1040^{o}C for about 100 h. Dislocation densities in the annealed specimens were not markedly decreased by a slow, controlled cooling rate from the annealing temperature (about 55^{o}C/h) so the normal furnace cooling rate was finally used. The maximum cooling rate for this tube furnace was about 72^{o}C/h.

Annealed specimens were kept in a dessicator until they were to be tested. This procedure avoided contamination of the observation surfaces.

IV. EXPERIMENTAL PROCEDURE

The sequence of operations in testing a given specimen was as follows. First, a thermal buffer was aligned and attached to a specimen holder with Eastman 910 adhesive. Next, the specimen was attached to the thermal buffer, also with Eastman 910. This last operation required some precaution. The alignment could not be accomplished in the customary V-block because of potential damage to the specimen and contamination of the observation surfaces. The method finally employed was to place the specimen on end on polyurethane foam and to bring the thermal buffer and specimen holder down gently on the specimen, aligning it by eye. After some practice, this could be done with sufficient accuracy, the misalignment of axes being less than 0.003 in. The flats at the {100} observation surfaces were then identified by letters a, b, c, d written on the thermal buffer. The thermal buffer was coated with Duco cement to prevent any contamination of the polishing and etching solutions used on the specimen.

Next, the specimen was chemically polished for 8 to 10 min, rinsed in distilled water, etched in either EB1 or EB2 etchants, and rinsed in hydrobromic acid and distilled water. Unless a specimen were to have fresh dislocations produced at the observation surfaces, that is, scratched, the etched surface produced in the above procedure was replicated as described previously. This replica was the "before" replica. If, as in the case of the first two specimens tested, the specimen were to be scratched, the first etch was removed by polishing for 8 to 10 min. Then the observation surfaces were scratched, the scratch running almost parallel to the <100> direction. The specimen

was polished for about 10 sec, etched in EB1 and rinsed in hydrobromic acid and water; and the {100} observation surfaces were replicated as described previously.

Next, the torsion machine was assembled and the static torque applied. All adhesive bonds in the torsion machine of a temporary nature were made with Eastman 910 adhesive. The torsion machine was completely ready to operate before the specimen holder- thermal buffer - specimen combination was attached to it. Immediately after the torsion pulse was applied, the specimen holder was removed from the load train by depolymerizing the Eastman 910 adhesive with heat from a propane torch. No heating of even the thermal buffer could be detected in this process, and the taper end of the specimen holder was quickly cooled in water.

Immediately after testing, the specimen was rinsed in distilled water, chemically polished for about 10 sec, etched in solutions EB1 or EB2, and rinsed in hydrobromic acid and distilled water. It should be noted that a ten-second chemical polish was not performed to remove material but to prepare the {100} surfaces so that the etchant did not produce general faceting and obscuring of the dislocation etch pits. After the above etching, the observation surfaces were replicated. This was the "after" replica. In case general faceting did occur upon etching, the specimen was chemically polished to remove that etch pattern and then re-etched and replicated. This latter procedure precluded use of the double etch technique of discerning dislocation displacement; however, dislocation movement could be determined from the 'before' and 'after' replicas with the aid of the comparison micro-

scope. Techniques and procedures in the acquisition of stress and dislocation displacement data are explained in the next section of this thesis.

Four such tests were performed with nominal resolved shear stresses ranging from 25 to 250 g/mm^2. A different annealed crystal was used in each test.

V. EXPERIMENTAL RESULTS

A. Specimen Substructure

There was a wide variation in dislocation substructure among the specimens examined in this study. The type of substructure of a specimen seems to be correlated with the crystal from which a specimen was machined. Specimens were from two parent crystals: crystal 3, obtained from Sandia Corporation; and crystal 6, grown as described in Section III of this thesis. The first digit of a specimen number is the number of the parent crystal.

The variation in dislocation substructure may be seen by comparing the photomicrographs of Figures 9 and 10. Figure 9 exhibits the dislocation etch pit configuration typical of specimens derived from crystal 3; and Figure 10, the configration typical of specimens derived from crystal 6. Large, very low dislocation density subgrains with high density subboundaries could be obtained after spark machining and annealing specimens from crystal 3, whereas specimens from crystal 6 had a much higher average dislocation density with no or low density subboundaries. While the motion of fresh dislocations from a scratch was studied in the low dislocation density crystal 3 specimens, only the motion of aged dislocations was studied in crystal 6 specimens because the introduction of fresh dislocations would have increased the density to the point that the dislocation displacements could not be determined with any certainty. There was found to be no significant difference between the motion of fresh and aged dislocations.

It would seem that the higher dislocation density in crystal 6

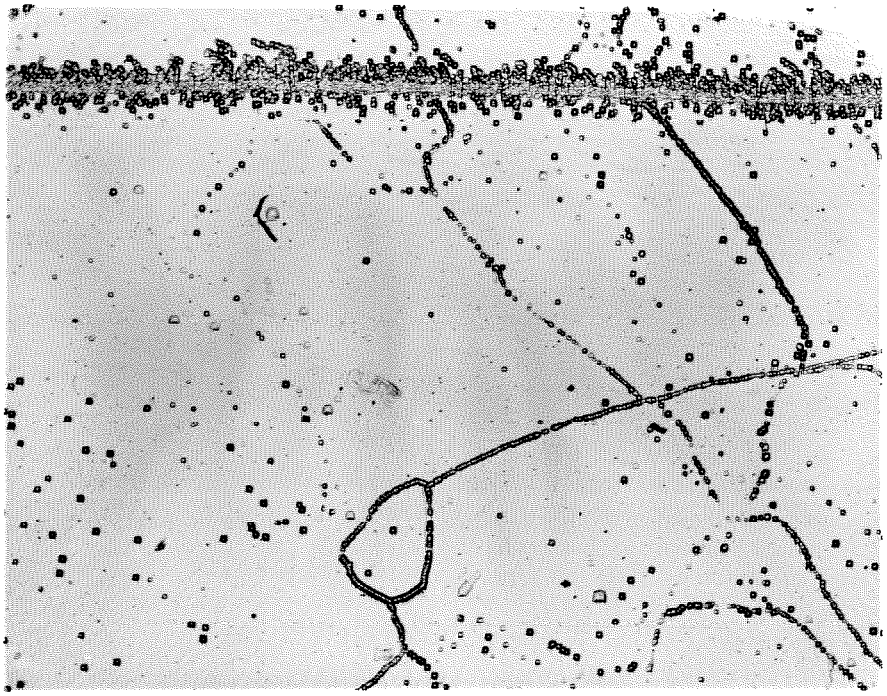

Figure 9. As Annealed and Scratched Dislocation Configuration, Typical of Specimens from Crystal 3. 100X.

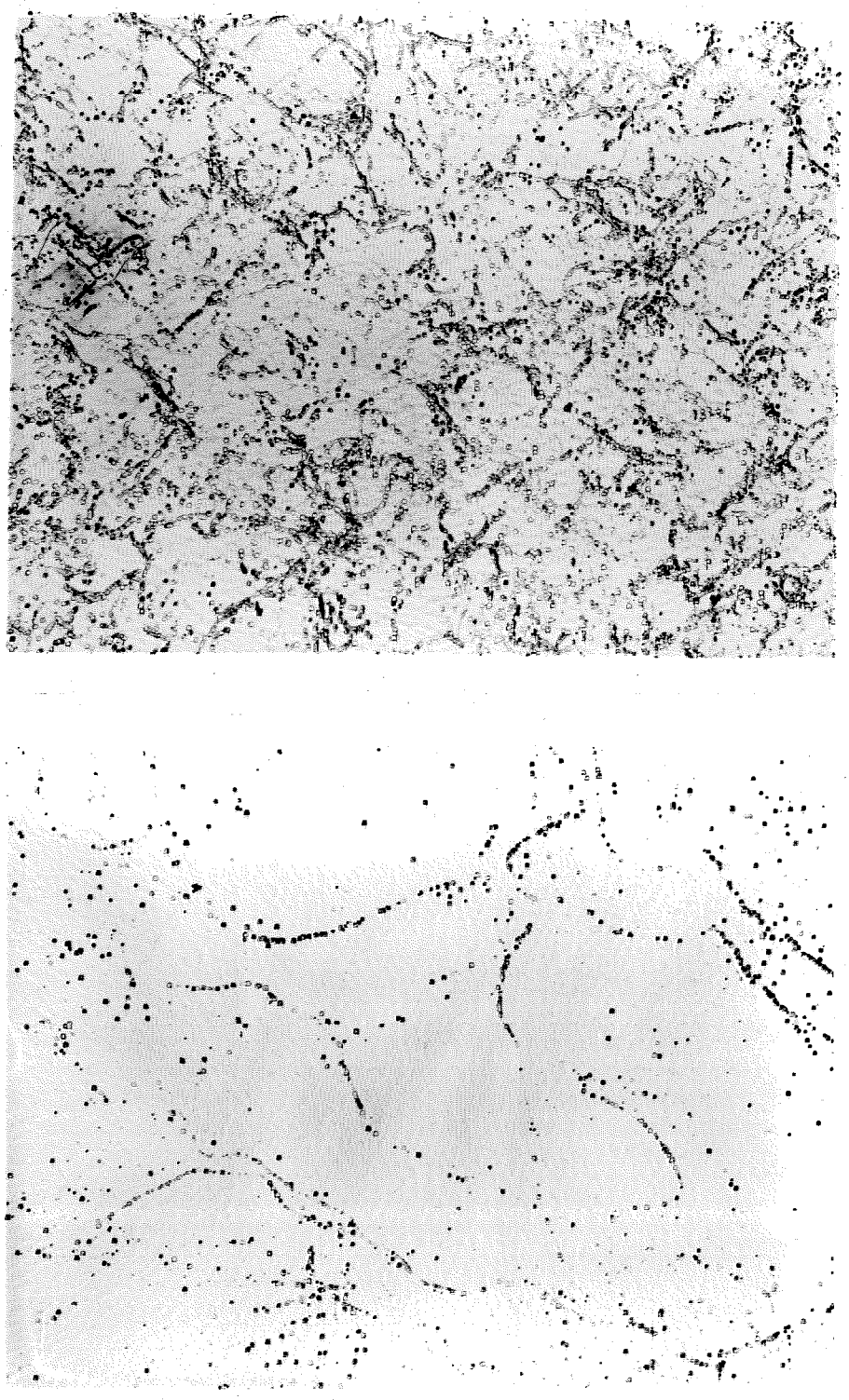

a

b

Figure 10. As Annealed Dislocation Configurations, Typical of Specimens from Crystal 6. 100X.

specimens is caused by spark machining. It is theorized that in crystals like number 3, the stable substructure is grown into the crystal and that this substructure limits motion and multiplication of the dislocations produced by spark machining. In crystals such as number 6, it is thought that the initial dislocation density is low with little or unstable substructure. Therefore, in these crystals, dislocations produced in the spark machining processes move large distances and multiply many times.

A further example of spark machining damage in copper single crystals is shown in the photomicrograph of Figure 11, which exhibits an etched observation surface of specimen 3-2-1 after annealing and scratching (the scratch damage extends across the top of the photomicrograph). The right edge of the photograph coincides with a spark-planed end of the specimen. This end, a (100) surface, was spark planed using ranges 6 and 7 in the Servomet machine. Spark machining damage extends some distance, approximately 450 μ, into the crystal after removal of about 50 μ by chemical polishing and after annealing. Gniewek, et al. (38) have investigated spark machining damage in copper due to spark planing on surfaces perpendicular to {111} planes. This is the first study of dislocation motion in copper where spark machining was the predominant means of shaping specimens, for Young (20, 22, 23) and Petroff (25) used chemical machining.

B. Stress Pulse Analysis

Several features of the torsion machine records need to be explained before proceeding to calculations which yield the maximum applied, resolved shear stress, and the shape of the stress pulse for

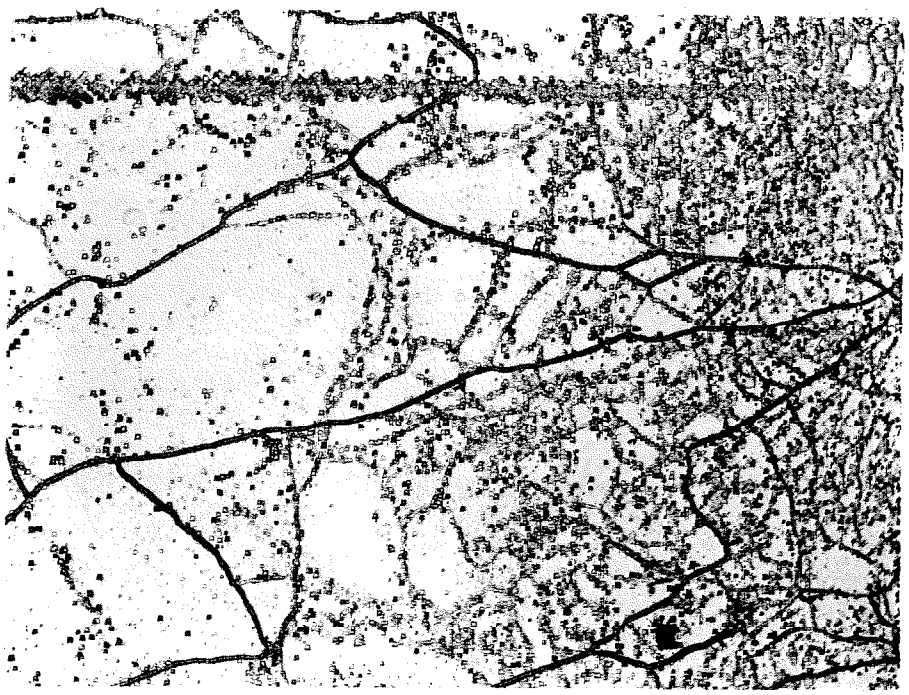

Figure 11. As Annealed and Scratched Dislocation Configuration, Exhibiting Spark Machining Damage. 100X.

each test. A typical torsion machine record is shown in Figure 12. This particular photograph is the record of the test on specimen 6-2-1, where the resolved shear stress was calculated to be 236 g/mm^2, the highest stress applied. Attention is called to several features of the lower trace. The rise time of the pulse is about 2 μsec. At about 60 μsec later on the trace there is a dip which shows the effect of an imperfectly matched taper joint where the specimen holder connects to the lower section of the torsion rod. Only one specimen holder was accurately fitted to the taper joint by lapping. When that specimen holder was used in the torsion machine, no dip was observed in the trace of the stress pulse. The effect of the imperfectly matched taper joint is not great since the stress rises to the value which it had before the wave encountered the taper joint. At about 110 μsec on the lower trace there is a slight dip due to the stress wave encountering the specimen holder - thermal buffer interface and diameter change.

The end of the pulse detected by the strain gages shows the effect of the specimen. If the acoustic impedance of the thermal buffer and the specimen were equal and if the specimen remained elastic upon application of the stress pulse, the trace would remain at that level which it had before the wave encountered the specimen and then would fall to zero in 2 μsec. In this particular case the diameter of the specimen was 0.491 in., less than the ideal 0.493 in. This decreased diameter should have caused only about 1 per cent decrease in the signal if the specimen had remained elastic. In addition, if the specimen had remained elastic, the signal would have fallen to the de-

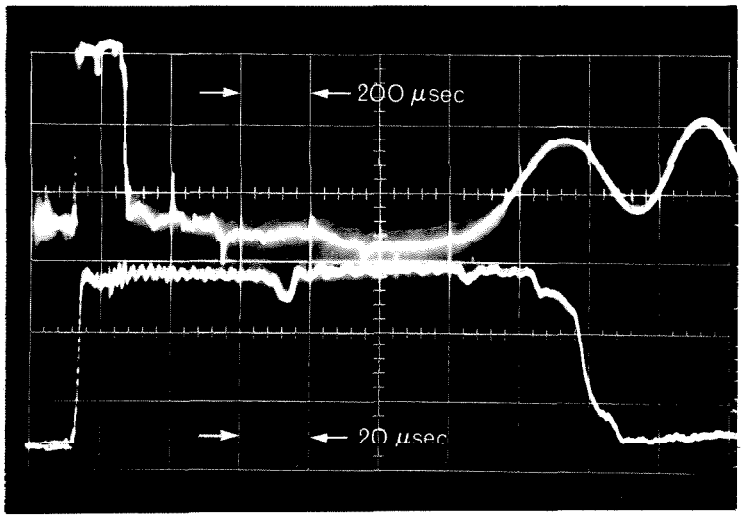

Figure 12. Typical Torsion Machine Record.

creased value, remained at that value for about 10 μsec, and then decreased in about 2 μsec to the zero level of the signal. Evidence of plastic flow in the specimen is seen in two features of the trace; the greater than calculated decrease of the signal when the pulse traversed the specimen (12 per cent), and the long decay time of the pulse. This trailing edge of the trace will be examined in greater detail in connection with the analysis of the applied stress.

The two pulses occurring at the end of the upper trace are caused by reflection of the stress wave from the damping section of the load train. The incomplete attenuation which causes these reflections is due to the fact that the composition of the Solithane viscoelastic material did not provide complete attenuation of the pulse traveling away from the specimen. That such long rise-time pulses cause a negligible increase to the resolved shear stress in the specimen can be seen by the following argument. If the rise time of a stress pulse is sufficiently long, it can be visualized that the stress in a short specimen might never reach the maximum stress of the pulse because the unloading stress wave propagating from the free end begins to decrease the stress before the maximum stress is reached. It can be shown that

$$\frac{\tau'}{\tau} = \frac{(A'/A)(2z/V_{cu})}{t'_{rise}} \qquad [12]$$

where

τ = maximum stress produced by a pulse,

A = amplitude of a pulse,

z = axial distance from the free end of the specimen,

t'_{rise} = rise time of a reflected pulse,

and the prime superscripts refer to a stress wave reflected from the damping section of the load train. Calculated in this manner, the maximum stress applied to the specimen by the reflected pulse was only about 3 per cent of the stress applied by the trapezoidal-shaped pulse and, therefore, was deemed negligible.

The analysis of the stress pulse requires further explanation before proceeding to the tabulation of the results of this investigation. First, a general analysis of the stresses transmitted by torsional waves in circular cross-section rods across interfaces between different diameters and materials will be presented. The boundary conditions at an interface, in this case between the thermal buffer and the specimen, are that the torque, T, and the angular velocity, $\dot{\theta}$, be continuous.

$$\begin{aligned} T_{tb} &= T_{cu} \\ \dot{\theta}_{tb} &= \dot{\theta}_{cu} \end{aligned} \qquad [13]$$

where the subscripts tb and cu again refer to the thermal buffer and the specimen, respectively. Then the assumption is made that the torsion shear stress distribution and its dependence on applied torque which has been derived for the static case is true for the dynamic case, i.e.,

$$\tau = Tr/J \qquad [14]$$

where

τ = torsion shear stress,

r = radial position of an elemental volume in the rod,

J = polar moment of the cross section = $\pi d^4/32$.

Then the boundary conditions in Equations 13 evaluated at the lateral surface of the thermal buffer or specimen become

$$\left(\frac{\tau J}{a}\right)_{tb} = \left(\frac{\tau J}{a}\right)_{cu} \qquad [15]$$

and

$$v_{tb} = \frac{a_{tb}}{a_{cu}} v_{cu} ,$$

where a is the radius of a cross section, v is the linear velocity of an elemental volume at the periphery of the cross section, and

$$v = a\dot{\theta} \quad . \qquad [16]$$

In addition, from equating the impulse applied to an elemental volume to its increased momentum,

$$\Delta\tau = \rho V \Delta v \qquad [17]$$

where $\Delta\tau$ is the change in stress across the wave front, ρ is the material density, V is the torsional wave velocity, and Δv is the change in linear velocity of an elemental volume due to passage of the wave front. Figure 13 shows a typical position - time diagram which is helpful in visualizing the stresses applied to the specimen and which defines the numeral subscripts in the equations to follow.

From Equations 15 and 17 the following relations may be derived:

$$\Delta\tau_2 = \Delta\tau_1 \left\{ \frac{\left[1 - \frac{(\rho VJ)_{tb}}{(\rho VJ)_{cu}}\right]}{\left[1 + \frac{(\rho VJ)_{tb}}{(\rho VJ)_{cu}}\right]} \right\} \quad . \qquad [18]$$

However, the product ρVJ may be seen to be the acoustic impedance for torsional waves, Z . Therefore, Equation 18 becomes

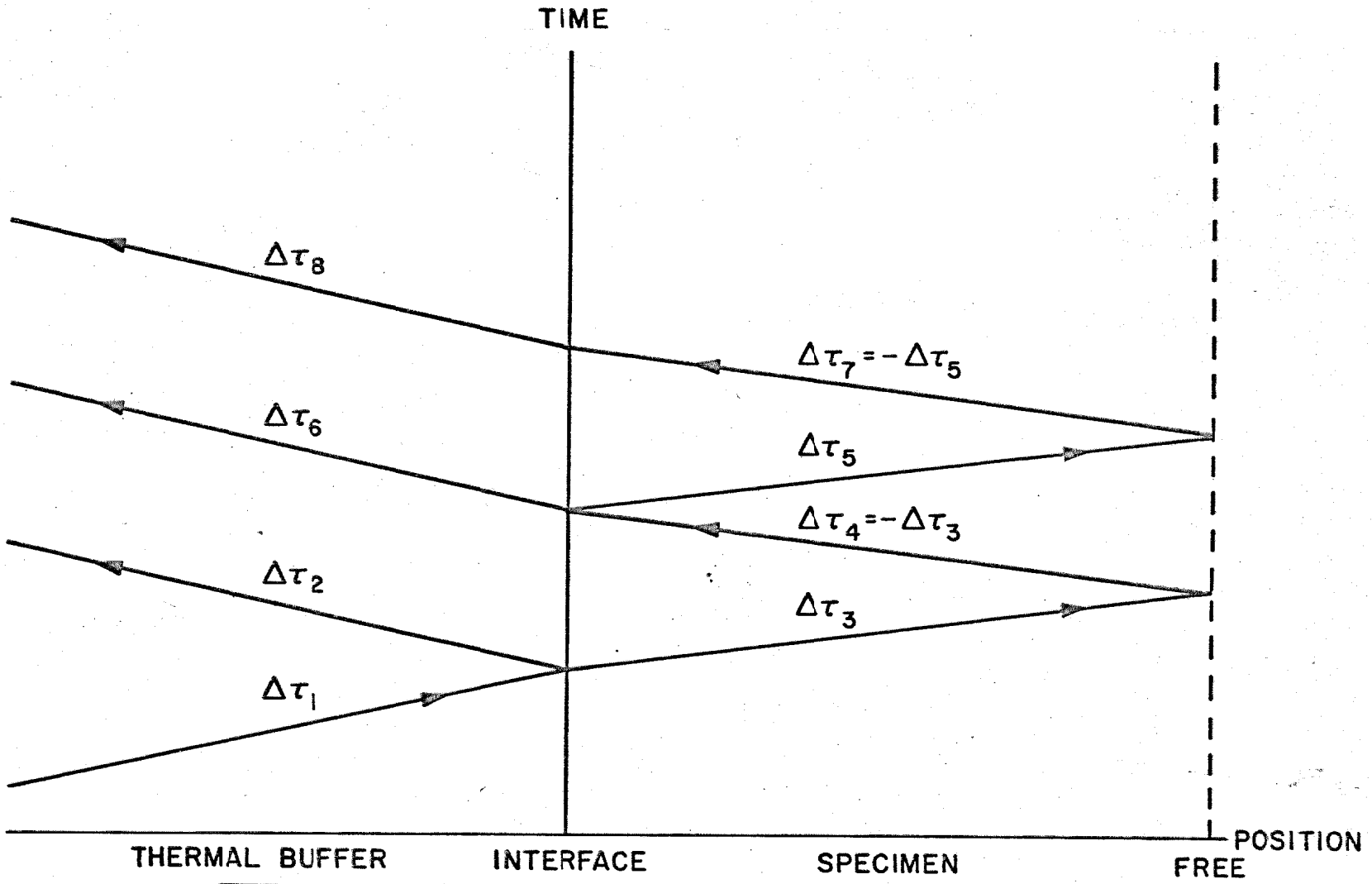

Figure 13. Position-Time Diagram for Torsion Waves in Thermal Buffer and Specimen.

$$\Delta\tau_2 = \Delta\tau_1 \left[\frac{(1 - Z_{tb}/Z_{cu})}{(1 + Z_{tb}/Z_{cu})} \right] \qquad [19]$$

and

$$\Delta\tau_3 = \Delta\tau_1 \left[\frac{2(d_{tb}/d_{cu})^3}{1 + Z_{tb}/Z_{cu}} \right] \qquad [20]$$

$$\Delta\tau_5 = -\Delta\tau_1 \left[\frac{2(d_{tb}/d_{cu})^3}{1 + Z_{tb}/Z_{cu}} \right] \left[\frac{(1 - Z_{cu}/Z_{tb})}{(1 + Z_{cu}/Z_{tb})} \right] \qquad [21]$$

$$\Delta\tau_6 = -\Delta\tau_1 \left[\frac{4}{(1 + Z_{tb}/Z_{cu})(1 + Z_{cu}/Z_{tb})} \right] \qquad [22]$$

It may seem that making the acoustic impedance Z continuous across an interface, as was done in Section II, is equivalent to requiring that $\Delta\tau_2 = 0$ (no stress reflected at the interface) and to deriving $\Delta\tau_3$ by matching torque at the interface since $Z_{tb}/Z_{cu} = 1$, thus making $\Delta\tau_3 = \Delta\tau_1 (d_{tb}/d_{cu})^3$.

The source of $\Delta\tau_1$ in the thermal buffer was the torsion stress pulse created in the steel torsion rod. The torsion stress in the steel rod was calculated from Equation 14 where $r = d/2$ and T, the torque, was one-half of the static torque applied to the rod, which was, in turn, equal to the product of the radius of the cranking disc and the weight hung on it. The stress in the steel rod was translated into $\Delta\tau_1$ in the thermal buffer by means of Equation 20.

The end of the stress pulse as detected by the strain gages shows the effect of the specimen. More specifically, the end of the pulse reveals the form of the stress pulse at the thermal buffer - specimen interface because there is no distortion of the pulse between that interface and the location of the strain gages, everything being

elastic. However, there is some plastic flow in the specimen, even apparently at the lowest stresses, and the stress pulse is thereby distorted. Considering this distortion, the only point on the specimen where the form of the stress pulse is known with any degree of accuracy is at the thermal buffer - specimen interface (aside from the free end). With the above considerations in mind, it was decided to analyze the data in the following manner. The stress pulse at the interface, on the fixed end of the specimen, was determined for each test from enlargements of the torsion machine records (cf. Figure 12). Graphs of the pulses are shown in Figures 14 through 17.

These pulses were analyzed in the following manner. The area under a given curve, the impulse, was determined with a planimeter. From the torsion machine record it was determined that the rise time of the pulse was either 2 or 3 μsec. Then a trapezoidal-shaped pulse was formed from the impulse of the actual pulse. The height, duration of the plateau, and decay time of the trapezoidal pulse were apportioned so as to conform as closely as possible to the shape of the original pulse. These trapezoidal-shaped pulses are shown by dashed lines in the Figures 14 through 17. The impulse contributed by any secondary lobes or pulses was less than 10 per cent of that of the original pulse and was not included in calculating the shape of the trapezoidal pulse.

If the specimens had remained elastic, the stresses $\Delta\tau_3$, etc., could have been calculated from Equations 19 through 22. The ratio of the decrease in the strain gage signal as the pulse encounters the thermal buffer - specimen interface to the prior signal level is equal to

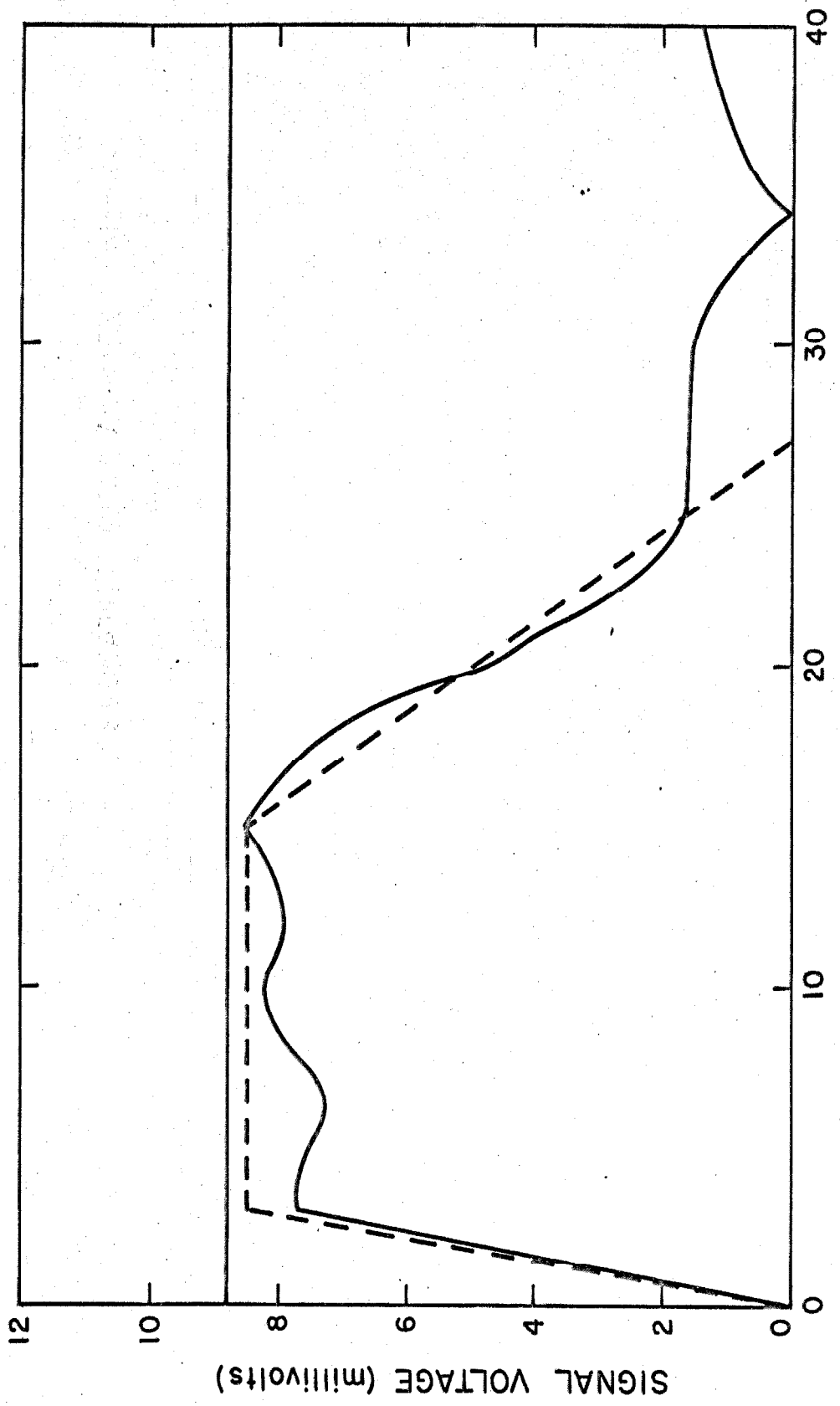

Figure 14. Stress Pulse at Fixed End of Specimen 6-3-1.

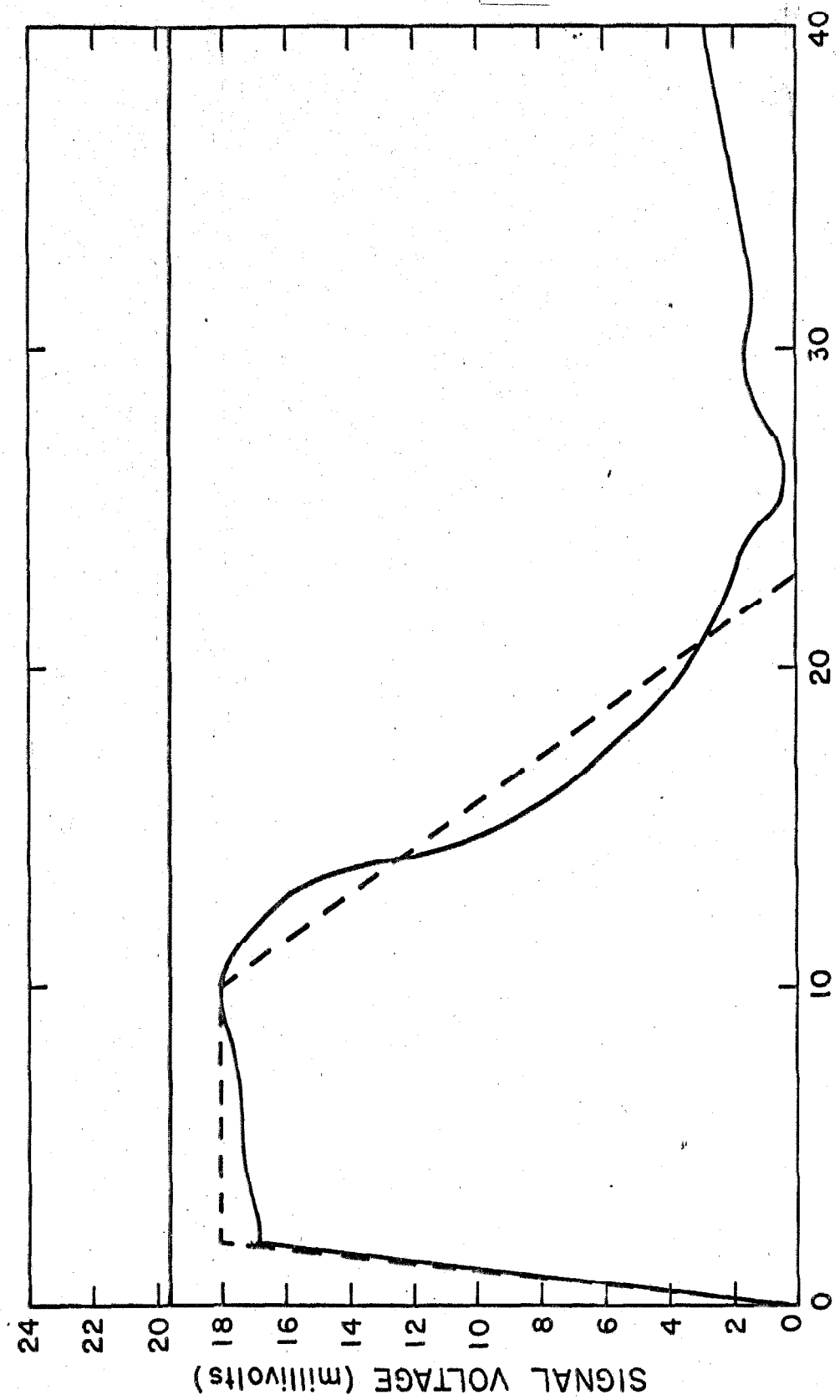

Figure 15. Stress Pulse at Fixed End of Specimen 3-2-1.

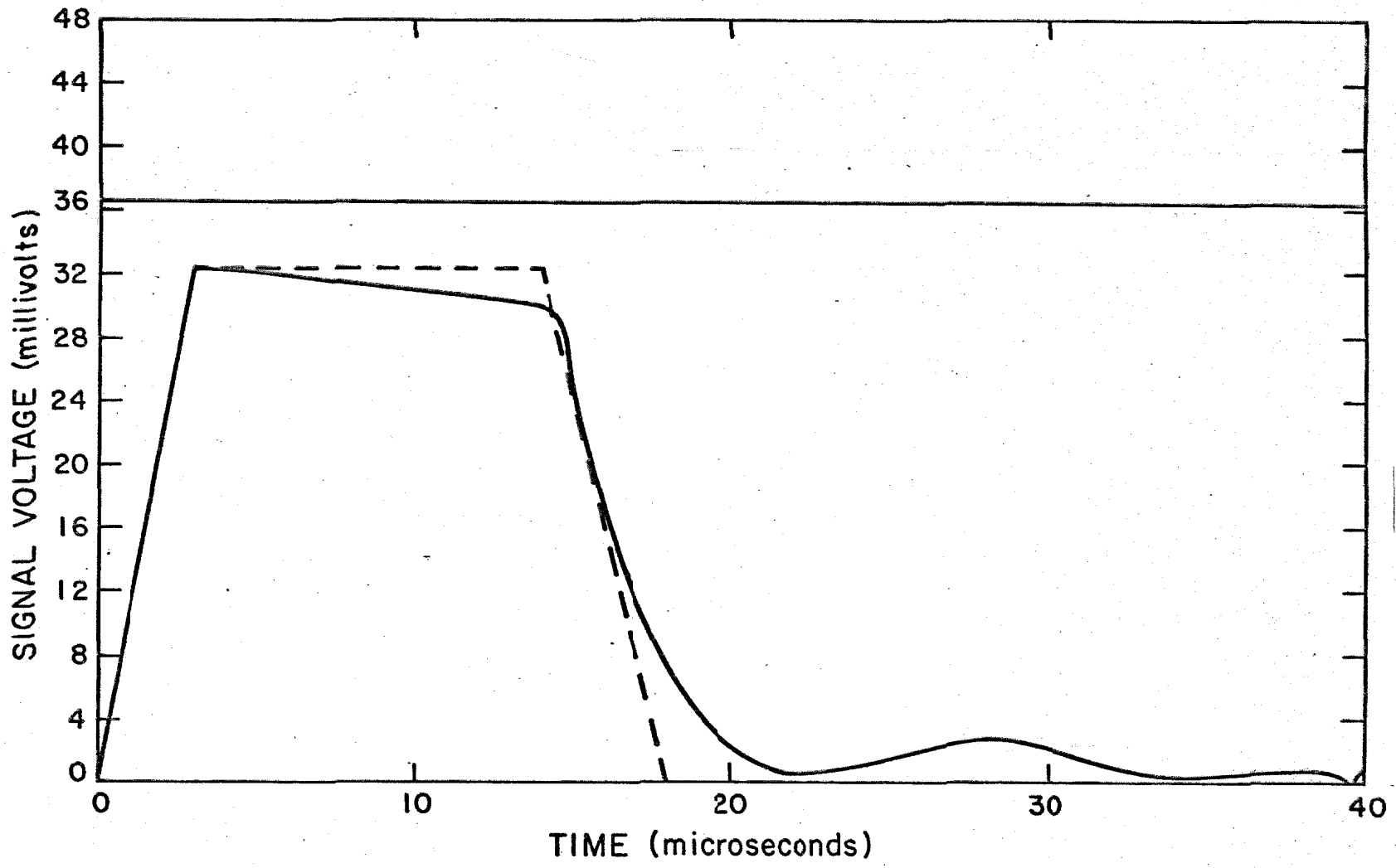

Figure 16. Stress Pulse at Fixed End of Specimen 3-3-1.

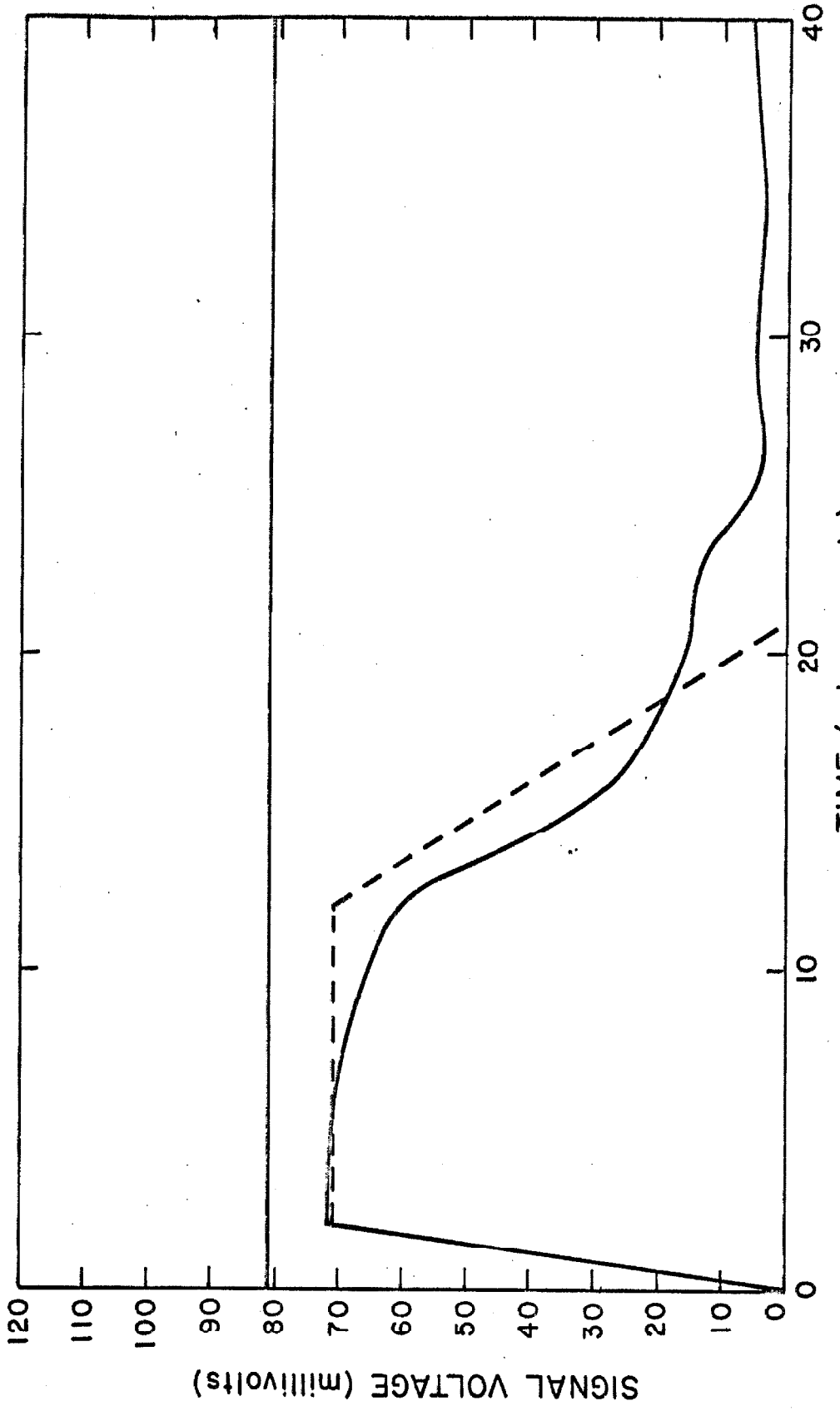

Figure 17. Stress Pulse at Fixed End of Specimen 6-2-1.

ratio $\Delta\tau_2/\Delta\tau_1$. If this ratio is calculated from Equation 19, assuming that the specimen remained elastic, the signal decrease is less than actually occurred. Therefore, the ratio of the signal decrease to the prior signal level was determined and used in calculating stresses in the specimen. This procedure is tantamount to determining the effective acoustic impedance of the specimen. The solid lines extending across the top of the graphs in Figures 14 through 17, for example at 8.8 mV in Figure 14, represent the signal level due to the stress pulse in the thermal buffer and the signal level which would have been obtained if the acoustic impedance had been continuous across the thermal buffer - specimen interface and/or plastic flow had not occurred in the specimen. The decrease of the signal from this level represents the stress $\Delta\tau_2$ reflecting from the interface.

The incident stress $\Delta\tau_1$ is considered decreased by the ratio of the signals after and before the pulse encounters the interface. This decreased $\Delta\tau_1$ is then used in calculating $\Delta\tau_3$, the stress in the specimen, by means of assuming the torque is equal across the thermal buffer - specimen interface. In resolving the stress on to the {111} <110> slip system, $\Delta\tau_3$ is decreased by a factor $1/\sqrt{6}$. The resolved shear stresses, τ_{max}, for each test corresponding to the plateau of the trapezoidal-shaped pulse are given in Table 1.

C. Etching Observations

Several features of the results using the {100} dislocation etchants require some explanation since this is the first study to employ them. In addition, since there is a wide variation in the features of the etched {100} surfaces of the specimens tested, the photomicro-

graphs of these surfaces in Figures 18 through 21 need to be explained. These photomicrographs display the dislocation configurations before and after the application of a torsion stress pulse. The "a" part of a figure refers to the configuration before testing; the "b" part, to the configuration after testing. In each micrograph the [100] specimen axis is horizontal, and the free end of the specimen is toward the right. The dislocation etch pits have a crystallographic shape, i.e., the edges are along <100> directions and the sides are {110} planes. The <110> slip directions are, therefore, along the diagonals of the square etch pits and at about 45° to the edges of the photographs.

Among these photomicrographs there is a variation in the clarity with which etch pits reveal the dislocation configuration. This variation is due to a problem with re-etching specimens after the application of the stress pulse. The only explanation of the problem which can be advanced is that some contaminant came in contact with the {100} surfaces of the crystal at some time between the before and and after etching. The contaminant altered the chemical reaction of the etchant to the surface sufficiently that the dislocation etch pits were less well-defined in relation to the general background. The ten-second chemical polish after testing was not effective in removing the contaminant. The only exception to the above remarks was that specimen 3-3-1 (Figure 20) re-etched well, and the clarity of the pits gave an excellent indication of the dislocation configuration.

The dislocation configuration in specimen 6-3-1, as observed on flat a , is shown in Figure 18. These photographs were taken at a point on the specimen where z , the axial distance from the free end

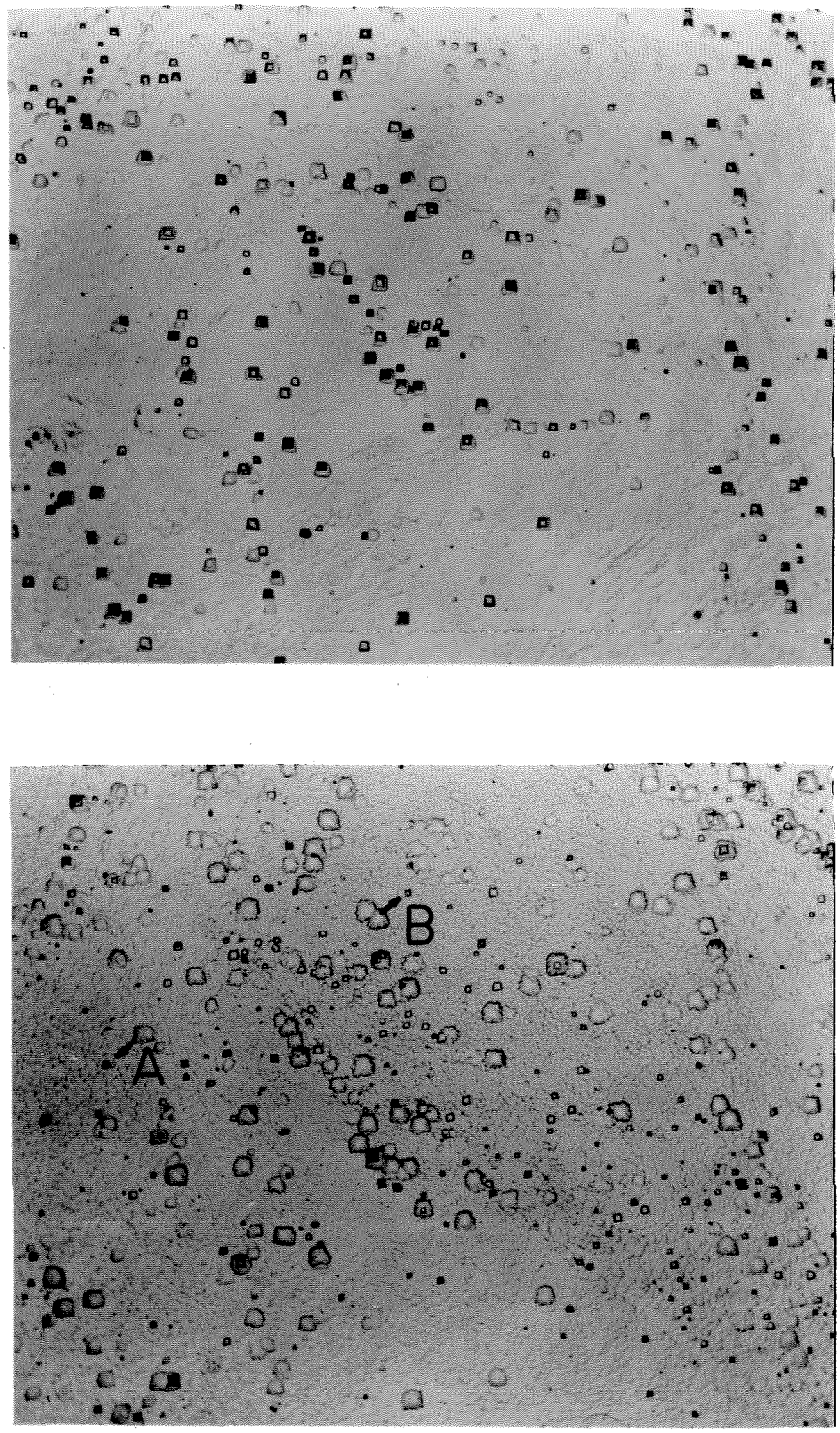

a

b

Figure 18. Etched {100} Surface of Specimen 6-3-1, 250X.

of the specimen, was 17.2 mm. The specimen was etched in both instances in etchant EB2, for 2 sec in the case of Figure 18a, for 5 sec in the case of Figure 18b. The dislocations revealed in Figure 18a are dislocations which existed in the specimen after annealing; thus, in this case, the motion of aged dislocations was studied.

At this point some observations will be made regarding the etching of dislocation sites on {100} planes in copper. These remarks are generally valid for Figures 18 through 21 and for both etchants. At least two types of pits may be distinguished in Figure 18a - small, light and small, dark pits. This difference in appearance may be explained in several ways. The etchants may be distinguishing between positive and negative edge dislocations as Livingston found for a {111} dislocation etchant (39). However, since dislocations revealed by both light and dark pits move in the same direction in the same slip system, it would seem that the differentiation is not between positive and negative edge dislocations.

On the other hand, the etchants may be distinguishing between screw- and edge-oriented dislocations. One fact which may militate against the latter possibility is the following. For this specimen orientation, there are three Burgers vectors connected with a given {111} plane, one lying in the {100} observation surface and two intersecting the surface at 45°, for which the resolved shear stress is one-half as large as that for the Burgers vector lying in the observation surface. Dislocations whose Burgers vectors intersect at 45° might reasonably be expected to be predominantly screw-oriented. Now, although both light and dark pits were included in the determi-

nation of dislocation displacement, no systematic variation of displacements between light and dark pits could be ascertained. If edge and screw dislocations move at different velocities at the same stress as Johnston and Gilman (7) found in lithium fluoride, a difference in the displacements between screw and edge dislocations should be evident unless the effect is cancelled by the difference in resolved shear stress described above. Therefore, it would seem either that the etchants do not distinguish between edge and screw dislocations or that screw dislocations move faster than edge dislocations in copper.

In Figure 18b can be seen another type of pit, a large, flat-bottomed pit. This type is interpreted as the site where a dislocation had been at the time of the first etch. The irregularity of the edges of the pit is due to the 10 sec chemical polish which preceded the "after" etching of the specimen. Also, due to this polishing, a dislocation which did not move is manifested in the superposition of a small pit on an irregular-shaped larger pit rather than a large, sharp-bottomed pit which is normally seen in the double etch technique. Dislocation motion can be seen at points A and B in Figure 18b.

The dislocation configuration in specimen 3-2-1, flat a , is shown in Figure 19. Etching was done in etchant EB1 for 4 and 3 sec, respectively. These photographs were taken at a point 11.6 mm from the free end of the specimen. The thick band of dislocation etch pits extending horizontally across the photographs is the result of scratching this observation surface with an alumina whisker in the scratching apparatus mentioned previously. The load on the whisker was 70 mg. The line of etch pits extending from the top to the bottom of the photo-

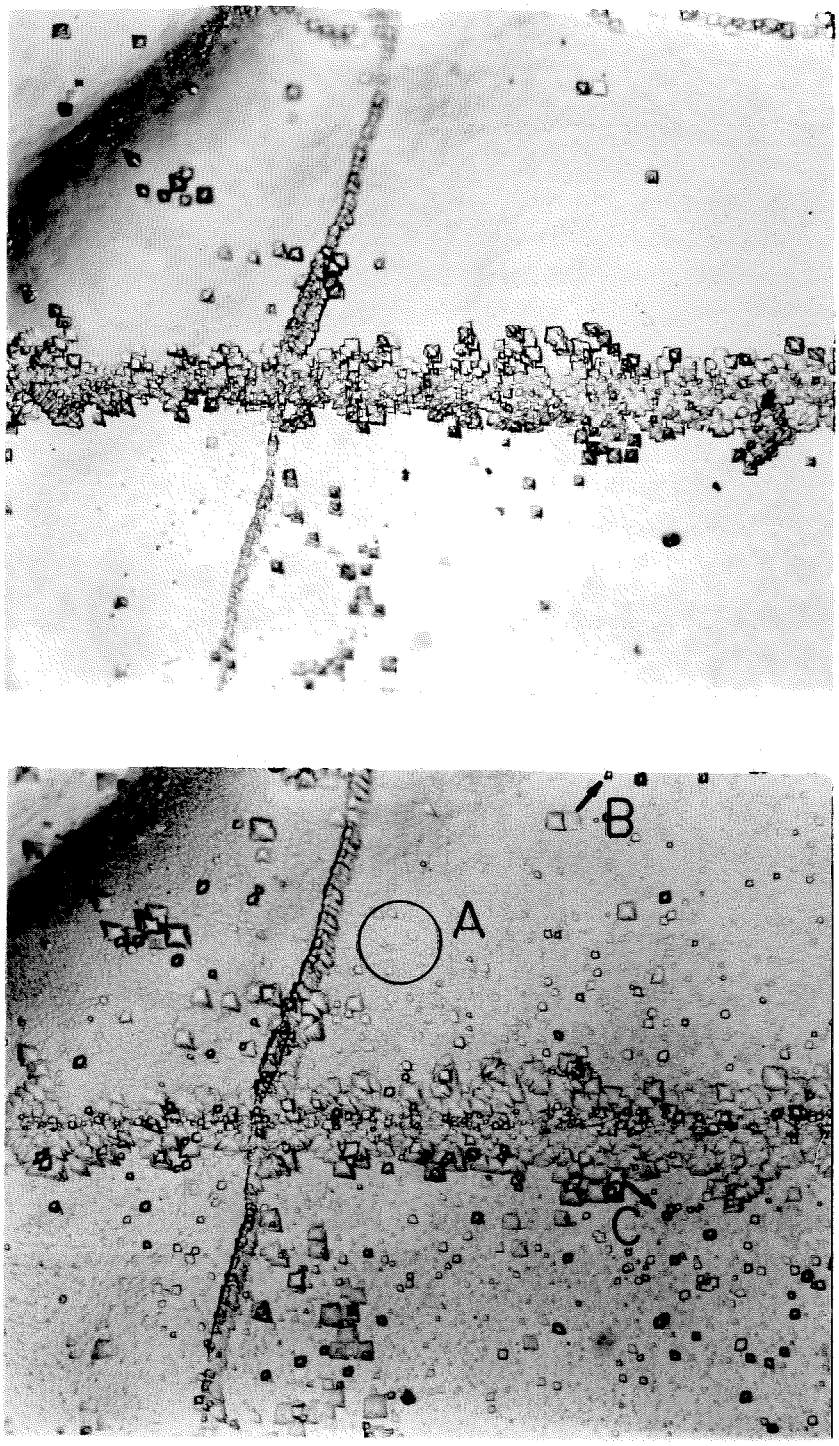

Figure 19. Etched {100} Surface of Specimen 3-2-1, 250X.

graphs is a subgrain boundary. It would appear that the density of dislocations has undergone a tremendous increase, but this is due to a faceting of the background, presumably caused by some contaminant which affects the etching behavior. This faceting produces a pebbled surface and features, such as in the circle at A, which might be confused with dislocation etch pits. Displacements of both aged and fresh dislocations produced by the scratch were included in the data used in determining the dislocation velocity. Dislocation motion can be seen at points B and C in Figure 19.

The dislocation configuration in specimen 3-3-1, flat d , is shown in Figure 20. Etching was done in etchant EB1 for 3 sec in each case. These photographs were taken at a point 13.5 mm from the free end of the specimen. As in Figure 19 the band of dislocation etch pits extending horizontally across the photographs is the result of scratching this observation surface. In this case, the scratching element was a diamond phonograph stylus, and the force was 330 mg. Note that the width of the band and, correspondingly, the damage done by the scratching element are about the same in both Figures 19 and 20 in spite of the different forces and scratching elements. In gathering data of dislocation displacement from this test, the motion of dislocations from the edge of the scratch was studied. In addition, displacements of aged dislocations far from the scratch were measured to determine the possible effect of residual stresses near the scratch and to determine any differences between the motion of aged dislocations and that of fresh dislocations. Motion of dislocations from the scratch is evident. In addition to the motion of single dislocations as

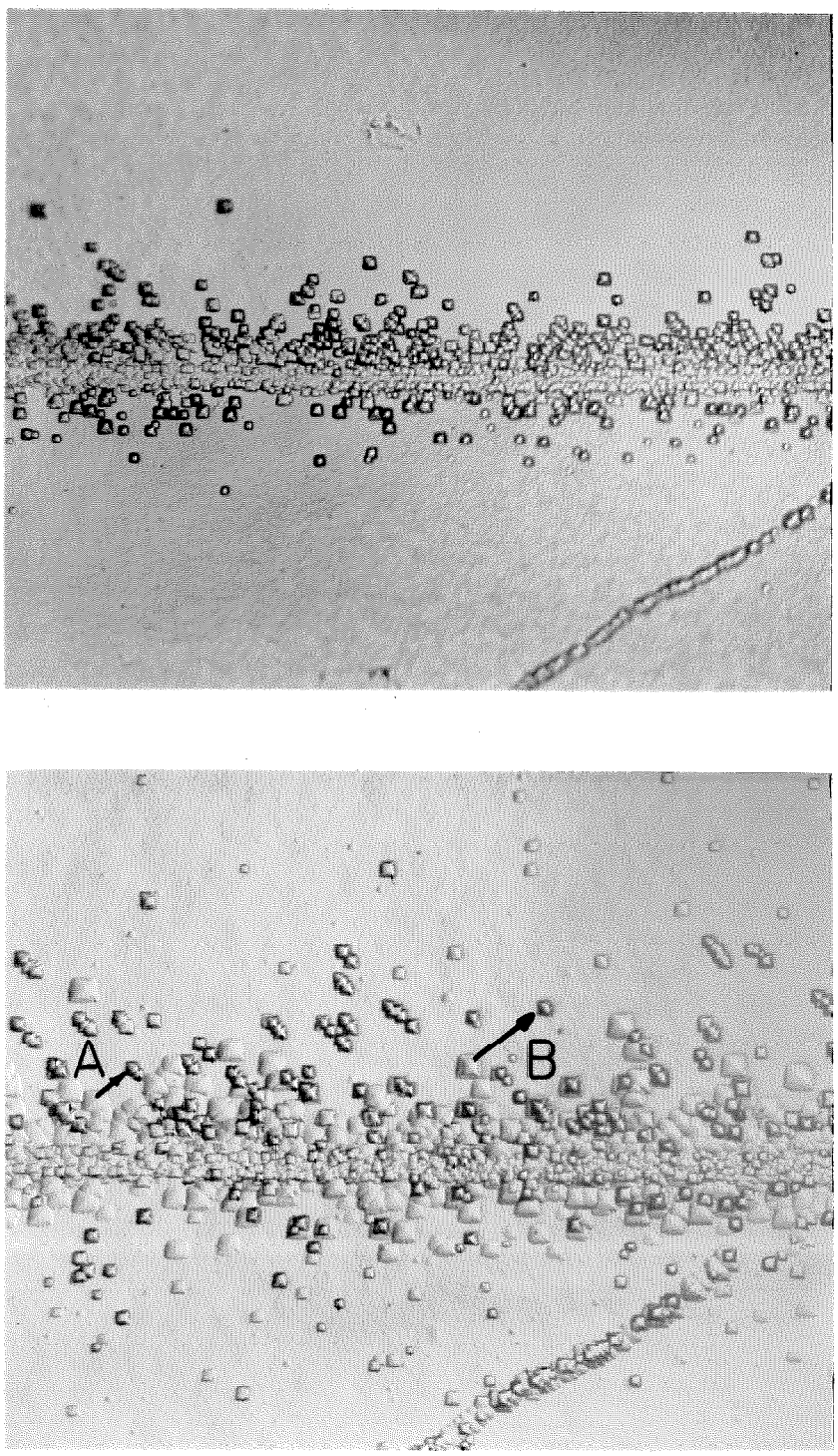

a

b

Figure 20. Etched {100} Surface of Specimen 3-3-1, 250X.

at B, there is also a cooperative motion of two and more dislocations as at A.

The dislocation configuration in specimen 6-2-1, flat a , is shown in Figure 21. This specimen was etched for 4 sec in EB1 before testing. Since the pits were rather large and somewhat indistinct (the sides of the pits are terraced), the specimen was etched for 5 sec in EB2 after the test. This etching was preceded by chemical polishing for 8 min in order to remove the pits from the previous etching. This was about a standard time to remove the pits from an etching by chemical polishing; therefore, the pits were about 8 to 16 μ deep, according to the previously stated polishing rate of 1 to 2 μ/min. The use of the double etch technique was not possible in this case because the "before" etch pits had to be removed; however, the comparison microscope system made it possible to determine dislocation displacements.

D. Dislocation Displacements

Acquisition of dislocation displacement data proceeded as follows. The 'before' and 'after' replicas of an observation surface for a given test were aligned in the comparison microscope system using the substructure as fiducial marks. Displacements were measured with a filar eyepiece which had been calibrated with a stage micrometer. It is not at all clear from viewing the areas shown in Figures 18 through 21 what the before and after positions of a moving dislocation might be. Indeed, it took considerable time examining the replicas of the observation surfaces to determine the position from which even one dislocation might have moved. In general, attention was focused

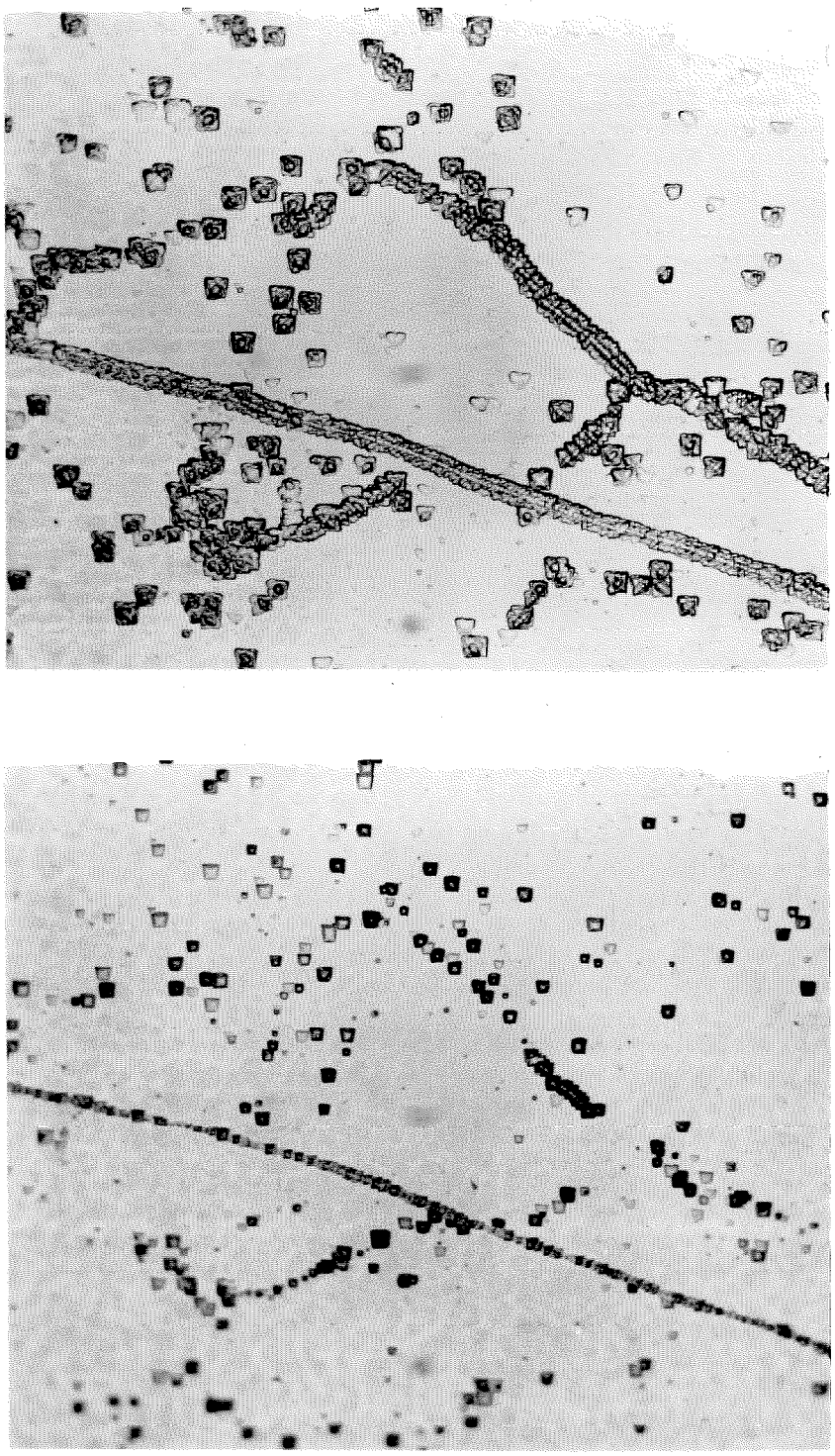

a

b

Figure 21. Etched {100} Surface of Specimen 6-2-1, 250X.

on a small, dark or light etch pit, and the problem of from where it came was posed. In some cases, as with a single aged dislocation, the dislocation could have moved from any one of four positions 90^{o} apart around the new position. However, in many cases, as with dislocations moving from a scratch or from a line-up of aged dislocations, the choice of before positions was restricted to two. Even when there were four positions from which the dislocation might have moved, the ambiguity could be resolved by aligning one cross-hair of the eyepiece along the diagonals of the etch pits, or along a pile-up of of dislocations (and thus, along the slip line) and then by observing which large, flat-bottomed etch pit lay along the slip line from the small, dark or light pit by means of the translating cross-hair. Nonetheless, much judgment was required even in the most obvious case shown in Figure 20.

After the problem of the before and after position of a dislocation was solved, the displacement was measured. The displacement was the distance between centers of the etch pits. It was determined that the center of an etch pit could be reproducibly determined within $2\,\mu$.

Increasing the duration of the stress pulse should increase the displacement of a dislocation in a linear manner. The duration of the stress pulse in these experiments increases with increasing distance from the free end of the single crystal specimen. Dislocation displacements were determined at a minimum of three different stations along the axial length of the specimen. At each station an average of 24 measurements of dislocation displacement, d , and distance of the

dislocation from the free end were taken. The mean of the displacement measurements at each station versus distance from the free end of the specimen, z , is shown in graphs in Figures 22 through 25. Figure 22 is for the lowest stress test (28.7 g/mm^2), and Figures 23, 24, and 25 are for increasingly higher stress tests. The circled points represent the mean of the displacement measurements, the number in parentheses is the number of measurements taken, and the length of the vertical lines through the points represents the standard deviation. In Figure 24 at z = 12.8 mm, the point represents displacements of aged dislocations situated at least 180 μ from the center of the scratch damage on the observation surface. Due to the slight difference between the displacements of aged and fresh dislocations at the same stress and pulse duration, the displacement of aged dislocations was measured in the high dislocation density specimens.

Several features of the graphs in Figures 22 through 25 are to be noticed. First, since the units of the abscissae can be converted into time at the constant stress, the slope of lines drawn through the data points is proportional to the dislocation velocity at that stress. Secondly, the rough linearity of the dependence of displacement on distance from the free end, or time, indicates that dislocations began to move and reached terminal velocity in a negligible time, that is, in a time negligible compared to the 2 or 3 μsec rise time of the stress pulse.

Further analysis of the data requires that the dislocation displacement at the axial station corresponding to the fixed end of the specimen be determined since the stress pulse applied to that point is

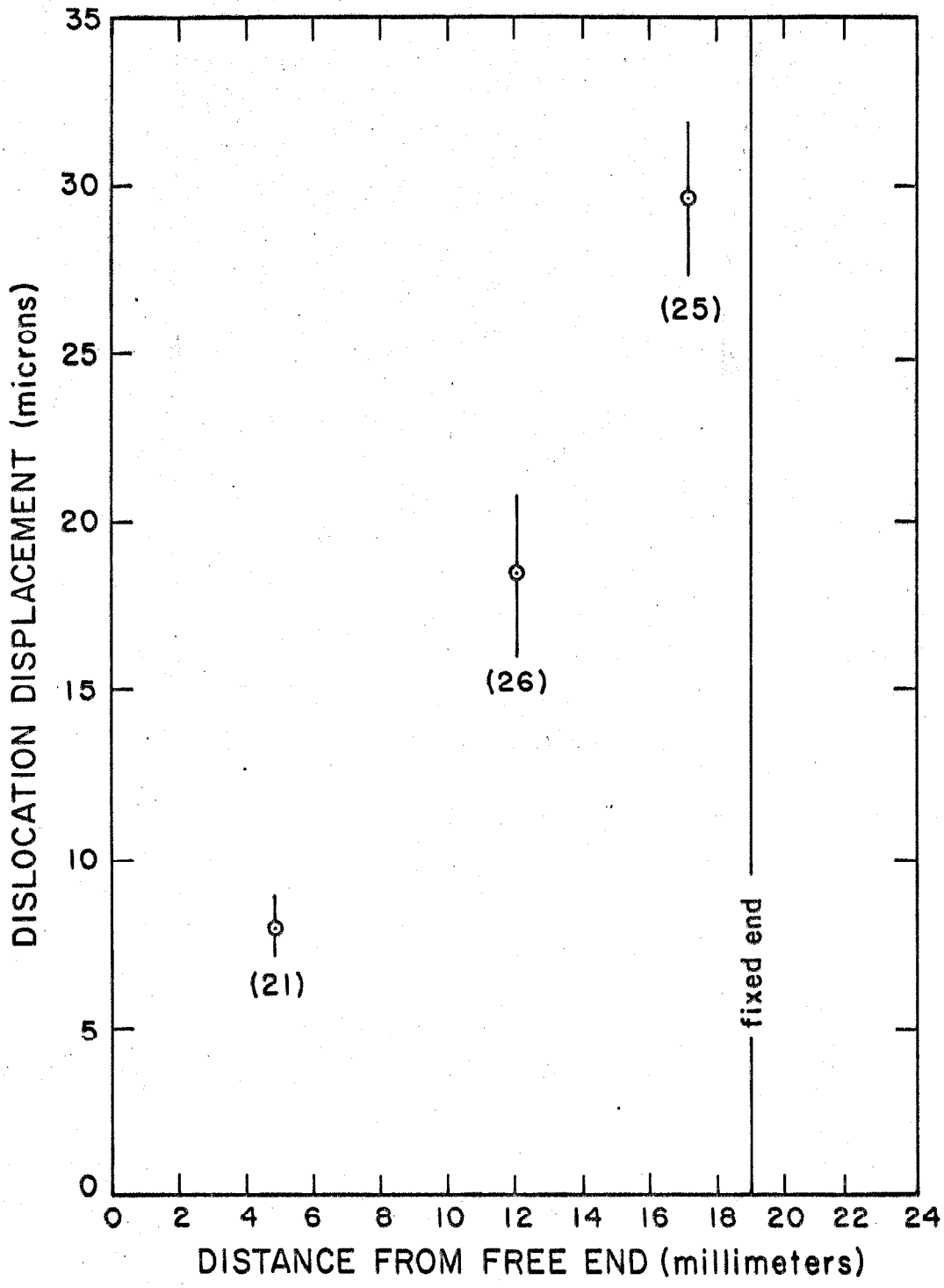

Figure 22. Dislocation Displacement Versus Distance from Free End for Specimen 6-3-1, $\tau_{max} = 28.7$ g/mm^2.

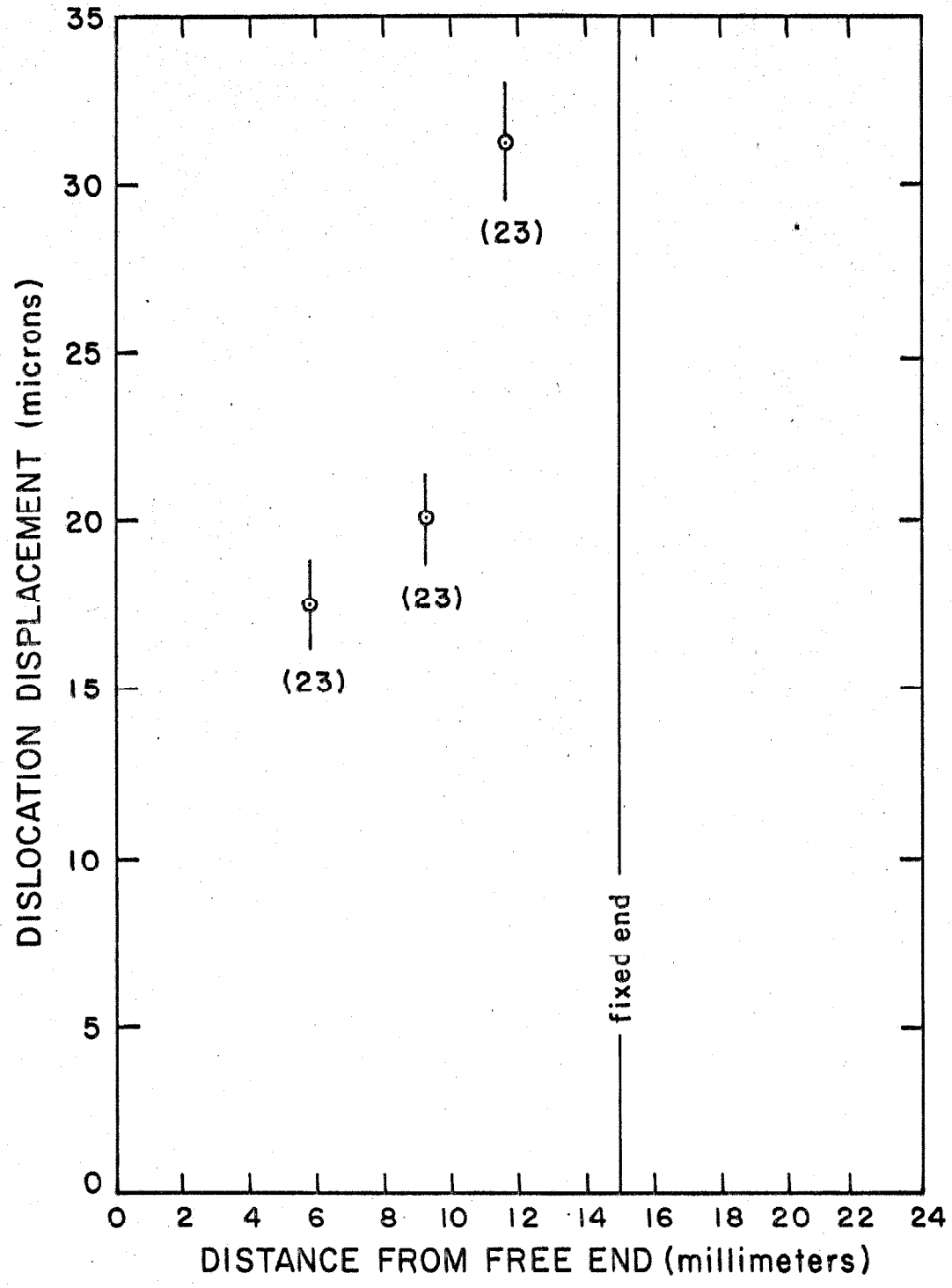

Figure 23. Dislocation Displacement Versus Distance from Free End for Specimen 3-2-1, $\tau_{max} = 68.8$ g/mm^2.

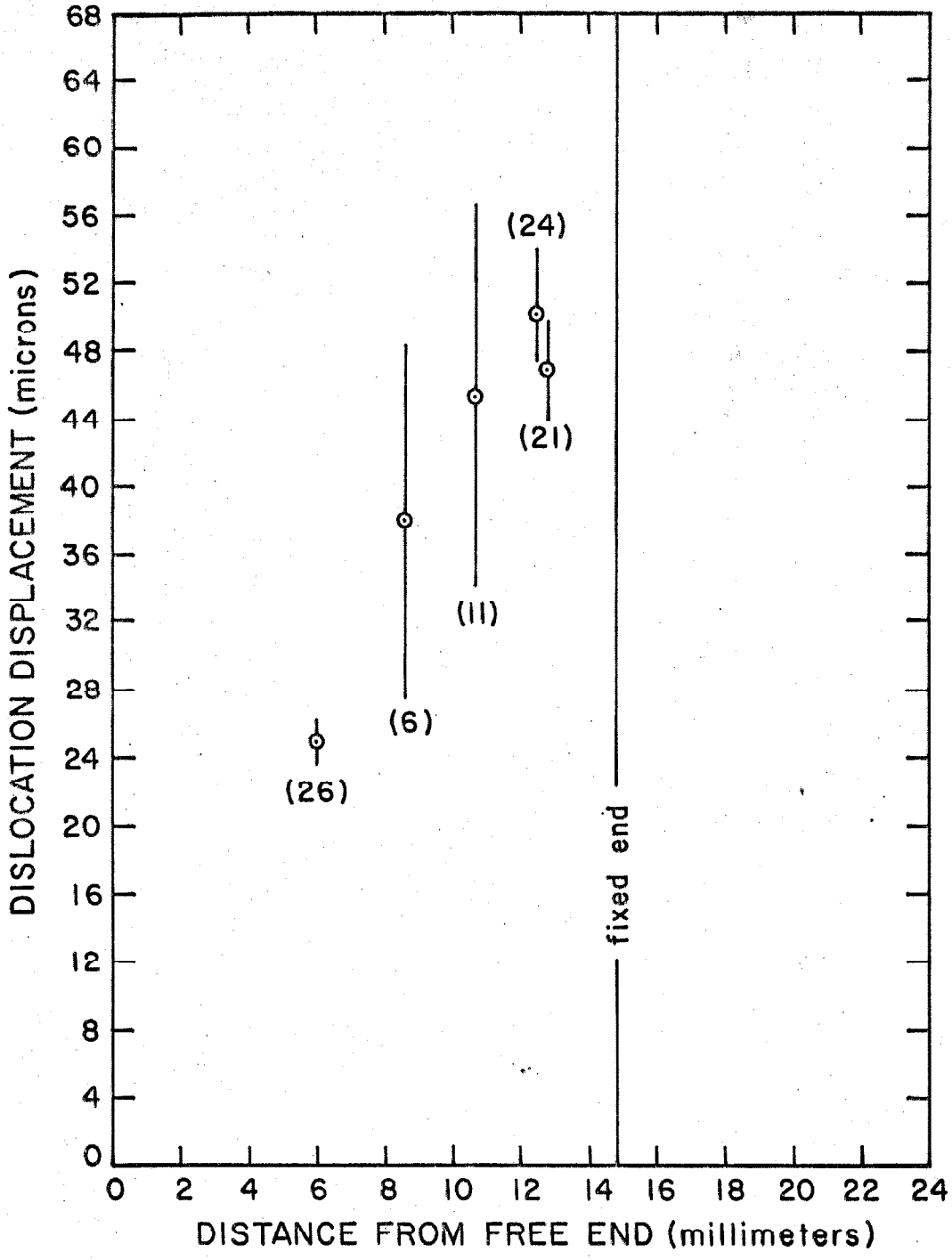

Figure 24. Dislocation Displacement Versus Distance from Free End for Specimen 3-3-1, $\tau_{max} = 134$ g/mm^2.

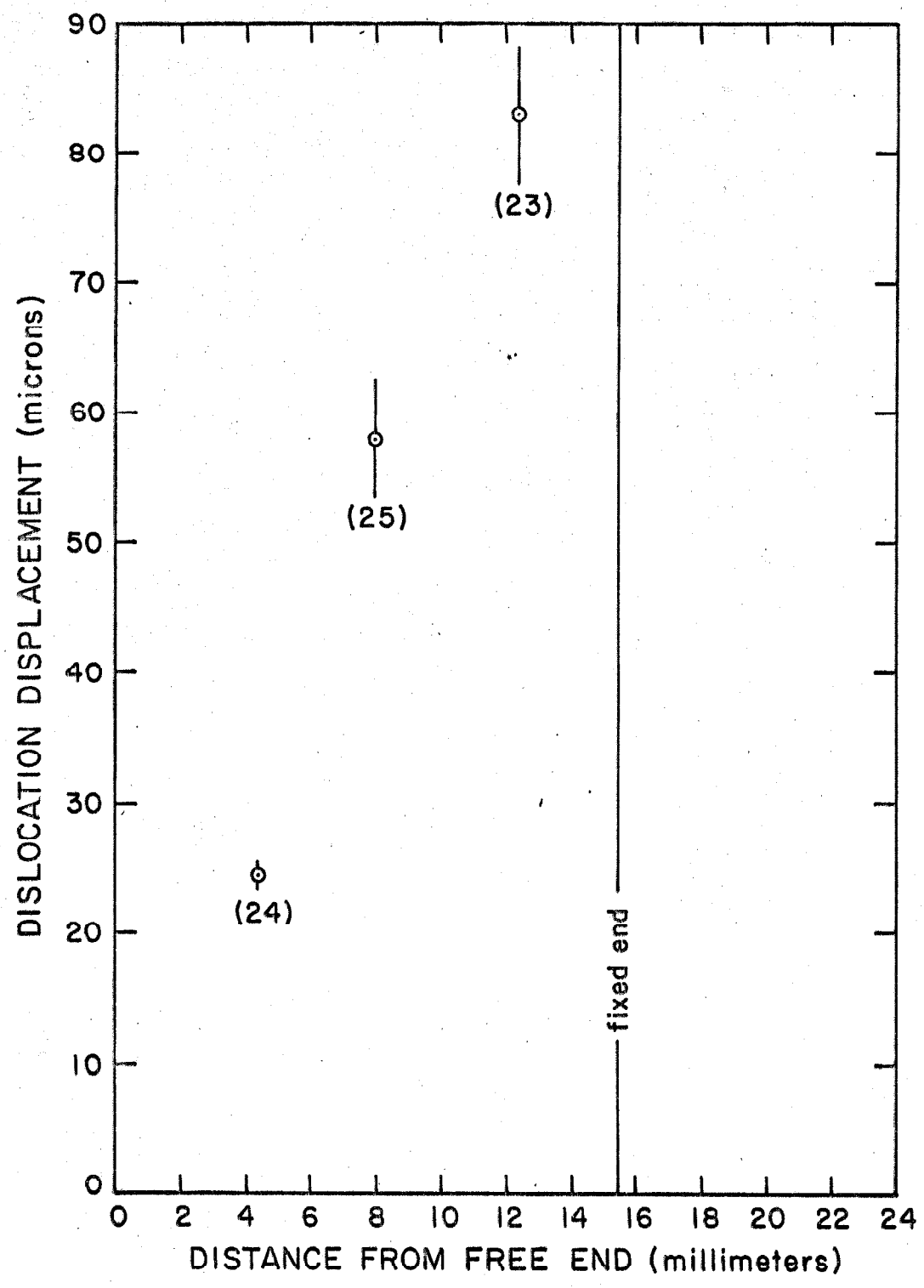

Figure 25. Dislocation Displacement Versus Distance from Free End for Specimen 6-2-1, $\tau_{max} = 236$ g/mm^2.

is known. The dislocation displacement at the fixed end of a given specimen can be obtained by extrapolation from the measured values of displacement. The position of the fixed end for each specimen is shown in the graphs in Figures 22 through 25. The displacement at the fixed end was taken to be the mean of the values obtained by extrapolating from pairs of points to the fixed end points. In Figure 23, however, the mean value (36.4 μ) of the displacement at the fixed end obtained in this way was judged too low. A line drawn through the three points yielded a value of dislocation displacement at the fixed end of 40 μ which was considered more accurate. The values of the dislocation displacement at the fixed end of the four specimens are given in Table 1.

TABLE I

Values of Stress and Dislocation Displacement, d ,

at Fixed End of Specimens

Specimen Number	d (μ)	τ_{max} (g/mm^2)	t_1 (μsec)	t_2 (μsec)	t_3 (μsec)
6-3-1	31.5	28.7	3	15	27
3-2-1	40	68.8	2	10	23
3-3-1	55.9	134	3	14	18
6-2-1	110.3	236	2	12	21

VI. DISCUSSION

The results presented in Table 1 are values of dislocation displacement in copper due to application of a controlled stress pulse. These results indicate in several ways that the velocity of dislocations in copper is relatively well-defined. The graphs in figures 22 through 25 demonstrate that dislocation displacement is a relatively smooth, if not linear, function of time at constant stress for stress pulses of the order of tens of microseconds and displacements of from 10μ to 110μ. The maximum standard deviation expressed as a percentage of the mean dislocation displacement was 13% in this investigation whereas for the work of Johnston and Gilman (7) it was 30%. Moreover, each velocity data point in this study represents the result of some 70 dislocation displacement measurements.

Young (22, 23) and Livingston (24) obtained dislocation displacements comparable to those in this investigation for stress pulses of somewhat lower magnitude but with durations of seconds. The explanation offered here for this discrepancy is that the dislocations were stopped by an internal stress barrier and actually moved during only a fraction of the pulse duration. The examples of dislocation displacement cited by Young and Livingston seem to be isolated instances, in contrast to this study, in which the displacements of many dislocations were averaged. Although in the investigations by Young and Livingston the dislocation displacements were generally less than 100μ, dislocations could move large distances, as predicted by the high velocities found in this study, when

barriers to these large displacements were small. For example, in the work by Young (23), dislocations traveled the width of a subgrain, a distance of at least 600μ before being stopped by a subboundary when the crystal was subjected to a stress pulse of 70 g/mm^2. Subboundaries in copper have been found to be effective barriers to dislocation motion (17).

It is of interest to examine the results of this study in the light of current theories of dislocation mobility to determine which theory most accurately predicts the velocity-stress relation. However, since the stress pulse was trapezoidal-shaped and not "square" i.e., since the applied stress was not constant during the entire period of dislocation motion, it is necessary to take this stress variation in time into account. Other investigators of dislocation mobility using the etch-pulse-etch technique have assumed that the dislocation velocity was adequately defined by dividing the dislocation displacement by the duration or time at constant stress of the stress pulse, thereby assuming a "square" stress pulse. It was not felt that this procedure for obtaining velocity was meaningful for the results of this investigation. Since the various formulae for dislocation mobility express the average dislocation velocity v as a function of applied shear stress τ and other variables, the problem of obtaining velocities from the data in Table 1 was posed. These data are analyzed below to give dislocation velocity versus stress. The procedure adopted was the following: A specific form of the velocity-stress relation was assumed to apply. This relation was integrated with respect to time to give dislocation displacement.

The functional dependence of stress on time was inserted in the stress-dependent half of the equation. The dislocation displacement as a function of the maximum resolved shear stress applied, the shape of the stress pulse, and various parameters in a given relation was thereby obtained. How closely a given velocity-stress formula predicted the displacements obtained in this investigation could be determined from this resulting equation for dislocation displacement. This procedure assumes that the dislocation velocity is in phase with the stress during the entire stress pulse, i.e., that the time of acceleration of the dislocation is negligible. The manner in which dislocation displacement increases with time of loading in each test indicates that the time of acceleration of the dislocation was negligible in this investigation.

The first representation of the stress dependence of dislocation velocity was not derived from a theory but from an empirical fit of the dislocation mobility data for lithium fluoride and silicon-iron. This relation was given in Equation 5 but is restated here in slightly different terms as

$$v = v_o(\tau/\tau_o)^m, \qquad [23]$$

where v is the dislocation velocity (equivalent to the $\bar{v}$ of Section I); τ is the applied, resolved shear stress; τ_o is the applied, resolved shear stress required to produce a velocity of v_o which is taken here as 1 cm/sec, and m is the mobility exponent. Assuming the

validity of Equation 23, an analysis is presented in Appendix B which yields a formula for dislocation displacement due to the application of a trapezoidal-shaped stress pulse. This formula for the displacement, d, is

$$d = \left(\frac{\tau_{max}}{\tau_o}\right)^m \left[\frac{t_3+m(t_2-t_1)}{m+1}\right] . \qquad [24]$$

The symbols τ_{max}, t_1, t_2, and t_3 are defined in Appendix B and Figure B-1. Having values of d, τ_{max}, and t_1, t_2, t_3, a value of m was assumed, and τ_o for each displacement and stress pulse was calculated from Equation 24. The mean of the four values of τ_o for each assumed value of m was calculated. This mean τ_o was used to calculate the displacement, d', by means of Equation 24. The error in determining displacement in this way is defined as

$$\frac{|d-d'|}{d} = e , \qquad [25]$$

and the mean error $\bar{e}$ for each value of m assumed was calculated. This procedure was followed for values of m = 0.5, 0.6, 0.7, 0.8, and 1.0. The results are given in Table 2. The calculated value of τ_o is quite sensitive to the value chosen for m. The mean error, $\bar{e}$, in calculating d from Equation 24 assuming values of m and, consequently, τ_o, is minimized for m = 0.7. Therefore, the form

$$v = (\tau/\tau_o)^{0.7} , \qquad [26]$$

where $\tau_o = 0.0248$ g/mm^2 gives a "best fit". Equation 26 and a reduced dislocation velocity which is defined as

Table 2

m	mean τ_o (g/mm^2)	$\bar{e}$
0.5	0.00111	0.136
0.6	0.00673	0.095
0.7	0.0248	0.088
0.8	0.0675	0.100
1.0	0.281	0.209

$$v' = d/\left[\frac{t_3+m(t_2-t_1)}{m+1}\right] \qquad [27]$$

with m = 0.7 are plotted in the graph of Figure 26. The vertical lines through the reduced dislocation velocity points represent the uncertainty in this quantity due to the uncertainty in the values of dislocation displacement at the specimen fixed end introduced by the extrapolation procedure.

In order to compare the experimental results of this investigation with theoretical predictions, it is of interest to fit the data to a linear relation (m = 1 in Equation 23). Figure 27 is a graph of this relation together with the reduced dislocation velocity defined by Equation 27 with m = 1. The vertical lines through the data points again represent the uncertainty in reduced dislocation velocity. The mean error is larger with m = 1, but the uncertainty in reduced velocities is such that the difference in $\bar{e}$ for m = 0.7 and m = 1 is not significant. A mean value of τ_o of 0.28 g/mm^2 was obtained with m = 1, giving

$$v = (\tau/0.28)^{1.0} . \qquad [28]$$

It can be seen that changing m from 0.7 to 1.0 has little effect on the values of reduced dislocation velocity.

The reduced dislocation velocity, v', defined by Equation 27, is the closest approximation which can be made from the displacement-stress pulse data to the actual average velocity of dislocations, v, given in Equation 23 and subsequent equations. Since the data were represented better by the relation in Equation 28 than

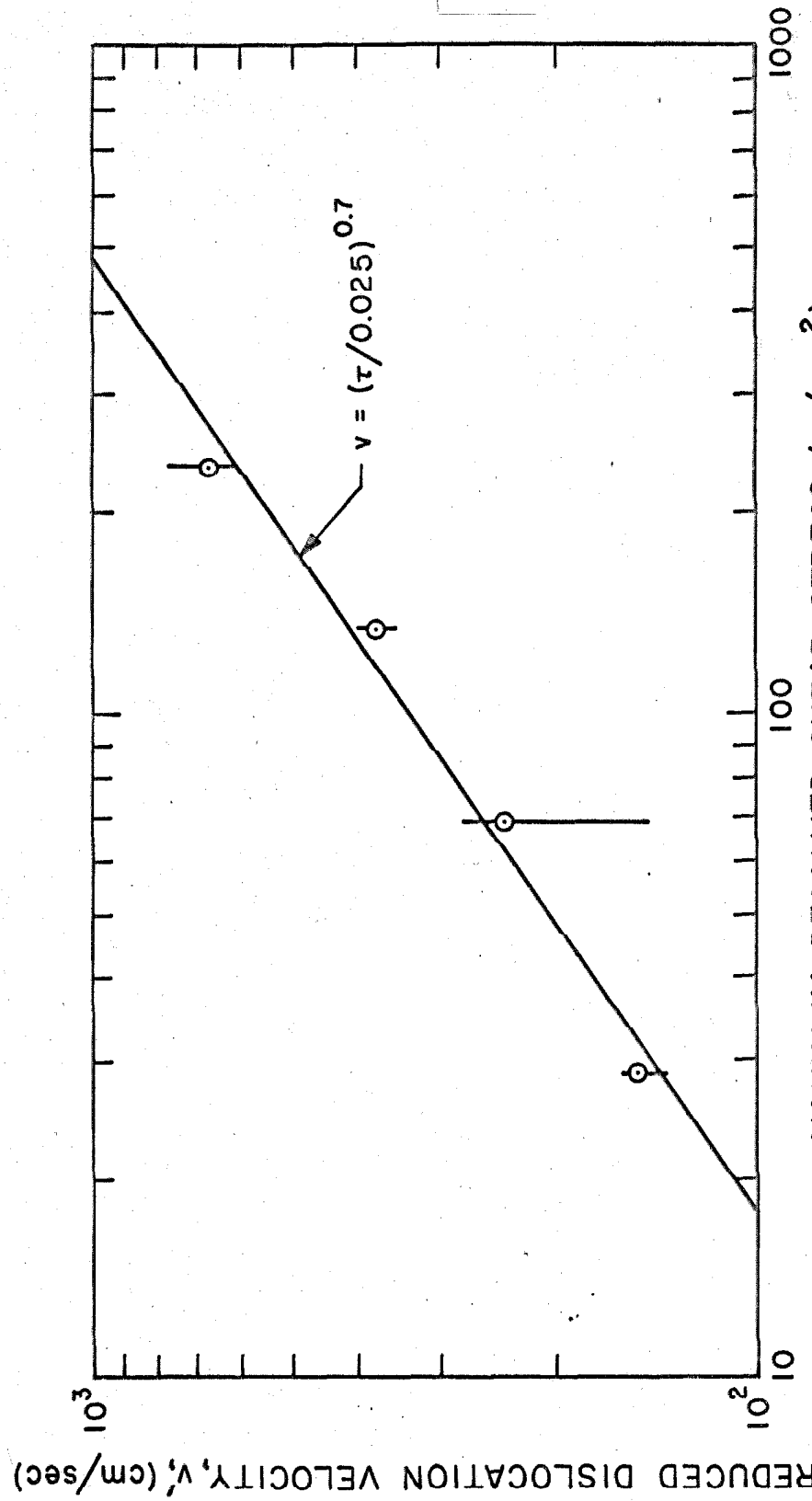

Figure 26. Reduced Dislocation Velocity Versus Maximum Resolved Shear Stress for m = 0.7.

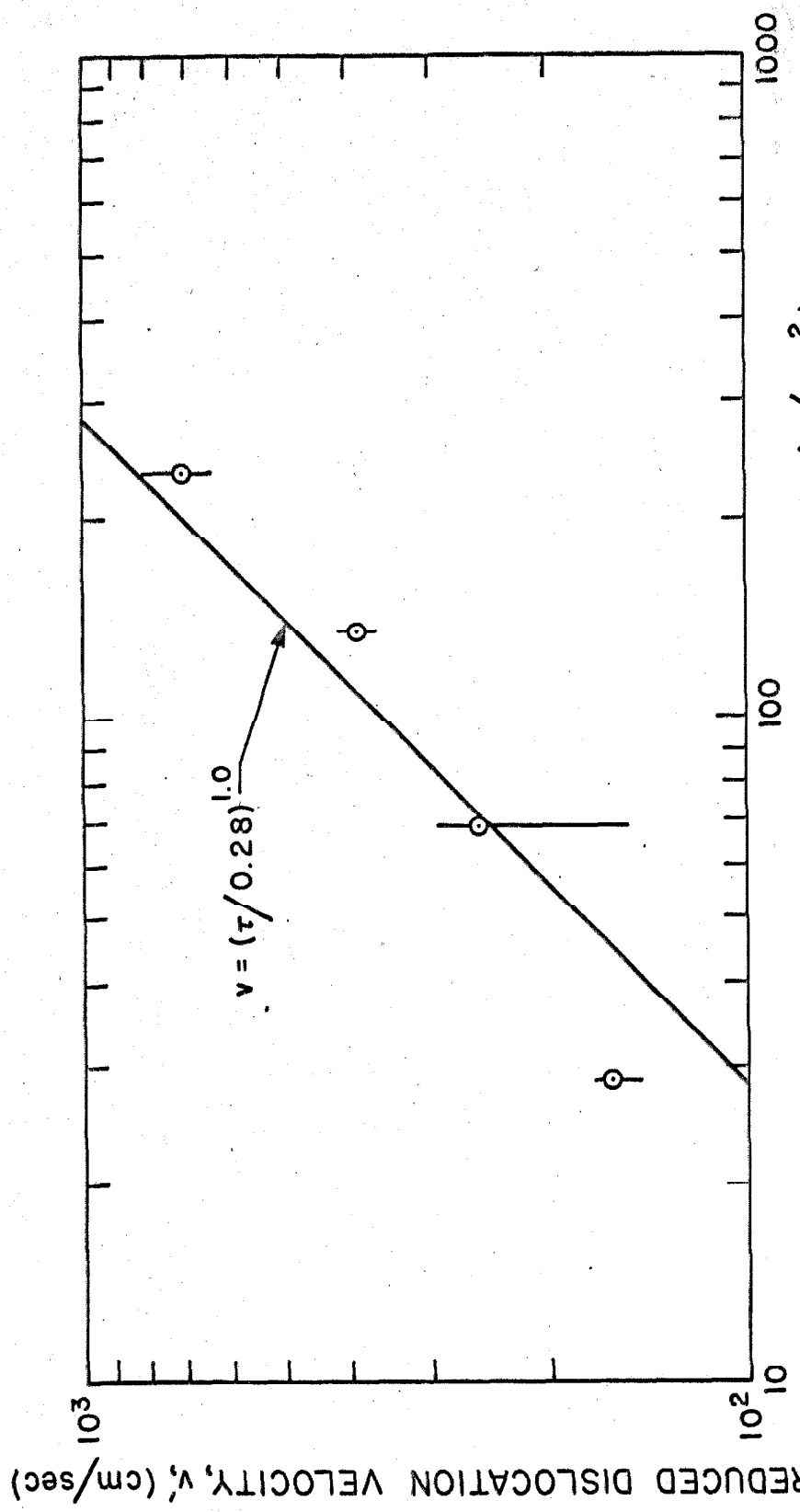

Figure 27. Reduced Dislocation Velocity Versus Maximum Resolved Shear Stress for m = 1.0 .

subsequent formulae, the reduced velocity for m = 1 was used as the value of actual velocity in analyzing the validity of other mobility formulae.

Another formulation of the stress-dislocation velocity relation has been suggested by Gilman (40). He has applied reaction rate theory to dislocation motion and has shown that when the activated complex is allowed two degrees of freedom the relation

$$v = v_o e^{-D/\tau} \qquad [29]$$

results, where v_o is a limiting velocity and D is a characteristic drag stress. The data shown in Table 1 were analyzed according to this formulation to determine whether it was a better representation of the data than Equation 28. The limiting velocity v_o is presumed to be the velocity of shear waves propagating in a $\langle 111 \rangle$ direction with the shear stress polarized so that it acts in a $\langle 110 \rangle$ direction on a $\{111\}$ plane. This velocity, evaluated from the stiffness moduli of the [111] specimen orientation as given in Appendix A, is 2.14×10^5 cm/sec.

As a first approximation to this analysis of the data, as it relates to Equation 29, the reduced dislocation velocity from the previous analysis (for m = 1) vs. $1/\tau_{max}$ is plotted in Figure 28. The data as interpreted in this way is not represented by Equation 29. More detailed calculations were made to ascertain the validity of the exponential formula for the data. Equation 29 was integrated as described above, to obtain a formula for dislocation displacement, and D was calculated for each test. The mean of the values for D

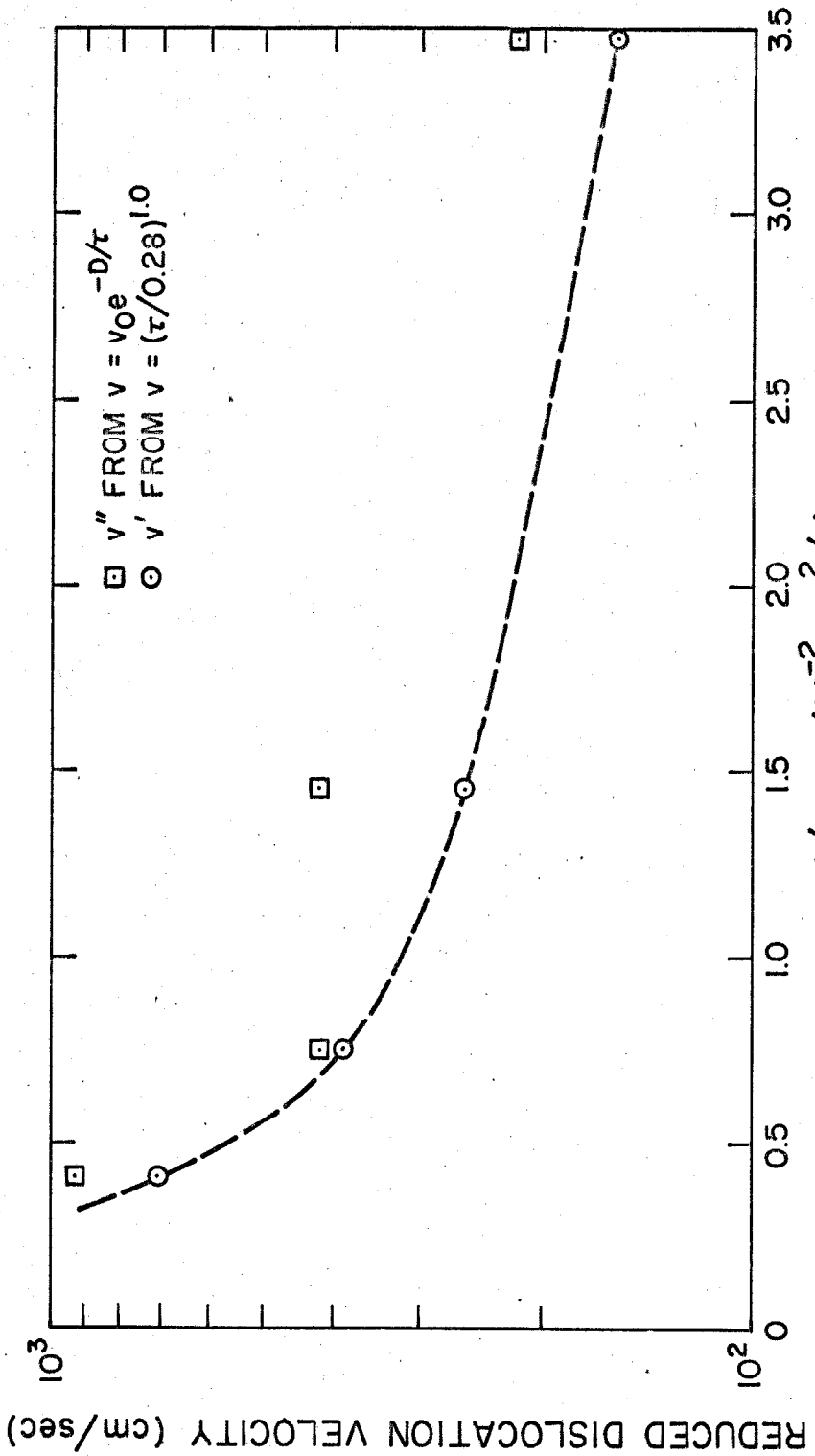

Figure 28. Reduced Dislocation Velocity Versus Reciprocal of Maximum Resolved Shear Stress.

was used to plot Equation 29, assuming the above value of v_o. A reduced dislocation velocity, v'', for this formulation does not lie on the straight line predicted by Equation 29.

Another theory for the relationship between dislocation velocity and stress has been presented by Fleischer (41). This theory is based upon the assumption that the velocity of dislocations is governed by their interaction with impurity atoms which are randomly distributed throughout the crystal. The theory is suitable to crystals in which the hardening is primarily due to tegragonal lattice distortions such as result from the introduction of magnesium into lithium fluoride. Although this mechanism is not thought to be operative in copper, the data were also analyzed on the basis of this theory. The formula given by Fleischer for dislocation velocity is

$$v = fL \exp\{-F_o b [1-(\tau/\tau_o)^{\frac{1}{2}}]^2 /kT\} , \qquad [30]$$

where f = frequency of vibration of a dislocation segment of length L,

F_o = the maximum force exerted on a dislocation due to the lattice distortion by the defect,

τ_o = the flow stress at 0^o K,

k = Boltzmann's constant,

and T = absolute temperature.

The logarithm of the reduced dislocation velocity defined by Equation 27 for m = 1 is plotted vs. the quantity $[(\tau/\tau_o)-(\tau/\tau_o)^{\frac{1}{2}}]$ in Figure 29. If the data of this investigation fit Equation 30, they should lie on a straight line in the graph; however, they do not.

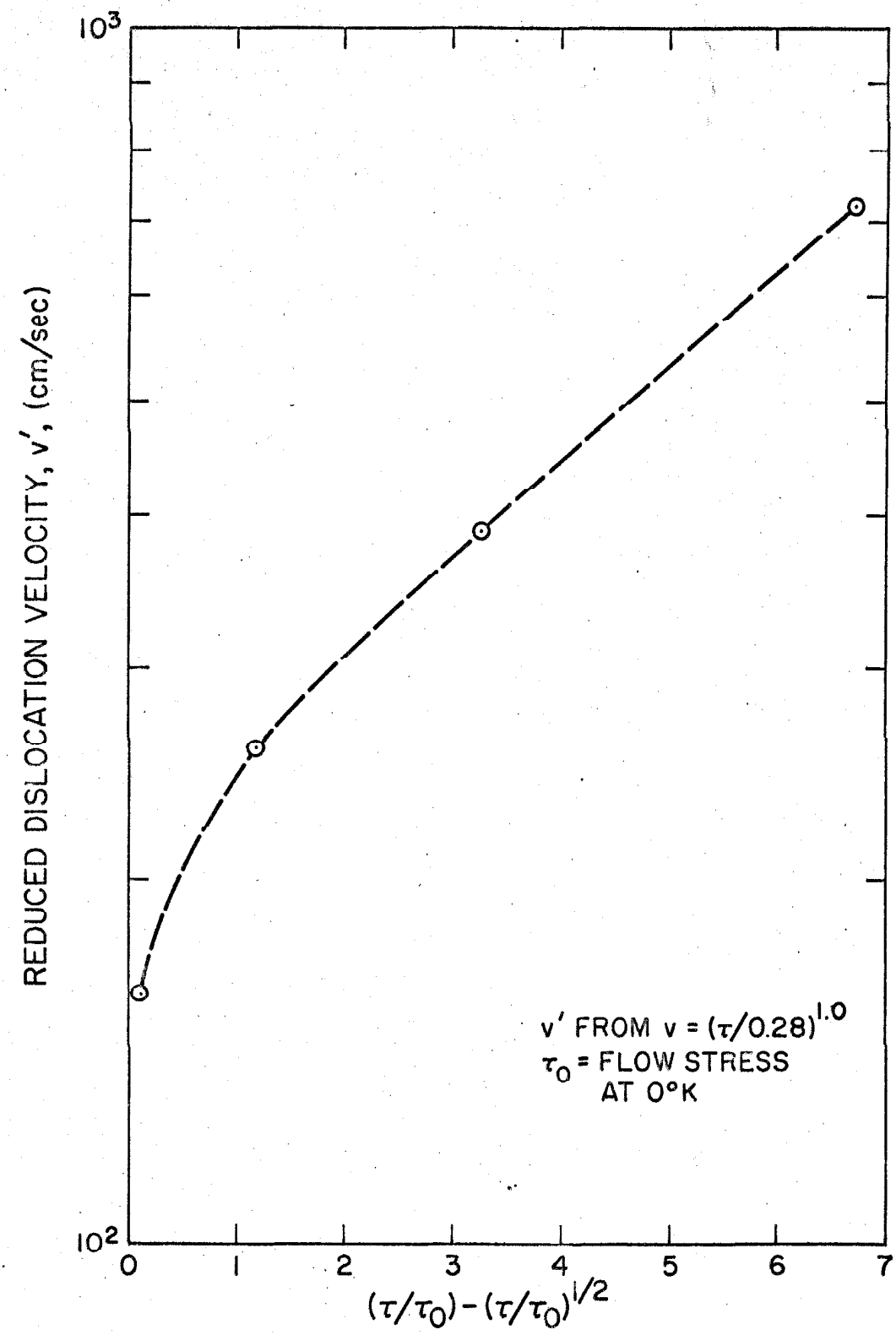

Figure 29. Analysis of Data According to Theory of Fleischer (41).

Physical mechanisms which might influence dislocation mobility in copper and their relation to the above theories will now be discussed. First, consider the assumptions and parameters of the velocity-stress relationships presented thus far. Several points should be mentioned here regarding the range of the variables in this study. The plastic strains imposed on the specimens were small compared to the elastic strains, and dislocation displacements were small, that is, small relative to the initial dislocation spacing. The dislocations were generally moving into dislocation-free areas. Different mechanisms and, consequently, a different dislocation velocity-stress relation may be obtained at higher strains where the dislocation displacement is equal to or greater than the initial dislocation spacing. However, for small displacements the relation of Equation 28 is valid, and the small value of τ_o indicates a low resistance of the lattice to the motion of dislocations.

The theories of Gilman (40) and Fleischer (41) involving point defect drag and, consequently, short-range interactions and small dislocation displacements would be attractive explanations of dislocation mobility in copper. However, the data are not represented by the formulae of these theories. It is, therefore, concluded that the type of thermally-assisted motion which is assumed by the theories is not applicable to dislocation mobility in copper.

The theory of Seeger et al. (42) assumes an Arrhenius relation for the strain rate as do those of Gilman (40) and Fleischer (41). The activation energy for this assumed form consists of two parts, one stress dependent, the other not. The data were analyzed

according to this theory and were found not to obey the relation predicted. The work of Conrad (26) on copper, as analyzed according to this theory, shows that the exponential term which should be dependent upon stress and temperature is actually relatively temperature independent.

It would seem plausible that dislocation motion in copper for the range of variables in this study need not depend upon assistance from thermal vibrations. A Peierls barrier to motion should be quite small, considering the extension of dislocations in copper, and might be surmounted by zero-point energy.

The foregoing discussion indicates that mechanisms whereby the velocity of dislocations is governed by thermally-activated surmounting of internal barriers to dislocation motion are not consistent with the experimental results obtained in this investigation. Another class of theories of the velocity of dislocations is based upon the assumption that the interaction between the strain field of the moving dislocation and the thermal vibrations of the crystal lattice, commonly known as the phonon drag and phonon viscosity effect. The most recent example of this type of theory is due to Lothe (43). Lothe predicts that for a straight, freely moving dislocation in metals, the anharmonicity in the core region and the phonon viscosity effect (lattice vibrations considered as a viscous phonon gas) give rise to a drag stress, τ_d, at ordinary temperatures $T \sim \theta$, where θ is the Debye temperature, of

$$\tau_d \sim \frac{1}{10} \epsilon \left(\frac{v}{V}\right) , \qquad [31]$$

where ϵ is the thermal energy density and V is again the shear wave velocity. The scattering of phonons by the dislocation is considered to produce a drag stress of the same order of magnitude so that the total drag stress due to anharmonicity, phonon viscosity, and phonon scattering is

$$\tau_d = \frac{1}{5} \epsilon \left(\frac{v}{V}\right) . \qquad [32]$$

Note that the drag stress is linear in velocity according to this theory. The thermal energy density is assumed to be the classical relation

$$\epsilon = \frac{3kT}{a^3/z} \qquad [33]$$

where a = the lattice parameter = 3.6×10^{-8} cm

and z = the number of atoms per unit cubic lattice cell = 4.

The drag stress calculated in this way is at most 55 per cent of the applied stress on the dislocation, being about 15 g/mm^2 at the lowest applied stress and velocity and about 68 g/mm^2 at the highest. Mason (44) has investigated the effect of phonon viscosity on dislocation motion, but this theory predicts, according to Suzuki et al. (45), the same order of magnitude of the drag stress as does the theory of Lothe.

The mechanisms due to lattice vibrations which might resist dislocation motion do not account entirely for the results of this study. Nonetheless, it is of interest to note that those theories which depend upon thermally-assisted dislocation motion predict that velocity will decrease with decreasing temperature whereas

those theories that depend upon the existence of a drag stress due to phonon scattering and viscosity predict that the dislocation velocity will increase with decreasing temperature. Stress pulse tests on copper specimens at low temperatures, which are in progress, should enable one better to select between the two types of theories of dislocation mobility.

Consider now the ramifications of the mobility relation, Equation 28, and the values of velocity and stress for copper. Table 3 gives mobility data for several materials, and one may see that at the flow stress (considered here as that stress at which the first deviation from linearity is observed in a stress-strain curve of the material) dislocations in copper are moving at a velocity several orders of magnitude greater than the velocity of dislocations at the flow stress in the ionic compounds, body-centered cubic metals, and semiconductor materials thus far studied. The easy glide flow or yield stress of the copper crystals used in this study was not measured, but Young (22, 23) obtained values of 35 g/mm^2 and 65 g/mm^2 for copper crystals of the same purity so an average of these two values was used as the flow stress given in Table 3 for the crystals of this investigation. Since the difference in dislocation velocities in copper and the other materials shown is so great, the comparison is not invalidated by an inexact value of the flow stress.

It is well-known that the strain rate sensitivity of the flow stress in copper is small. This is evidenced by a stress-strain relation which is very insensitive to the strain rate. Cottrell (46) interprets this phenomenon as due to a large mobility exponent in

Table 3

Dislocation Mobility Data for Several Materials

(at room temperature unless noted)

Material (reference to source in parentheses)	Flow stress (g/mm^2)	Velocity at flow stress (cm/sec)	Mobility exponent
Tungsten (11)	7400 (proportional limit)	1×10^{-3}	4.8
Lithium fluoride (7)	900 (critical resolved shear stress)	9×10^{-4} (screws) 1.5×10^{-2} (edges)	25
Sodium chloride (10)	30 (high purity)	1×10^{-5}	8
	170	1×10^{-5}	17
Silicon-iron (8)	12200 (0.3% offset yield strength)	1.5×10^{-6}	35
Germanium (12)	2900 (proportional limit) (500° C)	6×10^{-4} (500°C)	1.9
Copper*	~50	~200	1

* This investigation

copper, i.e., a small change in stress produces a large change in dislocation velocity. Silicon-iron with a relatively large strain rate sensitivity of the flow stress has a mobility exponent of 35, so that by this reasoning, the mobility exponent of copper should be large compared to 35. This investigation shows the mobility exponent in copper to be small. The small rate sensitivity of the flow stress in copper must therefore be due to a strong stress dependence of the density of moving dislocations and to the relatively high velocities which dislocations achieve at relatively low stresses. Such high velocities permit rapid dislocation multiplication so that the stress and strain are nearly in equilibrium even at relatively high strain rates. The sequence of events when stress is applied to a copper crystal is envisioned thusly: Dislocations are traveling at high velocities and multiplying at stresses below the macroscopic yield stress. The percentage of moving dislocations increases with stress as this author has observed qualitatively and Young (23) has checked semi-quantitatively. In a short time the dislocation density has increased to the point that the internal stress (from the strain fields of other dislocations) which opposes the motion of a dislocation equals the applied stress and dislocation motion ceases.

It is of interest to consider the effect of the internal stress further and to contrast the dynamical behavior of dislocations in a high-mobility-exponent material like silicon-iron to that in the low-exponent material copper. Vreeland (47) has studied the effect of a periodic internal stress field imposed on the constant applied stress level on the average velocity of a dislocation in a crystal,

considering the mobility exponent as a parameter. The stress in the dislocation mobility relation is taken as the local stress on the dislocation, not just the applied stress. He found that the form of the internal stress field had little effect on the analysis. As might be expected, the mobility exponent has a profound effect on the average velocity-average stress relation. The dislocation in a material with a high mobility exponent like silicon-iron spends much more time in the troughs of the periodic stress field than on the crests; consequently, as the amplitude of the internal stress field increases, the average dislocation velocity decreases rapidly. One may contrast this behavior of dislocation velocity to that in copper. When the velocity-stress relation is essentially linear, the amplitude of the internal stress field has no effect on the average velocity until it equals the applied stress when the average velocity goes to zero.

In copper, dislocations move and multiply rapidly at low stresses so that the dislocation density and, consequently, the internal stress need not increase too much before the internal stress amplitude equals the low applied stress and dislocation motion ceases. Phrased differently, the strain can essentially maintain its equilibrium value and be in phase with the stress at high strain rates. Since dislocations in silicon-iron move slowly at relatively high stresses, the dislocation density must become rather high before the internal stress amplitude approaches the applied stress. The strain cannot assume its equilibrium value and lags behind the stress at high strain rates.

The theory of yielding of a single crystal proposed by Johnston (2) states that for a small mobility exponent and a low density of moving dislocations, there will be a large yield drop when a stress-strain test is performed on the material. The density of mobile dislocations was assumed to be a function of strain but not explicitly a function of stress, whereas the mobile dislocation density must be strongly stress dependent in copper. Except in special cases, there is no yield drop in a stress-strain test of a copper crystal. Therefore, there must be a large density of moving dislocations at the flow stress, i.e., there must be weak pinning of aged dislocations compared to that provided by interstitials in body-centered cubic metals and divalent ions in lithium fluoride and sodium chloride. A cogent argument for this interpretation of the behavior of copper in light of this yield theory is in the paper by Cottrell (46) and is the stress-strain curve for a copper whisker which exhibits the largest known yield drop. The whisker must have been initially free of dislocations, and the upper yield stress of about 63 kg/mm^2 is interpreted as the stress necessary to create dislocations in the undislocated lattice. The yield drop to 3 kg/mm^2 is very abrupt because of the high velocity and rapid multiplication of the dislocations. Thus, in the case where there are no mobile dislocations or, more generally, a low density of moving dislocations, the low mobility exponent can give rise to a large yield drop.

SUMMARY AND CONCLUSIONS

The results of this investigation of dislocation mobility in copper and those of a previous one in zinc (14) indicate that the present theories of dislocation mobility cannot adequately predict the observed velocity-stress relations. Dislocations in copper move at high velocities at low stresses, and the velocity-stress relation is approximately linear. The low strain rate sensitivity of the flow stress is attributed to a strong stress dependence of the density of moving dislocations and to the high velocities at low stresses, rather than to a large mobility exponent.

The present theories of dislocation mobility may be divided into two categories. One which assumes that dislocation motion is thermally assisted; the other, that thermal assistance is negligible and that interaction with lattice vibrations causes a major portion of the drag force on a moving dislocation. The form of the velocity-stress relationship observed is in qualitative agreement with the latter, which predicts drag stresses of about 35% of the measured values. Which mechanism is operative in copper may be determined by low temperature tests of dislocation mobility, which are in progress. With such information, a more valid theory of dislocation mobility in FCC and HCP metals might be formulated. It would be of interest to extend the range of stresses for which dislocation velocities have been measured in this study by testing low dislocation density specimens in which large dislocation displacements can be followed.

Another result of this investigation which can be of use in other dislocation studies is that the dislocation etchants employed reliably reveal the sites of dislocations intersecting {100} planes.

APPENDIX A

The elastic properties of cylindrical, cubic-symmetry single crystals with three different crystallographic directions as the cylinder axis will be investigated in this appendix. Specifically, the elastic properties of the crystals when subjected to torsion about each of these three crystallographic directions will be examined, and it will be shown that a crystal with a [100] torsion and cylindrical axis is non-dispersive of a torsion stress pulse applied to it.

The generalized Hooke's law may be expressed in tensor notation as

$$\sigma_{ij} = c_{ijkl}\varepsilon_{kl} \qquad [A-1]$$

where σ_{ij} is the stress, c_{ijkl} are the elastic stiffness moduli, and ε_{kl} is the strain. The summation convention over repeated subscripts applies. The general transformation formulas relating the elastic moduli for a given Cartesian coordinate system which is rotated with respect to the crystallographic coordinate system are

$$c'_{\alpha\beta\gamma\delta} = \ell_{\alpha i}\ell_{\beta j}\ell_{\gamma k}\ell_{\delta l}c_{ijkl} \qquad [A-2]$$

where the $\alpha, \beta, \gamma, \delta$ subscripts range from 1 to 3 in the given rotated coordinate system, the i, j, k, l subscripts range from 1 to 3 in the crystallographic coordinate system, and $\ell_{\alpha i}$ is the direction cosine between the x'_α axis and the x_i axis. Equation A-2 can be simplified by introducing the reduced subscript notation where $c_{mn} = c_{ijkl}$, $\sigma_m = \sigma_{ij}$, and $\varepsilon_n = \varepsilon_{kl}$ according to the following prescription.

ij or kl	m or n
11	1
22	2
33	3
23 or 32	4
31 or 13	5
12 or 21	6

[A-3]

In addition, there are only three independent stiffness moduli for cubic symmetry crystals, c_{11}, c_{12}, c_{14}. Equation A-2 reduces to

$$c'_{\alpha\beta\gamma\delta} = \ell_{\alpha i}\ell_{\beta i}\ell_{\gamma i}\ell_{\delta i}C + \Delta_{\alpha\beta}\Delta_{\gamma\delta}c_{12}+(\Delta_{\alpha\gamma}\Delta_{\beta\delta}+\Delta_{\alpha\delta}\Delta_{\beta\gamma})c_{44} \quad [A-4]$$

where $\Delta_{\alpha\beta}$ is the Kronecker delta, i.e.,

$$\Delta_{\alpha\beta} = \begin{cases} 1 & \text{if} \quad \alpha = \beta \\ 0 & \text{if} \quad \alpha \neq \beta \end{cases} \quad [A-4a]$$

and

$$C = c_{11}-c_{12}-2c_{44} .$$

The stiffness moduli in the rotated coordinate system $c'_{\alpha\beta\gamma\delta}$ (or $c'_{\mu\nu}$ in the reduced notation) will be determined from Equation A-4 for the three single-crystal specimen orientations below.

Case 1. Cylindrical and torsion axis [111] (Figure A-1).

x'_1 axis - [111]

x'_2 axis - rotated angle θ from $[\bar{1}10]$

x'_3 axis - rotated angle θ from $[\bar{1}\bar{1}2]$

Direction cosines

	x_1	x_2	x_3
x_1'	$1/\sqrt{3}$	$1/\sqrt{3}$	$1/\sqrt{3}$
x_2'	$-\frac{1}{\sqrt{2}}\left(\cos\theta + \frac{\sin\theta}{\sqrt{3}}\right)$	$\frac{1}{\sqrt{2}}\left(\cos\theta - \frac{\sin\theta}{\sqrt{3}}\right)$	$\sqrt{2/3}\ \sin\theta$
x_3'	$-\frac{1}{\sqrt{2}}\left(\frac{\cos\theta}{\sqrt{3}} - \sin\theta\right)$	$-\frac{1}{\sqrt{2}}\left(\frac{\cos\theta}{\sqrt{3}} + \sin\theta\right)$	$\sqrt{2/3}\ \cos\theta$

The stiffness moduli are

$$c'_{11} = C/3 + c_{12} + 2c_{44}$$

$$c'_{12} = C/3 + c_{12}$$

$$c'_{13} = C/3 + c_{12}$$

$$c'_{14} = 0$$

$$c'_{15} = 0$$

$$c'_{16} = 0$$

$$c'_{22} = C/2 + c_{12} + 2c_{44}$$

$$c'_{23} = C/6 + c_{12}$$

$$c'_{24} = 0$$

$$c'_{25} = \frac{C\cos\theta}{3\sqrt{2}}(1 - 2\cos 2\theta)$$

$$c'_{26} = -\frac{C\sin\theta}{3\sqrt{2}}(1 + 2\cos 2\theta)$$

$$c'_{33} = C/2 + c_{12} + 2c_{44}$$

$$c'_{34} = 0$$

$$c'_{35} = -\frac{C\cos\theta}{3\sqrt{2}}(1 - 2\cos 2\theta)$$

$$c'_{36} = \frac{C\sin\theta}{3\sqrt{2}}(1 + 2\cos 2\theta)$$

$$c'_{44} = C/6 + c_{44}$$

$$c'_{45} = \frac{C\sin\theta}{3\sqrt{2}}(1 + 2\cos 2\theta)$$

$$c'_{46} = \frac{C\cos\theta}{3\sqrt{2}}(1 - 2\cos 2\theta)$$

$$c'_{55} = C/3 + c_{44}$$

$$c'_{56} = 0$$

$$c'_{66} = C/3 + c_{44}$$

Case 2. Cylindrical and torsion axis [110] (Figure A-2).

x'_1 axis - [110]

x'_2 axis - rotated angle θ from $[\bar{1}10]$

x'_3 axis - rotated angle θ from [001]

Direction cosines

	x_1	x_2	x_3
x'_1	$1/\sqrt{2}$	$1/\sqrt{2}$	0
x'_2	$-\cos\theta/\sqrt{2}$	$\cos\theta/\sqrt{2}$	$\sin\theta$
x'_3	$\sin\theta/\sqrt{2}$	$-\sin\theta/\sqrt{2}$	$\cos\theta$

The stiffness moduli are

$$c'_{11} = \frac{1}{2}(c_{11}+c_{12}+2c_{44})$$

$$c'_{12} = \frac{C}{2}\cos^2\theta + c_{12}$$

$$c'_{13} = \frac{C}{2}\sin^2\theta + c_{12}$$

$$c'_{14} = -\frac{C}{4}\sin 2\theta$$

$$c'_{15} = 0$$

$$c'_{16} = 0$$

$$c'_{22} = C\left(\sin^4\theta + \frac{\cos^4\theta}{2}\right) + c_{12} + 2c_{44}$$

$$c'_{23} = \frac{3C}{8}\sin^2 2\theta + c_{12}$$

$$c'_{24} = \frac{C}{2}\sin 2\theta\left(\sin^2\theta - \frac{\cos^2\theta}{2}\right)$$

$$c'_{25} = 0$$

$$c'_{26} = 0$$

$$c'_{33} = C\left(\frac{\sin^4\theta}{2} + \cos^4\theta\right) + c_{12} + 2c_{44}$$

$$c'_{34} = \frac{C}{2}\sin 2\theta\left(\cos^2\theta - \frac{\sin^2\theta}{2}\right)$$

$$c'_{35} = 0$$

$$c'_{36} = 0$$

$$c'_{44} = \frac{3C}{8}\sin^2 2\theta + c_{44}$$

$$c'_{45} = 0$$

$$c'_{46} = 0$$

$$c'_{55} = \frac{C}{2}\sin^2\theta + c_{44}$$

$$c'_{56} = -\frac{C}{4}\sin 2\theta$$

$$c'_{66} = \frac{C}{2}\cos^2\theta + c_{44}$$

Case 3. Cylindrical and torsion axis [100] (Figure A-3).

x_1' axis - [100]

x_2' axis - rotated angle θ from [010]

x_3' axis - rotated angle θ from [001]

Direction cosines

	x_1	x_2	x_3
x_1'	1	0	0
x_2'	0	$\cos\theta$	$\sin\theta$
x_3'	0	$-\sin\theta$	$\cos\theta$

The stiffness moduli are

$$c'_{11} = c_{11}$$

$$c'_{12} = c_{12}$$

$$c'_{13} = c_{12}$$

$$c'_{14} = 0$$

$$c'_{15} = 0$$

$$c'_{16} = 0$$

$$c'_{22} = C(\cos^4\theta + \sin^4\theta) + c_{12} + 2c_{44}$$

$$c'_{23} = \frac{C}{2}\sin^2 2\theta + c_{12}$$

$$c'_{24} = -\frac{C}{2}\sin 2\theta \cos 2\theta$$

$$c'_{25} = 0$$

$$c'_{26} = 0$$

$$c'_{33} = C(\cos^4\theta + \sin^4\theta) + c_{12} + 2c_{44}$$

$$c'_{34} = \frac{C}{2} \sin 2\theta \cos 2\theta$$

$$c'_{35} = 0$$

$$c'_{36} = 0$$

$$c'_{44} = \frac{C}{2} \sin^2 2\theta + c_{44}$$

$$c'_{45} = 0$$

$$c'_{46} = 0$$

$$c'_{55} = c_{44}$$

$$c'_{56} = 0$$

$$c'_{66} = c_{44}$$

Whether any or all of the three specimen orientations is dispersive of the torsion pulse will be determined in the following manner. The application of a pure twisting deformation, with no warping of the cross section and no radial displacement, is presumed equivalent to the application of the torsion stress pulse to the specimen. The stresses resulting from the torsional shear strain, ϵ'_5, will be determined from the stiffness moduli calculated above for the three specimen orientations. Dispersion of the stress pulse will result if the initial σ'_5 is converted into other stresses due to the elastic anisotropy. This method of determining wave dispersion allows the relative magnitude of the dispersive stresses to be calculated.

The stresses resulting from ϵ'_5 for the [111] torsion axis orientation are

$$\sigma_1' = c_{15}'\epsilon_5' = 0$$

$$\sigma_2' = c_{25}'\epsilon_5' = \frac{C\cos\theta}{3\sqrt{2}}(1 - 2\cos 2\theta)\,\epsilon_5'$$

$$\sigma_3' = c_{35}'\epsilon_5' = -\frac{C\cos\theta}{3\sqrt{2}}(1 - 2\cos 2\theta)\epsilon_5'$$

$$\sigma_4' = c_{45}'\epsilon_5' = \frac{C\sin\theta}{3\sqrt{2}}(1 + 2\cos 2\theta)\epsilon_5'$$

$$\sigma_5' = c_{55}'\epsilon_5' = (\frac{1}{3}C + c_{44})\epsilon_5'$$

$$\sigma_6' = c_{56}'\epsilon_5' = 0$$

Thus, σ_2', σ_3', and σ_4' arise to give dispersion. The numerical values of the stiffness moduli for copper in units of 10^{11} dynes/cm^2 (33) are given below in order to be able to evaluate the relative magnitudes of the above stresses.

$$c_{11} = 17.02$$

$$c_{12} = 12.3$$

$$c_{44} = 7.51$$

$$C = -10.3$$

The magnitudes of these stresses relative to σ_5', evaluated at $\theta = 0$, are

$$\left|\frac{\sigma_2'}{\sigma_5'}\right| = \left|\frac{\sigma_3'}{\sigma_5}\right| = 0.6$$

and

$$\left|\frac{\sigma_4'}{\sigma_5'}\right| = 0 \ .$$

This solution is not exact, as there are the stresses σ_2', σ_3', σ_4' occurring at the stress-free cylindrical surface. However, there is evidence of transfer of energy from shear to dilatational waves and

consequent dispersion of the torsion stress pulse.

The stresses resulting from ϵ'_5 for the [110] torsion axis orientation are

$$\sigma'_1 = c'_{15}\epsilon'_5 = 0$$

$$\sigma'_2 = c'_{25}\epsilon'_5 = 0$$

$$\sigma'_3 = c'_{35}\epsilon'_5 = 0$$

$$\sigma'_4 = c'_{45}\epsilon'_5 = 0$$

$$\sigma'_5 = c'_{55}\epsilon'_5 = (\frac{C}{2}\sin^2\theta + c_{44})\epsilon'_5$$

$$\sigma'_6 = c'_{56}\epsilon'_5 = -(\frac{C}{4}\sin 2\theta)\epsilon'_5$$

Thus, σ'_6 arises to give dispersion. The magnitude of this stress relative to σ'_5 evaluated at $\theta = \pi/4$, is

$$\left|\frac{\sigma'_6}{\sigma'_5}\right| = .52 .$$

In addition, σ'_5 varies with θ around the specimen axis. As in the case of the [111] torsion axis, the occurrence of a stress, σ'_6, at the cylindrical surface, which was presumed stress-free, indicates the solution is not exact.

The stresses resulting from ϵ'_5 for the [100] torsion axis orientation are

$$\sigma'_1 = c'_{15}\epsilon'_5 = 0$$

$$\sigma'_2 = c'_{25}\epsilon'_5 = 0$$

$$\sigma'_3 = c'_{35}\epsilon'_5 = 0$$

$$\sigma'_4 = c'_{45}\epsilon'_5 = 0$$

$$\sigma'_5 = c'_{55}\epsilon'_5 = c_{44}\epsilon'_5$$

$$\sigma'_6 = c'_{56}\epsilon'_5 = 0$$

In this case, no dispersion results, and there are four {100} surfaces available for observation of dislocation motion.

The inverse problem of applying a pure torsional moment, $M_{zz} = M_{11}$, about the specimen axis, thereby producing only the torsional shear stress $\tau_{\theta z} = \sigma'_5$, has been solved for the [110] orientation by Wood (48). He calculated the compliance moduli, $s'_{\mu\nu}$, for this orientation, imposed the stress σ'_5, determined strains and displacements, and concluded that

> "the stress distribution is the same as that for pure torsion of a circular rod of isotropic elastic material. The strain distribution, however, differs from that in the isotropic rod, and, furthermore, the cross sections are warped." (48).

It should be noted that the analysis applies to a long, single crystal rod in which the radial and axial displacements, u_r and u_z, must be independent of the axial coordinate z and in which the tangential displacement u_θ must be a linear function of z. Of course, this was not the experimental situation in this investigation.

The above procedure developed by Wood was attempted for the case of a [111] specimen and torsion axis. However, the resulting differential equations involving the displacements appear intractable and are perhaps insoluble. The results of applying this procedure to the case of the [100] oriented specimen show that the stress and strain distribution is the same as in the case of pure torsion of a circular rod of elastically isotropic material.

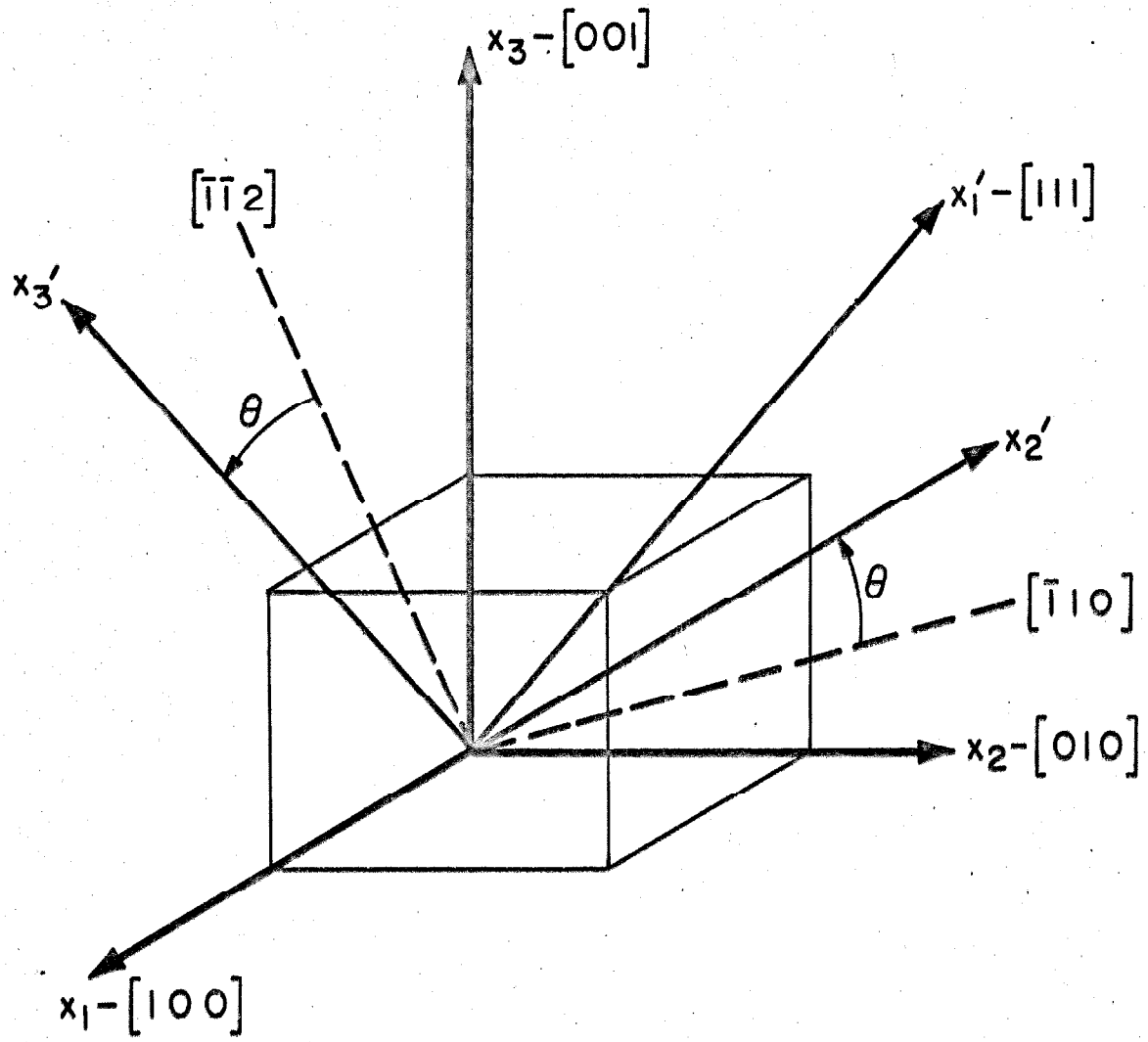

Figure A-1. [111] Specimen Orientation.

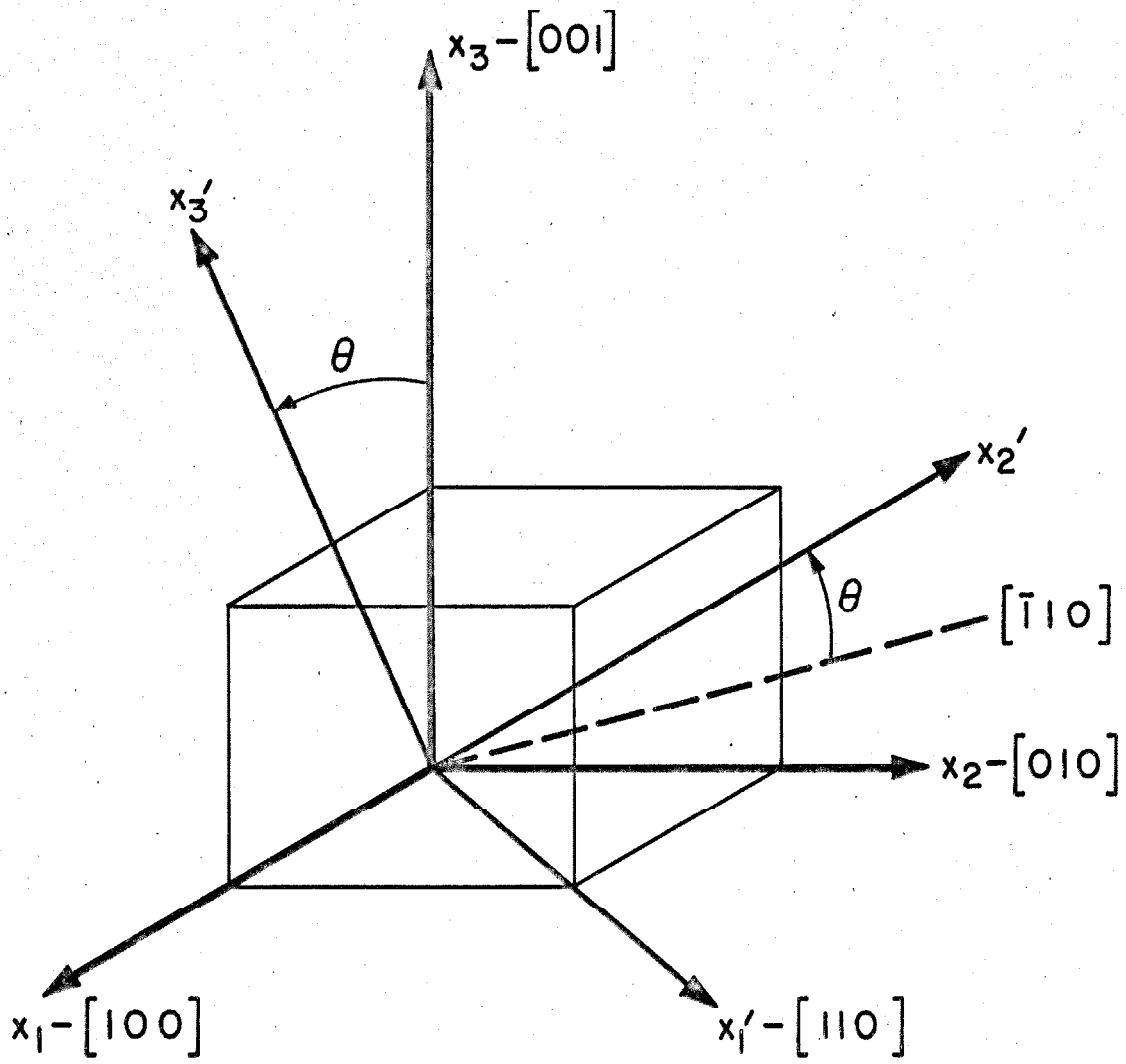

Figure A-2. [110] Specimen Orientation.

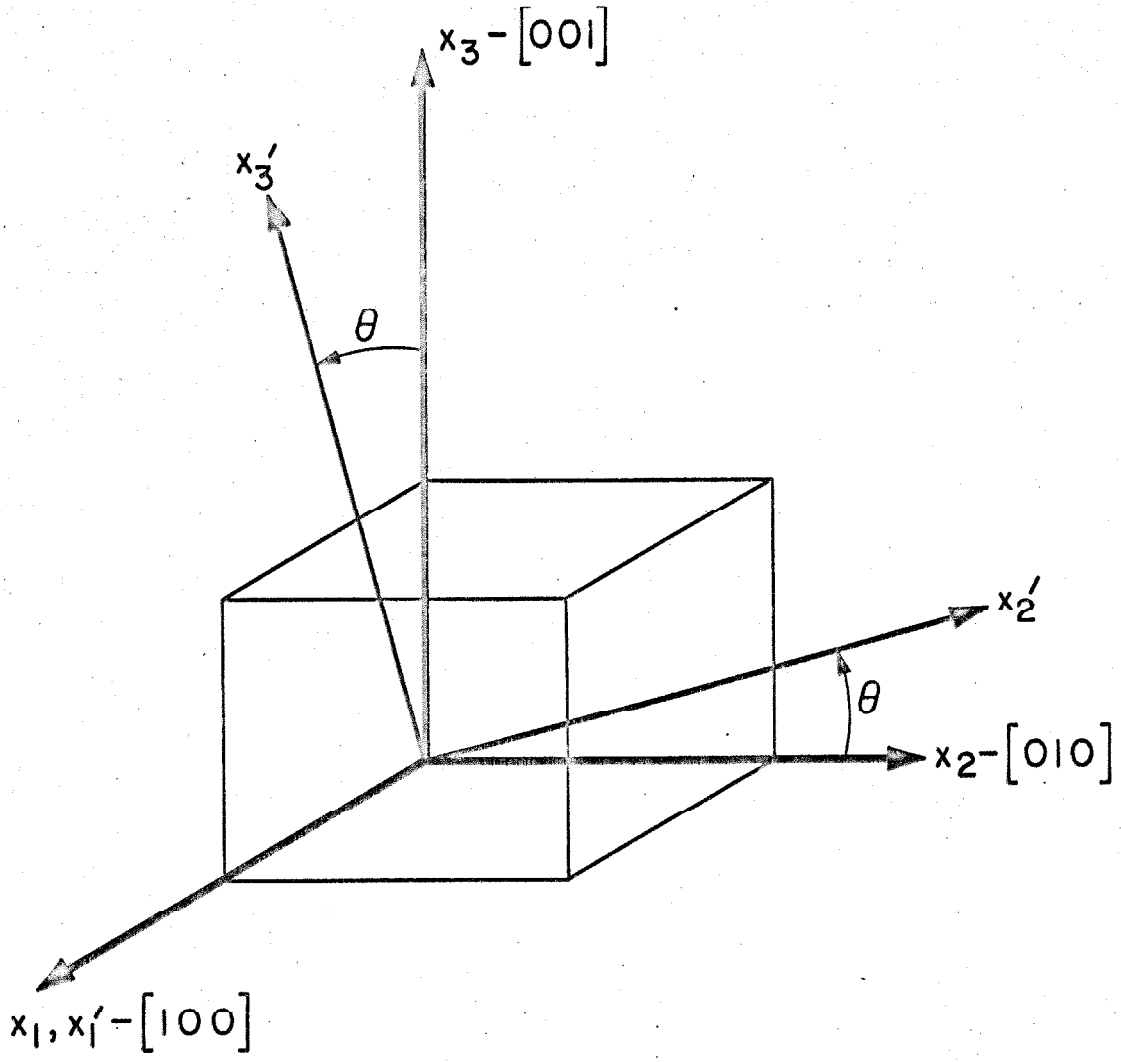

Figure A-3. [100] Specimen Orientation.

APPENDIX B

Assume that the stress dependence of dislocation velocity can be expressed as

$$v = (\tau/\tau_o)^m \qquad [B-1]$$

where v is the dislocation velocity, τ is the applied stress, τ_o is the applied stress which produces a velocity of 1 cm/sec, and m is the mobility exponent. Then the displacement, d, of a dislocation can be written as

$$d = \int v\,dt = \frac{1}{\tau_o^m} \int \tau^m(t)\,dt \ . \qquad [B-2]$$

The stress as a function of time, t, for a trapezoidal-shaped stress pulse is displayed in Figure B-1. The functional dependence of stress on time is given below.

$$\tau = \frac{\tau_{max}}{t_1}\, t \qquad 0 \le t \le t_1 \qquad [B-3]$$

$$\tau = \tau_{max} \qquad t_1 \le t \le t_2 \qquad [B-4]$$

$$\tau = \tau_{max} \left(\frac{t_3 - t}{t_3 - t_2}\right) \qquad t_2 \le t \le t_3 \qquad [B-5]$$

Subscripts are defined in Figure B-1. Substituting these functions in Equation B-2, and integrating over the appropriate ranges, yields

$$d = \left(\frac{\tau_{max}}{\tau_o}\right)^m \left[\frac{t_3 + m(t_2 - t_1)}{m+1}\right] \ . \qquad [B-6]$$

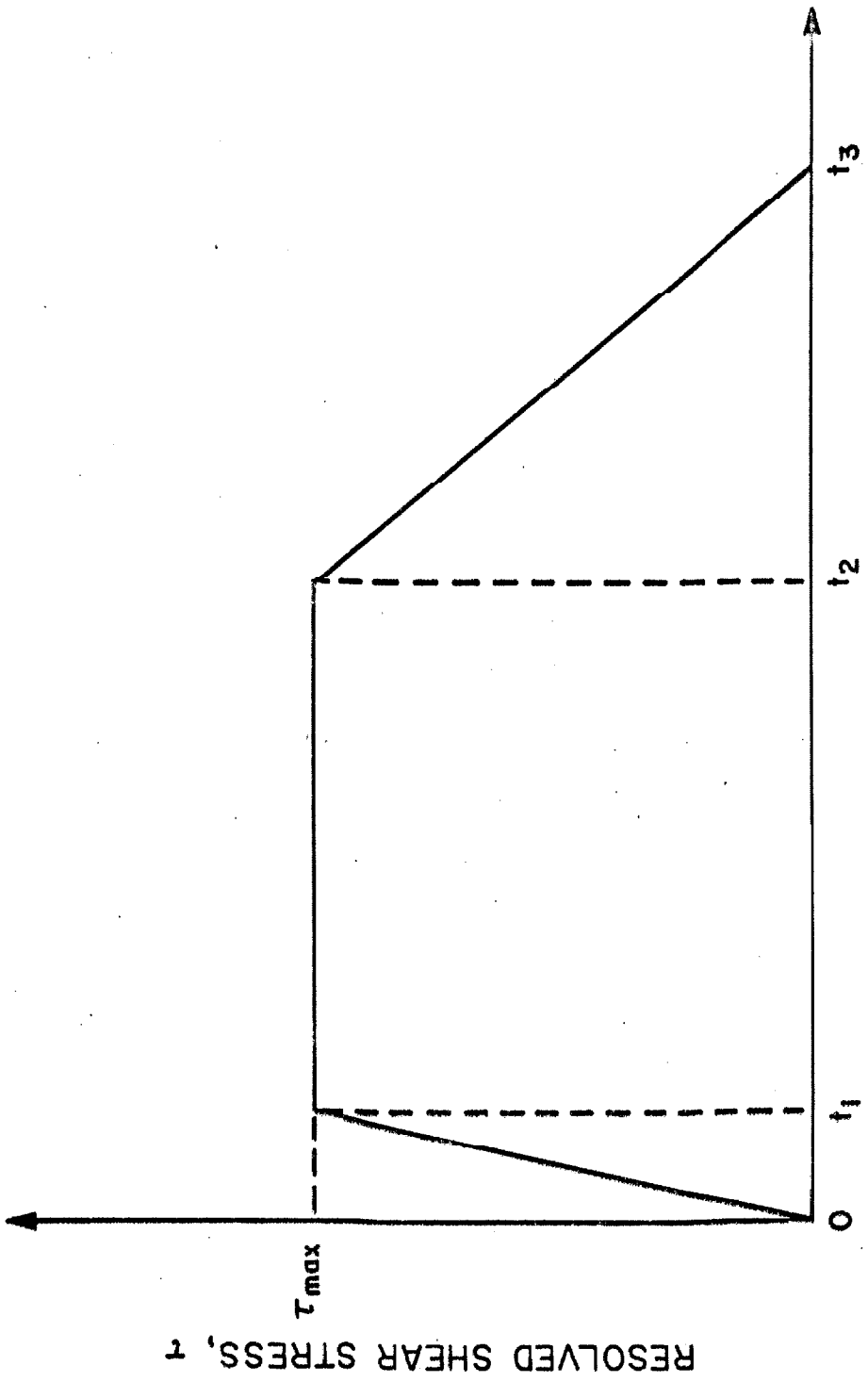

Figure B-1. Schematic Representation of Stress Pulse.

LIST OF REFERENCES

1. J. J. Gilman, "Progress in the Microdynamical Theory of Plasticity," Proceedings 5th U. S. Nat. Congr. Appl. Mech., Amer. Soc. Mech. Engrs. (1966), p. 385.

2. W. G. Johnston, "Yield Points and Delay Times in Single Crystals," J. Appl. Phys. 33, 2716 (1962).

3. J. C. M. Li, "A Dislocation Mechanism of Transient Creep," Acta Met. 11, 1269 (1963).

4. J. W. Taylor, "Dislocation Dynamics and Dynamic Yielding," J. Appl. Phys. 36, 3146 (1965).

5. D. P. Pope, research in progress, W. M. Keck Laboratory of Engineering Materials, California Institute of Technology.

6. T. Suzuki and H. Kojima, "A New Method and Results of Observation on Dislocation Motion in Silicon Crystals," Technical Report of the Institute for Solid State Physics, Series A, No. 173, The University of Tokyo (1965).

7. W. G. Johnston and J. J. Gilman, "Dislocation Velocities, Dislocation Densities, and Plastic Flow in Lithium Fluoride Crystals," J. Appl. Phys. 30, 129 (1959).

8. D. F. Stein and J. R. Low, Jr., "Mobility of Edge Dislocations in Silicon-Iron Crystals," J. Appl. Phys. 31, 362 (1960).

9. J. S. Erickson, "Mobility of Edge Dislocations on {112} Slip Planes in 3.25% Silicon-Iron," J. Appl. Phys. 33, 2499 (1962).

10. E. Yu. Gutmanas, E. M. Nadgornyi, and A. V. Stepanov, "Dislocation Movement in Sodium Chloride Crystals," Soviet Phys. - Solid State (5), 743 (1963).

11. H. W. Schadler, "Mobility of Edge Dislocations on {110} Planes in Tungsten Single Crystals," Acta Met. 12, 861 (1964).

12. A. R. Chaudhuri, J. R. Patel, and L. G. Rubin, "Velocities and Densities of Dislocations in Germanium and Other Semiconductor Crystals," J. Appl. Phys. 33, 2736 (1962).

13. M. N. Kabler, "Dislocation Mobility in Germanium," Phys. Rev. 131, 54 (1963).

14. K. H. Adams, "Dislocation Mobility and Density in Zinc Single Crystals," Ph. D. Thesis, California Institute of Technology, Pasadena, California (1965).

15. H. J. Levenstein and W. H. Robinson, "Etch Pits at Dislocations in Silver Single Crystals," J. Appl. Phys. 33, 3149(1962).

16. L. C. Lovell and J. H. Wernick, "Dislocation Etch Pits and Polygonization in High Purity Copper," J. Appl. Phys. 30, 590 (1959).

17. J. D. Livingston, "Etch Pits at Dislocations in Copper," J. Appl. Phys. 31, 1071 (1960).

18. J. D. Livingston, "The Density and Distribution of Dislocations in Deformed Copper Crystals," Acta Met. 10, 229 (1962).

19. F. W. Young, Jr., "Etch Pits at Dislocations in Copper," J. Appl. Phys. 32, 192 (1961).

20. F. W. Young, Jr., "On the Yield Stress of Copper Crystals," J. Appl. Phys. 33, 963 (1962).

21. M. J. Hordon, "Dislocation Density and Flow Stress of Copper," Acta Met. 10, 999 (1962).

22. F. W. Young, Jr., "Elastic-Plastic Transition in Copper Crystals as Determined by an Etch-Pit Technique," J. Appl. Phys. 32, 1815 (1961).

23. F. W. Young, Jr., "Etch Pit Studies of Dislocations in Copper Crystals Deformed by Bending: I. Annealed Crystals; II. Irradiated Crystals," J. Appl. Phys. 33, 3553 (1962).

24. J. D. Livingston, "Dislocation Studies in Copper Using Etch Pits," J. Aust. Inst. Metals 8, 15 (1963).

25. P. Petroff, "The Motion of Dislocations in Copper Single Crystals," M. S. Thesis, Department of Mineral Technology, University of California, Berkeley, California (1964).

26. H. Conrad, "An Investigation of the Rate Controlling Mechanism for Plastic Flow of Copper Crystals at 90°K and 170°K," Acta Met. 6, 339 (1958).

27. R. W. Guard, "Rate Sensitivity and Dislocation Velocity in Silicon Iron," Acta Met. 9, 163 (1961).

28. W. G. Johnston and D. F. Stein, "Stress Dependence of Dislocation Velocity Inferred from Strain Rate Sensitivity," Acta Met. 11, 317 (1963).

29. W. P. Mason, Physical Acoustics and the Properties of Solids, D. Van Nostrand Co., Inc. Princeton, New Jersey (1958), p. 48.

30. D. P. Pope, T. Vreeland, Jr., and D. S. Wood, "Machine for Producing Square Torsion Pulses of Microsecond Duration," Rev. Sci. Instr. 35, 1351 (1964).

31. W. P. Mason, op. cit., p. 35.

32. ibid, p. 17.

33. ibid., p. 358.

34. ibid., p. 49.

35. D. P. Pope, T. Vreeland, Jr., and D. S. Wood, "Comparison System for Microscope Images," Rev. Sci. Instr. 37, 377 (1966).

36. F. W. Young, Jr. and J. R. Savage, "Growth of Copper Crystals of Low Dislocation Density," J. Appl. Phys. 35, 1917 (1964).

37. F. W. Young, Jr. and T. R. Wilson, "Acid Cutting and Acid Polishing of Copper Crystals," Rev. Sci. Instr. 32, 559 (1961).

38. J. J. Gniewek, A. F. Clark, and J. C. Moulder, "Spark Planing Damage in Copper," National Bureau of Standards, Technical Note No. 321 (Sept. 6, 1965).

39. J. D. Livingston, Direct Observations of Imperfections in Crystals, ed. J. B. Newkirk and J. H. Wernick, Interscience Publ., New York (1962), p. 115.

40. J. J. Gilman, "Dislocation Mobility in Crystals," J. Appl. Phys. 36, 3195 (1965).

41. R. L. Fleischer, "Rapid Solution Hardening, Dislocation Mobility, and the Flow Stress of Crystals," J. Appl. Phys. 33, 3504 (1962).

42. A. Seeger, S. Mader, and H. Kronmüller, "Theory of Work-Hardening of FCC and HCP Single Crystals," Electron Microscopy and Strength of Crystals, Interscience Publ., New York (1963), p. 665.

43. J. Lothe, "Theory of Dislocation Mobility in Pure Slip," J. Appl. Phys. 33, 2116 (1962).

44. W. P. Mason, "Phonon Viscosity and Its Effect on Acoustic Wave Attenuation and Dislocation Motion," J. Acoust. Soc. Am. 32, 458 (1960).

45. T. Suzuki, A. Ikushima, and M. Aoki, "Acoustic Attenuation Studies of the Frictional Force on a Fast Moving Dislocation," Acta Met. 12, 1231 (1964).

46. A. H. Cottrell, "Discontinuous Yielding," The Relation Between the Structure and Properties of Metals, Her Majesty's Stationery Office, London (1963), p. 455.

47. T. Vreeland, Jr., private communication.

48. D. S. Wood, private communication.